University of Calgary

PRISM Repository **https://prism.ucalgary.ca**

The Vault Open Theses and Dissertations

2013-09-27

Investigating the changes in phagosomal function in Porcine Reproductive and Respiratory Syndrome Virus infection

Chaudhuri, Sibapriya

Chaudhuri, S. (2013). Investigating the changes in phagosomal function in Porcine Reproductive and Respiratory Syndrome Virus infection (Master's thesis, University of Calgary, Calgary, Canada). Retrieved from https://prism.ucalgary.ca. doi:10.11575/PRISM/26637 http://hdl.handle.net/11023/1058

Downloaded from PRISM Repository, University of Calgary

UNIVERSITY OF CALGARY

Investigating the changes in phagosomal function in Porcine Reproductive and Respiratory Syndrome Virus infection

by

Sibapriya Chaudhuri

A THESIS

SUBMITTED TO THE FACULTY OF GRADUATE STUDIES

IN PARTIAL FULFILMENT OF THE REQUIREMENTS FOR THE

DEGREE OF MASTER OF SCIENCES

DEPARTMENT OF VETERINARY MEDICAL SCIENCES

CALGARY, ALBERTA

SEPTEMBER, 2013

© Sibapriya Chaudhuri 2013

Abstract

Porcine Reproductive and Respiratory Syndrome is one of the most economically devastating diseases of the swine industry and affects all swine producing countries worldwide. The disease is caused by Porcine Reproductive and Respiratory Syndrome Virus (PRRSV). The virus is macrophage-tropic and infects tissue macrophages in the host animal. However, nothing is known about how the phagosome lumenal microenvironment in the macrophages may be modified in PRRSV infection. Such knowledge is crucial for understanding how microbicidal and antigen presentation functions of the macrophage may be compromised during PRRSV infection. The field of PRRSV biology also suffers from the dearth of existence of a good *in vitro* system for studying the virus biology in a methodical and reductionist fashion. This thesis establishes an *in vitro* system for studying PRRSV infection. Using this newly established *in vitro* system of PRRSV infection in porcine bone marrow derived macrophages, this study investigates how the phagosome microenvironment changes in porcine macrophages in PRRSV infection. This study also investigates how phagosome lumenal properties are modified in porcine alveolar macrophages isolated from PRRSV infected pregnant gilts.

Acknowledgements

I would like to thank my supervisor Dr. Robin Yates for his guidance and support for this study. Working under the supervision of a scientist as enthusiastic and motivated as him, has been a great experience. Not only was his door always open for discussions, but he was also always enthusiastic to troubleshoot, teach or work at the bench together.

I would like to thank Dr. Yan Shi, Dr Faizal Careem and Dr. Derek Mckay for investing their time to be on my supervisory committee.

I would like to thank Dr. Neil McKenna for helping me carry out some of the *ex vivo* experiments, proof-reading my thesis, and for all his invaluable suggestions for troubleshooting experiments. He is a great co-worker who always greatly contributes to making working in lab super fun for all lab members. I would also like to thank him for his patience when I was slow to learn, and for having faith in my abilities.

I would like to thank everyone in the Yates lab - Dale Balce for his invaluable suggestions on phagosomal assays, Jason Lemmon for valuable tips on improving writing skills. I would like to thank Euan Allan, Jason Abboud, Pankaj Tailor, Paymon, Bernard Euanchak, Raymond Lam, Samuel Lee for being great people to work with.

I would like to thank our collaborator Dr. John Hardings for sending us *exvivo* samples.

Finally, I would like to thank my family and friends for their moral support, particularly my parents for having faith in my abilities and my sister who made me see “the other side of the coin”. Moving half way across the globe can be challenging. I would like to thank all who made this transition easy – particularly Meenakshi Rawat, Demyana Boles and my flatmate Liane Babes.

Dedication

Dedicated to my parents - who inspired me to dream big and believed in me at all times, even when I did not believe in myself.

TABLE OF CONTENTS

CHAPTER 1 : INTRODUCTION	**1**
1.1: Phagocytosis	2
1.2: Professional phagocytes	3
1.3: The macrophage	4
1.3.1: Alveolar macrophages	9
1.4: Phagosome formation	10
1.5: Phagosome maturation	14
1.6: Microbicidal effectors of the phagolysosome	19
1.7: Porcine Reproductive and Respiratory Syndrome Virus (PRRSV)	23
1.7.1: Clinical symptoms:	25
1.8: PRRSV genome organization and structural proteins:	25
1.9: PRRSV cell tropism:	28
1.10: Entry of PRRSV into the host cell: PRRSV receptors	30
1.11: Immune responses of the host animal to PRRSV	35
1.12: Hypothesis and Specific Aims:	38
1.12.1: HYPOTHESIS:	38
1.12.2: Specific Aim I	38
1.12.3: Specific Aim II	39
1.12.4: Specific Aim III	39
CHAPTER 2: METHODS	44
2.1: Cell lines used	45
2.1.1: MARC 145 cell line	45
2.1.2: L929 cell line	45
2.2: Virus strain used	46
2.3: Growing PRRSV isolate NVSL 97-7895 in MARC 145 cells	46
2.4: Titration of virus by plaque assay	47
2.5: Cultivation of L929 supernatant	50
2.6: In vitro differentiation of porcine bone marrow cells into porcine bone marrow derived macrophages	51
2.7: Freezing and thawing of porcine bone marrow cells	55
2.8: Infection of pBMMØ	55
2.9: Maintenance and infection of pregnant gilts:	56
2.10: Isolation of porcine alveolar macrophages (PAM) from BAL samples by density gradient centrifugation	57
2.11: Assays for studying phagosomal lumenal properties	60

2.11.1: Preparation of experimental particles: 60
2.11.1.1: Preparation of experimental particles for phagocytic index calculation 60
2.11.1.2: Preparation of proteolysis reporter experimental particles 61
2.11.1.3: Preparation of oxidation-sensitive experimental particles 61
2.11.1.4: Preparation of pH-sensitive experimental particles 62
2.11.1.5: Preparation of fluorescent latex beads with or without Fc receptor ligand 62
2.11.1.6: Preparation of serum-opsonised zymosan 63
2.11.2: Measuring phagocytic index 63
2.11.2.1: Measuring phagocytic index by microscopy 63
2.11.2.2: Measuring phagocytic index using flow cytometry 64
2.11.3: Measuring phagosomal proteolysis 65
2.11.4: Measuring intra-phagosomal oxidative burst through phagocytosis of oxidation- sensitive experimental particles 68
2.11.5: Detection of phagosomal ROS by amplex red assay 69
2.11.6: Fluorometric measurement of phagosomal acidification in real time 69
2.12: Statistical analysis 71
2.13: Imaging 71

CHAPTER 3: RESULTS
3.1: *In vitro* differentiation of porcine bone marrow cells into porcine bone marrow derived macrophages (pBMMØ) using L929 cell supernatant 73
3.2: *In vitro* differentiated pBMMØ exhibit FcγR -mediated phagocytosis of experimental particles 77
3.3: *In vitro* differentiated pBMMØ show characteristic phagosomal acidification 78
3.4: *In vitro* differentiated pBMMØ show characteristic phagosomal proteolysis 79
3.5: PRRSV isolate NVSL 97-7895 was propagated in MARC 145 cells 87
3.6: *In vitro* infection of pBMMØ is productive 87
3.7: pBMMØ infected i*n vitro* with PRRSV isolate NVSL 97-7895 did not show cell death 24 hours post-infection 93
3.8: pBMMØ infected *in vitro* with PRRSV isolate NVSL 97-7895 exhibited significantly lower levels of phagosomal proteolysis than uninfected cells 96
3.9: Infected pBMMØ do not show any significant difference in phagocytic efficiency compared to uninfected cells 97
3.10: pBMMØ infected *in vitro* with PRRSV isolate NVSL 97-7895 show no significant difference in acidification pattern from uninfected cells 98
3.11: pBMMØ infected *in vitro* with PRRSV isolate NVSL 97-7895, produce significantly lower levels of phagosomal ROS than uninfected cells 99

3.12: Alveolar macrophages isolated *ex-vivo* from PRRSV-infected gilts exhibit significantly higher levels of proteolysis than alveolar macrophages from uninfected animals 108
3.13: Alveolar macrophages from PRRSV infected gilts show no significant difference in phagocytic index than alveolar macrophages from uninfected animals 110
3.14: ROS production in alveolar macrophages from PRRSV-infected gilts was not significantly different than from alveolar macrophages from uninfected animals 111

CHAPTER 4: DISCUSSIONS 119
4.1: Establishment of a novel *in vitro* system to study PRRSV infection 120
4.1.1: Advantages of the established system over the existing systems 120
4.1.2: L929 cells can be used to differentiate porcine bone marrow cells into porcine bone marrow derived macrophages 122
4.1.3: Fluorometric analysis of phagosomal microenvironment can be used as functional assays to identify macrophages 123
4.1.4: Future Directions Aim I 124
4.2: pBMMØ when infected *in vitro* with PRRSV show different phagosomal lumen properties 126
4.2.1: PRRSV-infected pBMMØ exhibit significantly lower levels of phagosomal proteolysis 126
4.2.2: Future directions Aim 2 129
4.3 : PAM isolated from PRRSV-infected pregnant gilts showed significantly higher levels of phagosomal proteolysis than cells isolated from healthy animals 131
4.3.1: Future directions Aim 3 134

4.4: Overall future directions: 136

List of Figures and Illustrations

Figure 1.1	A simplified cartoon illustrating phagosomal maturation in relation to the endo-lysosomal network
Figure 1.2	Microenvironment within mature phagosome
Figure 1.3	PRRSV genome
Figure 1.4	PRRSV entry mediators
Figure 1.5	PRRSV internalization
Figure 1a.1	Workflow for specific aim 1
Figure 1a.2	Workflow for specific aim 2
Figure 1a.3	Workflow for specific aim 3
Figure 2.1	Schematic diagram for PRRSV NVSL 97-7895 titration on MARC 145 cells
Figure 2.2	Important timelines in cultivation and harvest of L929 cell supernatant
Figure 2.3	A simplified protocol highlighting the most important steps in differentiation of porcine bone marrow cells into porcine bone marrow derived macrophages
Figure 2.4	Schematic representation of the most important steps in the isolation of alveolar macrophages from BAL samples
Figure 2.5	Schematic representation of how proteolytic reporter experimental particles are used to assay phagosomal proteolysis
Figure 3.1	Porcine bone marrow cells isolated from mid costal (rib) bones can be differentiated *in vitro* by culturing in the presence of L929 cell supernatant containing murine M-CSF
Figure 3.2	pBMMØ showed significantly higher levels of FcR-mediated phagocytosis
Figure 3.3	Phagosomes formed by *in vitro* differentiated pBMMØ, upon ingestion of experimental particles, showed characteristic acidification
Figure 3.4	*In vitro* differentiated pBMMØ showed characteristic phagosomal proteolysis
Figure 3.5	PRRSV isolate NVSL-97-7895 was propagated in MARC-145 cells
Figure 3.6	Infection of pBMMØ with PRRSV isolate NVSL-97-7895 is productive
Figure 3.7	Infection of pBMMØ with PRRSV isolate NVSL-97-7895 does not result in

	significant cell death 24 hours post-infection
Figure 3.8	pBMMØ infected *in vitro* with PRRSV showed significantly lower levels of phagosomal proteolysis than uninfected cells
Figure 3.9	pBMMØ infected with PRRSV (NVSL-97-7895) at a MOI of 0.1 showed no significant differences in efficiency of phagocytic uptake than uninfected cells
Figure 3.10	There is no significant difference in the phagosomal pH between uninfected and PRRSV-infected pBMMØ
Figure 3.11	pBMMØ infected *in vitro* with PRRSV isolate NVSL 97-7895 exhibit significantly lower levels of phagosomal ROS production than uninfected control cells
Figure 3.12	PAM isolated from pregnant gilts infected with PRRSV (isolate NVSL 97-7895) show significantly higher phagosomal proteolysis than PAM from uninfected control animals
Figure 3.13	There is no significant difference in the phagocytic index between alveolar macrophages isolated from PRRSV-infected and uninfected pregnant gilts
Figure 3.14	Alveolar macrophages isolated from PRRSV-infected pregnant gilts and uninfected control animals showed no significant difference in phagosomal ROS production.

List of Abbreviations:

BAL	Broncho-alveolar lavage
conA	Concanamycin A
CORVET	Class C core vacuole/endosome tethering
CPE	Cytopathic effects
DMEM	Dulbecco's Modified Eagle's Medium
DMSO	Dimethyl sulfoxide
DPI	Diphenyleneiodonium
EAV	Equine arteritis virus
EDTA	Ethylene diaminetetraacetic acid
EEA1	Early endosomal antigen 1
EV-SS	Electronic voltage-Side scatter
FCS	Fetal Calf Serum
FcγR	Fcγ receptor
GEFs	Guanine nucleotide exchange factors
H2HFF	Dihydro-2',4,5,6,7,7'-hexafluorofluorescein
HOPS	Homotypic fusion and protein sorting
IFN-γ	Interferon-gamma
Ig	Immunoglobulin
iNOS	Inducible nitrous oxide synthase
ITAM	Immunoreceptor tyrosine-based activation motifs
LAMP	Lysosome-associated membrane proteins

LBPA	Lysobiphosphatidic acid
LPS	Lipopolysaccharide
M-CSF or CSF1	Murine macrophage colony stimulating factor
MOI	Multiplicity of infection
ORF	Open reading frame
PAM	Porcine alveolar macrophages
PAMPs	Pathogen-associated molecular patterns
PBS	Phosphate Buffer Saline
PCR	Polymerase chain reaction
PFU	Plaque forming unit
$PI(4,5)P_2$	Phosphatidylinositol-4,5-bisphosphate
PI3K	Phosphatidylinositol 3-kinase
PLCγ	Phospholipase Cγ
PRDC	Porcine respiratory disease complex
PRR	Pattern recognition receptors
PRRS	Porcine Reproductive and Respiratory Syndrome
PRRSV	Porcine Reproductive and Respiratory Syndrome Virus
RCF	Relative centrifugal force
RFU	Relative fluorescence intensity
SE	Succinimidyl ester
SH2	Src homology 2
SHFV	Simian hemorrhagic fever virus
SJPL	St-Jude porcine lung cell
TIM	T cell immunoglobulin mucin

TLR	Toll-like receptor
TNF	Tumor necrosis factor
UTR	Untranslated regions
VCA	Verprolin homology, cofilin homology and acidic
WASP	Wiskott-Aldrich syndrome protein

CHAPTER 1: INTRODUCTION:

1.1: Phagocytosis

Phagocytosis is a process of particle uptake by a cell. Phagocytosis was first described in the late nineteenth century by Elie Metchnikoff when he observed phagocytes in starfish larvae clustering around rose thorns that were introduced into the larvae. This led to the postulation of the "phagocytosis theory" which earned him the Nobel Prize in 1908[2]. Since then, the process has been studied intensively; however gaps still exist in our understanding of the intricate details of the process. Phagocytosis occurs across the different phyla of the animal kingdom – from unicellular organisms to mammals. However, in different organisms, phagocytosis may serve different functions. The unicellular amoeba *Dictyostelium discoideum* uses phagocytosis for uptake of nutrients from its environment[3]. In the nematode *Caenorhabditis elegans*, phagocytosis plays an active role during embryogenesis for removal and recycling of dying cells. In adult worms, phagocytosis is involved in tissue remodeling, but the phagocytes do not stimulate any inflammatory response and are not considered to be a part of an "immune system"[4]. In *Drosophila*, along with humoral immune responses, phagocytosis by cells in the hemolymph plays an important role in providing protection against infection[5]. In mammals, phagocytosis functions at the fulcrum of innate and adaptive immune responses. Professional phagocytes constitute the body's first line of defense and are actively involved in clearing invading micro-organisms[6]. Ingested particles are degraded inside the phagosome and the antigens derived from the degraded products are presented to T cells[7]. Phagocytes can also stimulate an inflammatory response during an infection[8] as well as play active roles in clearing apoptotic cells of the body[9] for tissue homeostasis, remodeling and

repair[10]. During tissue remodeling functions, phagocytes can release or stimulate the release of anti-inflammatory cytokines to prevent further tissue damage[11].

1.2: Professional phagocytes:

Professional phagocytes, a term popularized by Rabinovitch, include monocytes, macrophages, dendritic cells and neutrophils[12]. They have an overall higher phagocytic efficiency than paraprofessional and nonprofessional phagocytes which broadly includes fibroblasts, epithelial cells and endothelial cells[13]. The non professional phagocytes do not produce pro-inflammatory or anti-inflammatory immune responses, do not produce a phagosomal respiratory burst and are limited in the range of target particles they internalize as they lack the arsenal of phagocytic receptors expressed by professional phagocytes[12]. Among professional phagocytes, macrophages and neutrophils are functionally more skewed towards killing and removing infectious agents. Dendritic cells, on the other hand, are more actively involved in capturing and processing antigenic peptides and subsequently presenting antigenic peptides to T cells[14]. Neutrophils are the first cells to be recruited to a site of inflammation in the body. They employ various intracellular and extracellular microbicidal mechanisms to kill invading pathogens[15,16]. They are particularly known for producing a high phagosomal respiratory burst[17]. Dendritic cells principally reside in tissues where they survey their immediate environment for foreign antigens. Once captured, antigens are processed by dendritic cells and presented to CD4+ or CD8+ T cells[14]. Dendritic cells also play an important function in T cell activation and immune tolerance[18].

1.3: The Macrophage:

Macrophages are primary host cells for Porcine Reproductive and Respiratory Virus infection[19]. Macrophages are an anatomically and functionally diverse population of cells belonging to the mononuclear phagocytic system[20]. Macrophages function in immunity, homeostasis, development and tissue repair in the body[21-24]. Macrophages reside in different tissues throughout the body and they constantly patrol their immediate environment for danger signals such as molecular patterns from invading micro organisms, apoptotic cells and necrotic debris[22,24]. A high degree of heterogeneity exists between macrophages in different tissues which make them better equipped to perform the specialized function of that tissue[25,26]. As such, macrophages are often categorized into different subsets based on their anatomical location in the body[27]. Osteoclasts are macrophages in bones – they are actively involved in bone remodeling, repair and growth[28,29]. Liver-resident macrophages, called Kupffer cells, are important for bilirubin metabolism[30]. Microglia, perivascular macrophages, meningial macrophages and choroid plexus macrophages populate the central nervous system. Microglia are involved in brain development[31]. Gut macrophages have high microbicidal and phagocytic activity but are poor in the secretion of proinflammatory cytokines[32]. Macrophages residing in the colon do not respond readily to various stimuli and are generally very tolerant to the existing gut microflora and their products[33]. Thymic macrophages play a role in maturation and development of thymic lymphocytes[34,35]. Splenic macrophages exhibit functional heterogeneity based on their location. The red pulp macrophages inside the spleen can recycle iron from ingested red blood cells. The marginal zone macrophages in spleen express a unique set of

pattern recognition receptors and are involved in clearing blood borne pathogens and apoptotic cells[36,37]. Metallophilic macrophages reside adjacent to the marginal sinus in the spleen, surrounding the white pulp. They may play an important role in responding to viral infections[38]. Tingle body macrophages present in white pulp of spleen are important for clearing apoptotic cells[39]. Alveolar macrophages populate the respiratory tract and lungs and function at the blood-air interface. They have high expression levels of pattern recognition receptors and scavenger receptors and play an active role in removing and degrading inhaled allergens and invading micro-organisms[40].

The origin of macrophages in adults is quite different from that in the embryo and fetus[41]. In adults, tissue macrophages differentiate from circulating monocytes during steady state and in response to inflammation[27]. Monocytes originate from a common myeloid progenitor derived from hematopoietic stem cells in the bone marrow. In addition to macrophages, circulating monocytes also differentiate into dendritic cells[42]. Increased recruitment and differentiation of monocytes have been observed in response to proinflammatory, metabolic and immune signals[43,44]. However, what influences the choice of monocyte differentiation is still debatable[45,46]. Monocytes in the blood are heterogeneous in terms of size, trafficking, receptors expressed and their ability to differentiate upon being exposed to cytokines and microbial products[47-49]. As monocyte heterogeneity is not yet completely understood, disputes still exist over if macrophages in a particular tissue are derived from a specific lineage-committed monocyte population or from a random pool of circulating monocytes[50]. In addition to being replenished by circulating monocytes, tissue macrophages

also have self-renewal capacities and can be generated through local proliferation of existing macrophages in the tissue. However, it is yet to be determined if local proliferation of macrophages is tissue-restricted or is a universal property of all tissue macrophages[27]. Also considerable debate exists over if local proliferation of tissue macrophages occurs both during steady state and in response to inflammation. To date, alveolar macrophages, microglia, Kupffer cells, white pulp and metallophilic macrophages in the spleen have been shown to originate from two sources – from circulating monocytes and through self renewal of existing local macrophages[51-54].

In addition to differentiation and tissue distribution, the activation state of the macrophage contributes to heterogeneity of the macrophage population. Activation state of macrophages is determined by their responsiveness to microbial products, cytokines and adaptive immune signals[55]. Based on activation states, three distinct populations of macrophages can be identified – classically activated macrophages, alternatively activated macrophages or wound healing macrophages and regulatory macrophages[56]. However, macrophages exhibit a great deal of plasticity in terms of their activation states. In a disease state or under a given set of conditions of tissue microenvironment, tissue macrophages can exist in more than one state of activation or may exhibit combined features of different activation states. For example, tumour-associated macrophages exhibit features of regulatory macrophages and alternatively activated macrophages[56-58].

Classically activated macrophages (also known as M1 macrophages) are activated by a combination of interferon-gamma (IFN-γ) and tumor necrosis factor (TNF)[59,60]. IFN-γ can be

produced from innate or adaptive immune sources. During an infection, natural killer (NK) cells produce IFN-γ to activate macrophages[61]. Also, antigen-specific T_H1 cells are a source of IFN-γ for macrophage activation[62]. The source of TNF can be exogeneous or endogeneous. TNF transcription in macrophages can be activated in response to Toll-like receptor (TLR) ligands such as bacterial lipopolysaccharide (LPS) in a MyD88-dependent or independent manner[56,63]. Classically activated macrophages exhibit high phagosomal microbicidal properties, have a high phagosomal respiratory burst (thereby producing copious amounts of reactive oxygen species - ROS and nitric oxide)[64]. However, they exhibit lower levels of phagosomal hydrolytic activities including lower phagosomal proteolysis[65]. They produce proinflammatory cytokines such as TNF, IL 1, IL 6, IL 12 and IL 23 and hence play an important role in host defense[55]. Such inflammatory responses, along with ROS, can mediate extensive tissue damage[66]. Classically activated macrophages, similar to alternatively activated macrophages, have higher expression of MHC class II molecules and show enhanced antigen presentation[67].

When stimulated by IL 4 and/or IL 13, macrophages are polarized to an alternative activation or M2 state[68]. M2 activated macrophages, otherwise known as wound healing macrophages, play an active role in wound healing and tissue repair[69]. IL 4 and IL 13 are cytokines typically produced by T_H2 T cells in response to allergic conditions, parasitic infections or extracellular pathogens[70]. IL 4 can also be produced in response to tissue damage by basophils, eosinophils and mast cells[71]. M2 macrophages exhibit upregulated expression of mannose receptor, MHC II molecules, and arginase[68,72-74]. Arginase inhibits production of nitric oxide and facilitates ornithine production[75]. Ornithine is a precursor to proline, polyamines, and

collagen and contributes to building extracellular matrix and hence facilitates tissue repair[73]. Alternatively activated macrophages have a lower phagosomal respiratory burst but exhibit higher levels of phagosomal proteolysis[76]. Some studies suggest that due to lower respiratory burst, alternatively activated macrophages may be more susceptible to intracellular infections[77,78].

Like classically activated macrophages and alternatively activated macrophages, regulatory macrophages are polarized by innate or adaptive immune responses. Regulatory macrophages are often found to arise during control of inflammation and can sufficiently dampen the immune responses mediated by classically activated macrophages[55,79]. Various factors including immune complexes, prostaglandins, G-protein coupled receptor ligands, and apoptotic cells can polarize macrophages into their regulatory subtype[55,80,81]. IL 10 and TGF-β induces macrophages to exhibit regulatory phenotype and at the same type, these anti-inflammatory cytokines are produced by regulatory macrophages[82]. In addition, production of proinflammatory cytokines such as IL 12 and IFN-γ is down-regulated[79]. Invading viruses and bacteria may mimic one of the stimuli for polarization of macrophages to regulatory phenotype and thereby inhibit the secretion of proinflammatory cytokines. This provides conditions conducive for replication and growth of invading pathogens[83]. Some tissue macrophages such as alveolar macrophages and gut macrophages have been reported to exhibit the deactivated phenotype under steady state conditions[84-86].

1.3.1: Alveolar Macrophages:

Alveolar macrophages reside in alveolar spaces in the lung tissue at the blood-airway interface. They are the major phagocytes in the lower respiratory tract[87]. In the steady state, resident alveolar macrophages are continuously challenged with inhaled particulate matter including dust and pollutants. To ensure that such harmless antigens do not provoke an inflammatory immune response and thereby lead to tissue damage, alveolar macrophages usually exhibit "deactivated phenotype" and have been known to express IL 10 and TGF-β in steady state[88]. Alveolar macrophages express a broad range of pattern recognition receptors (PRR)[88]. During an infection initiated by a microbial influx through the respiratory tract, they provide the first line of defense in phagocytosing and removing the microbes before the adaptive immune system is stimulated[89]. Binding of PRR (most importantly TLRs) and non pattern recognition receptors to their ligands can activate alveolar macrophages, leading to inhibition of TGF β expression and production of proinflammatory cytokines[90]. Activated alveolar macrophages contribute to several lung diseases[91]. In addition to being replenished by circulating monocytes, alveolar macrophages can undergo local proliferation and exhibit self-renewing properties[88,92]. In vitro studies mainly rely on isolation of alveolar macrophages from broncho-alveolar lavage (BAL) samples[93,94]. BAL samples are obtained by non invasive bronchoscopy of living subjects (human or animals)[94]. In mammals, under normal physiological conditions, alveolar macrophages constitute 95% of the cellular component of BAL[93].

1.4: Phagosome formation:

The complex series of events leading to phagosome formation can be conceptually divided into two steps: 1) particle recognition and 2) particle internalization.

1. Particle recognition:

Target particles typically larger than 500 nm are taken up by phagocytosis. *In vitro*, spherical targets are usually used for studying phagocytic uptake[95,96]. In nature, phagocytic targets can be of diverse shape and can be electrostatically charged or neutral. The relation between target charge and target recognition and internalization is complex and poorly understood. *In vitro*, phagocytosis has been reported to be affected by target geometry and surface charge on the phagocytic target[97-99]. Particles smaller than 500 nm are internalized by the cell through one of many endocytic mechanisms[100,101].

Particle recognition in phagocytosis is largely thought to be receptor-mediated. Phagocytosis is initiated when receptors on the surface of a phagocyte bind to their cognate ligands. Receptor-ligand interaction is direct in case of non-opsonic pattern recognition receptors (PRRs)[102]. Such receptors can recognize innate components on the surface of microbes called pathogen-associated molecular patterns (PAMPs). Among pattern recognition receptors, dectin-1 and mannose receptor recognize glucan and mannan on the surface of yeast cells respectively[103]. Scavenger receptors are a family of diverse receptors which can recognize a wide range of targets including bacterial LPS, bacterial lipoteichoic acids and CpG

DNA[104]. In case of opsonic receptors, receptor-ligand interaction is indirect and is mediated by opsonins, which are exogenous host derived molecules such as antibody or complement. Opsonins bind to pathogen surface and facilitate their recognition by opsonic receptors[105]. Integrin receptor CR3 primarily binds to complement fragment iC3b of complement-coated targets[106]. The IgG-opsonized targets are recognized by Fcγ receptor (FcγR)[107]. *In vivo*, multiple opsonic and non-opsonic receptors may interact simultaneously or in sequence with the target[105]. The strength of a receptor-ligand interaction depends on their mutual affinity and their density of occurrence on the surface of phagocyte and target particles[105]. In addition, an activation stimulus can sometimes enhance the affinity of some receptor-ligand interactions. For example, downstream signaling from activation of TLRs may induce conformational changes in integrin receptor and increase its affinity for its ligand[108]. Pathogens may exhibit strategies to avoid being phagocytosed. The most common strategies developed by pathogens to do so are to avoid receptor binding or prevent opsonin deposition[109-111]. Recognition of apoptotic cells occurs through similar, yet different mechanisms. Cells undergoing apoptosis release soluble chemoattractants such as ATP, fractalkine, sphingosine-1-phosphate, *etc,* which recruit phagocytes[112]. Phagocytes recognize specific signals on apoptotic cells that differentiate them from healthy cells. For example, apoptotic cells have phosphatidylserine on the outer leaflet of the plasma membrane instead of on the inner leaflet, as found in normal cells[113]. A number of phagocytic receptors such as T cell immunoglobulin mucin (TIM), BAI-1, and Stabilin-2 families can bind directly to phosphatidylserine and facilitate their phagocytosis[114-116]. Sometimes healthy cells such as activated T cells may express considerable amounts of phosphatidylserine

on their surface. To escape being phagocytosed, they also express “do not eat me” molecules such as CD31[117].

2. Particle internalization:

The downstream signaling after particle recognition and the process of particle internalization depend hugely on the nature of receptors engaged and type of ligands involved. The complex series of events leading to the internalization of targets are regulated by many important mediators in a non linear fashion[105]. A phagocytic target is internalized by extensions of plasma membrane forming pseudopodia-like structures, creating a phagosomal cup around the target circumference, and enclosing it to form a phagosome[118]. This mechanism of particle internalization is otherwise known as the zipper model of phagocytosis[119]. Particle internalization involves local rearrangement of the actin cytoskeleton consisting of F-actin or actin filaments. This is mediated to a large extent by *de novo* actin nucleation[120]. Actin nucleation refers to the initiation of actin polymerization from its free monomeric units or G-actin. After sealing of the phagosomal cup, the actin network rapidly depolymerizes rendering the phagosomal membranes flexibile enough to fuse with the endolysosomal system during the maturation process[120]. The best-studied model of phagocytosis is the uptake of IgG-opsonized targets through FcγR[121]. Fc receptors (FcR) belong to the immunoglobulin (Ig) superfamily and bind to the constant region (Fc portion) of immunoglobulin molecules[121,122]. Interactions of FcRs with their targets can initiate a wide range of immune responses including phagocytosis, inflammatory responses, and antibody-dependent cell-mediated cytotoxicity. Among the different classes of Fc receptors, FcγRs are in particular known to mediate phagocytosis[105].

Among the different classes, FcγRI, FcγRIIA, FcγRIII, and FcγRIV are known to activate phagocytosis, while FcγRIIB negatively regulates phagocytosis[123]. Phagocytosis by FcγR is initiated by multivalent receptor-ligand binding resulting in receptor clustering[124]. FcγRs are characterized by the presence of two immunoreceptor tyrosine-based activation motifs (ITAM) separated by 7-12 amino acids. ITAM motifs contain the consensus sequence of YXXI/L[125]. Receptor clustering brings ITAM motifs of several Fc receptors close together. This is followed by phosphorylation of both tyrosine residues on ITAM motifs by Src family tyrosine kinases[126]. Src kinases which can phosphorylate ITAM motifs on FcγRs include, but may not be limited to, Hck, Lyn, and Fgr[127,128]. Syk kinase then binds to doubly phosphorylated ITAMs through two of its Src homology 2 (SH2) domains[129]. Subsequent to its ITAM motifs, Syk is phosphorylated and activated by Src kinases. Phosphorylated Syk recruits an arsenal of adaptor proteins including LAT, Grb2, and Gab2[130-132]. Syk may phosphorylate neighbouring ITAM motifs in a given Fc receptor cluster on being recruited, as suggested by studies which show that Syk can phosphorylate ITAM motifs *in vitro*[133]. Activated Syk, along with the adaptor proteins, plays an active role in lipid signaling by activating multiple lipid modification enzymes. Lipid signaling is important for membrane remodeling and phagocytic cup formation[105]. Under regular physiological conditions, phosphatidylinositol-4,5-bisphosphate ($PI(4,5)P_2$) is present on the inner leaflet of the plasma membrane of phagocytes[105]. During phagocytic cup formation, levels of $PI(4,5)P_2$ increase transiently in the pseudopods forming the cup, and then disappear suddenly[120]. This accumulation of $PI(4,5)P_2$ followed by its complete disappearance is important for internalization of targets[134]. Also this may help in the actin depolymerization process after

sealing of the phagocytic cup. Several overlapping mechanisms contribute to the rise and fall in the levels of $PI(4,5)P_2$. One mechanism involves hydrolysis of $PI(4,5)P_2$ by phosphoinositide-specific phospholipase Cγ (PLCγ) in its phosphorylated form. PLCγ is recruited to the phagocytic cup by Syk kinase and its adaptor proteins[135]. In another pathway, $PI(4,5)P_2$ is phosphorylated to $PI(3,4,5)P_3$ at the phagocytic cup by class I phosphatidylinositol 3-kinase (PI3K)[120]. PI3K is also recruited to the phagocytic cup by Syk and its adaptor protein complex[136]. Syk kinase along with its adaptor proteins are also known to recruit guanine nucleotide exchange factors (GEFs). GEFs convert GDP to GTP and facilitate shuttling of small GTPases between an inactive GDP-bound state and an active GTP-bound state. Rac, Cdc42, and RhoA are Rho family GTPases that regulate actin polymerization and cytoskeletal rearrangement during phagocytosis[137]. Cdc42 and $PI(4,5)P_2$ bind simultaneously to Wiskott-Aldrich syndrome protein (WASP) bringing about a conformational change in the protein such that its VCA (verprolin homology, cofilin homology and acidic) domain is exposed which binds and activates the Arp2/3 complex[120,138]. Arp2/3 is an evolutionarily conserved seven protein actin nucleator complex that mediates actin polymerization. Rac does not bind to WASP family proteins directly; it instead activates the Scar/WAVE family proteins which also serve as nucleation promoting factors[120]. Signaling from Rac may also promote actin nucleation in Arp2/3-independent manner[107].

1.5: Phagosome maturation:

Phagosome maturation refers to a series of complex biochemical reactions occurring sequentially and resulting in gradual conversion of the newly formed neutral, relatively

nonreactive phagosome into an acidic, oxidative, degradative, and microbicidal organelle. The cytotoxic, degradative, and microbicidal milieu of the mature phagosome is a cumulative effect of its acidification, the generation of ROS, and acquisition of hydrolytic enzymes and antimicrobial products[139]. The process of maturation is initiated immediately after, or possibly before[140], the sealing of the phagosomal membrane. During maturation, the phagosome undergoes a series of fusion and fission reactions with the endolysosomal system. According to the "kiss and run" model of phagosome maturation, phagosomes undergo a series of multiple transient fusion reactions, consisting of the "kiss" with the endolysosomal system, followed by immediate separation or a "run" phase[141]. The maturing phagosome progressively acquires the membrane and lumenal components and characteristics of the fusing vesicles. However, the size of the phagosome remains fairly constant[142]. Recycling of the phagosomal membrane to the cell surface through formation and budding off multi-vesicular bodies is believed to be one of the mechanisms contributing to keeping phagosome size constant[143,144]. The phagosome preferentially fuses with, in sequence, early, then late endosomes, and finally lysosomes. The fusion reactions eventually result in the formation of the phagolysosome which marks the completion of the maturation process. The kinetics of maturation may depend on the nature of the ingested target[145,146]. The process of maturation is tightly regulated at the molecular level. Among other molecules, Rab GTPases play an important role in maturation of phagosome and co-ordinating vesicular traffic[105]. In the GTP-bound form, Rab GTPases can interact with adaptor proteins, tethering factors, kinases, phosphatases, motor proteins, mediate vesicular fission and fusion events, direct motor-driven vesicular traffic and can even activate other Rab

GTPases through Rab conversion[147]. An interesting feature of Rab GTPases is their distinct intracellular localization patterns. For example, Rab5 is found only in early endosomes and early phagosomes but not in the late endo/phagosome[148]. Analogous to the sequence of maturation of the endolysosomal system, phagosomal maturation consists of the following stages:

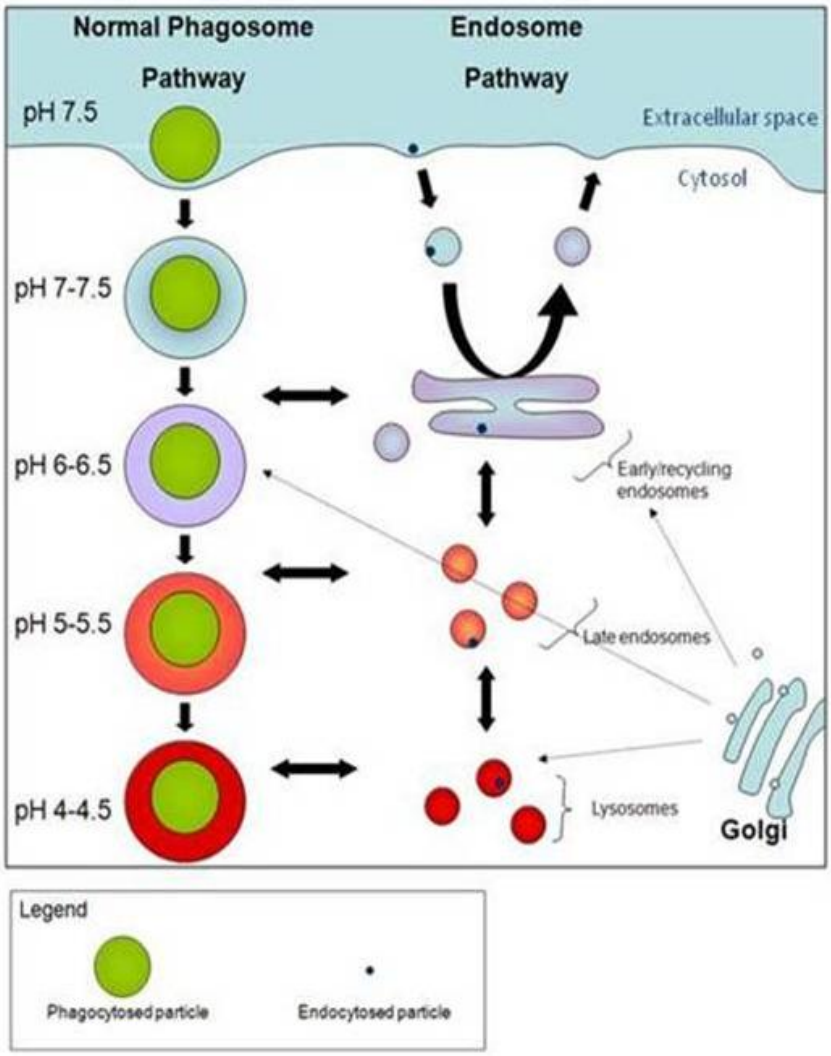

Figure 1.1: A simplified cartoon illustrating phagosomal maturation in relation to the endo-lysosomal network.

Figure courtesy of Dr. Robin Yates

The early phagosome:

Newly formed phagosomes tend to fuse with early endosomes and not late endosomes or lysosomes[142,149]. The early phagosomal lumen resembles that of early endosomes and is mildly acidic with a pH of 6-6.5, and poorly hydrolytic. Rab5, recruited to early phagosome, promotes fusion of the phagosome with the early endosome. *In vitro*, constitutive expression of an active GTP-locked mutant Rab5 has been reported to lead to the formation of enlarged phagosomes[150]. Disruption of Rab5 function on the other hand can arrest maturation of the phagosome[151]. The early phagosome also contains other markers of the early endosome such as early endosomal antigen 1 (EEA1), and transferrin receptors[148]. EEA1 is believed to play an active role in phagosome maturation by tethering early phagosomes to incoming early endocytic vesicles. Also,EEA1 interacts with Rab5 and SNARE proteins which are required for membrane fusion[152]. EEA1 is believed to be recruited by Rab5[153]. Rab5 also recruits other effector molecules to the early phagosome such as Rabaptin, Rabankyrin, p150-Vps34 complex, Mon1a/b and SNARE proteins[154].

The late phagosome:

The early phagosome matures into the late phagosome which is characterized by a more acidic pH (5.5 -6), higher hydrolytic activities, and expression of lysosome-associated membrane proteins (LAMPs)[154]. There is a transition of Rab5 to Rab7[148]. The exact mechanism of conversion of Rab5 to Rab7 is yet to be elucidated in mammalian phagocytes; however, in yeast, the transition is mediated by the class C core vacuole/endosome tethering (CORVET) complex and the homotypic fusion and protein sorting (HOPS) complex[155,156]. The late

phagosome also contains lysobiphosphatidic acid (LBPA), a unique lipid found in multivesicular bodies.

Phagolysosome:

The phagolysosome is the terminal stage of the maturation of the phagosome and is characterized by a highly acidic lumen (ph 4.5-5) and high hydrolytic and microbicidal characteristics[154]. The fusion of late phagosomes with lysosomes occurs in a Rab7-dependent manner[157]. Rab7 recruitment to the phagosomes has been reported to be essential for its fusion with late endosomes and/or lysosomes[157] The phagolysosome differs from the late lysosome in having a dearth of LBPA or PI(3)P enriched internal membranes[146]. They also contain higher levels of active cathepsins[154].

1.6: Microbicidal effectors of the phagolysosome:

Acidic pH:

The phagolysosomal lumen is acidic, with a pH of 4.5-5, while the nascent phagosome is mostly neutral with a pH of around 7.5. This decrease in pH is essential for the maturation of the phagosome as inhibition of acidification actually inhibits phagosome-lysosome fusion[158]. Vacuolar ATPases (vATPases) play a key role in the acidification process by translocating protons into the phagosome across the phagosomal membrane[158,159]. Inhibitors of the vATPases such as concanamycin A (conA) completely prevent acidification of the phagosome[160]. The acidic pH facilitates ingested target degradation, helps in impairing metabolic pathways of the microorganisms, and is also essential for activation of some of the acquired lysosomal

hydrolytic enzymes[161].

Generation of ROS:

ROS have direct cytotoxic and microbicidal effects. Superoxide anion is produced by the activities of NADPH oxidase by transferring electrons from NADPH to an oxygen molecule[162]. Superoxide anion can be converted to various ROS. For example, in the presence of superoxide dismutase, superoxide anion combines with water to form hydrogen peroxide. Hydrogen peroxide may act upon different chemical species to generate hydroxyl radicals and hypochlorous acid in polymorphonuclear leukocytes[163]. Superoxide can also combine with nitric oxide intermediates to form reactive nitrogen species, a reaction facilitated inside the phagosome by the enzyme inducible nitrous oxide synthase 2 (iNOS)[164]. Some of the ROS such as hydrogen peroxide are membrane permeable and leak out of the phagosome. In addition to reactive oxygen species, reactive nitrogen intermediates generated in the mature phagosome also contributes to the phagosomal respiratory burst and bacterial killing[165].

Presence of hydrolytic enzymes and antimicrobial products:

The mature phagosome possesses an arsenal of hydrolytic enzymes including lipases, proteases, glycosidases, etc. Their combined actions lead to the degradation of the engulfed matter[166]. The proteases play a crucial role in either completely digesting foreign proteins so that they can be recycled, or in processing them into peptides of optimal size so that they can be presented in complex with MHC class II molecules to CD4+ T cells[167]. Where and how these proteases cut determine the fate of the peptides and the immune response generated[168]. Cathepsins are a major group of lysosomal proteases found in the mature phagosome that play

an active role in antigen processing and presentation[169]. The mature phagosome also contains antimicrobial peptides such as defensins, which mediate broad spectrum bacterial killing[170]. There is also a general lack of nutrients inside the phagosome which offers a very unfavorable environment for microbial survival[161].

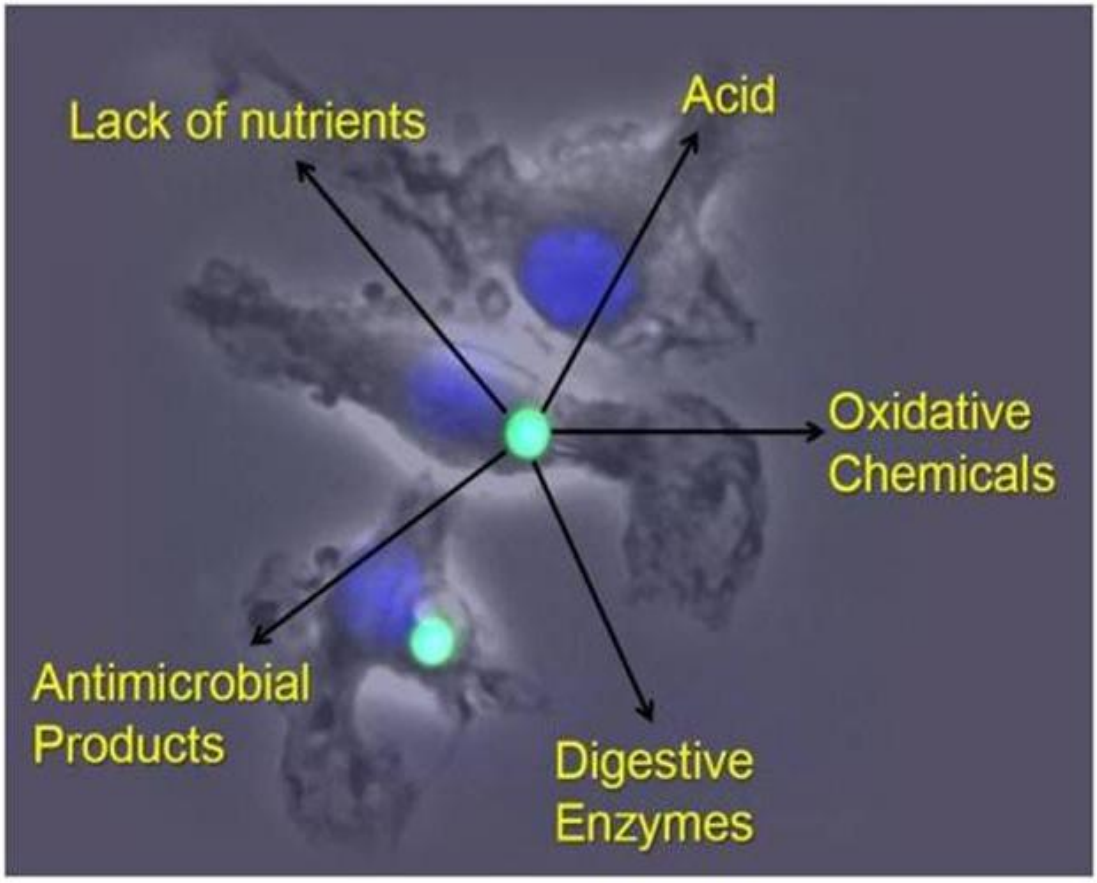

Figure 1.2: Microenvironment in the mature phagosome

Figure courtesy of Dr. Robin Yates

1.7: Porcine Reproductive and Respiratory Syndrome Virus (PRRSV):

Porcine Reproductive and Respiratory Syndrome (PRRS) is one of the major economically devastating diseases of the swine industry. It is prevalent in all major swine producing countries across the globe. According to estimates in 2005, the disease causes a loss of around $560 million per year to the swine industry in the United States alone[171]. The clinical symptoms of the disease were first reported in United States in late 1980s and a year later from different parts of Europe. The etiological agent, now known as the Porcine Reproductive and Respiratory Syndrome Virus (PRRSV) was first isolated and described in 1991 – fulfilling the requirements of Koch's postulates by Wensvoort *et al.* in the Netherlands. The virus was isolated using porcine alveolar macrophages and was designated as the Leystad Virus[172]. A year later, a different strain of the virus, VR2332, was isolated from swine herds in the United States, using a continuous cell line (CL2621)[173]. In 2006, pandemic outbreaks of the disease were reported from different parts of China. The strain was identified to be a highly virulent mutant of the North American genotype of the virus[174,175]. The same mutant was reported in American swine herds in 2007 [176]. Currently, two distinct genotypes of the virus exist – the European isolate or type I genotype represented by the Leystad Virus as the prototype strain, and the North American isolate or type II genotype, represented by VR2332. These two genotypes share about 60% DNA sequence identity[177]. Genomic sequence analyses indicate that the two strains diverged prior to the appearance of the disease on farms, suggesting that the virus has existed for far longer than the observed clinical disease outbreaks[178].

The PRRSV virion is an enveloped, positive-sense single-stranded RNA virus belonging to

the *Arteriviridae* family, and is grouped with the *Coronaviridae* and *Roniviridae* in the order *Nidovirales*[179,180]. Other viruses belonging to *Arteriviridae* include the equine arteritis virus (EAV), lactate dehydrogenase-elevating virus (LDH) and simian hemorrhagic fever virus (SHFV) – all of which are monocyte/macrophage-tropic and cause persistent infections. The host range of arteriviruses is restricted to animals: EAV infects horses and donkeys, LDV infects mice and SHFV infects different species of Asian and African monkeys[180]. Other than pigs, PRRSV is found to infect some avian species[181].

RNA viruses have a high mutation rate compared to DNA viruses primarily due to errors introduced during genome replication by the error-prone RNA-dependent RNA polymerase[182]. In Poliovirus, the positive-sense ss-RNA genome is replicated by RNA-dependent RNA polymerase having an error rate of 10^{-3} to 10^{-4}/bp[183]. In contrast, DNA polymerase in bacterial or mammalian system exhibits much higher fidelity and has an error rate of 10^{-9} to 10^{-11}/bp[184]. RNA genomes are also more susceptible to environmental damaging agents such as UV radiation, alkylating agents, modifying enzymes of the host immune system, *etc*. The low fidelity of RNA-dependent RNA polymerase allows viral genomes the flexibility to form quasi-species under environmental stress and have a high mutation rate to adapt to the environment[185]. Hence, it is not surprising that there exists so much genetic diversity among the different field isolates of PRRSV[186]. The PRRSV isolates differ in not only genome sequence, but also in antigenic properties and characteristics of the plaques formed *in vitro*[187,188].

1.7.1: Clinical symptoms:

Despite differences in genome sequences and antigenic properties, both the European and North American strains of the virus cause identical clinical syndromes; however, virulence of different field isolates of PRRSV may differ. PRRSV causes respiratory infections in both growing and adult pigs, resulting in porcine respiratory disease complex (PRDC). In sows, PRRSV causes reproductive failure including premature farrowing, and stillborn or mummified piglets[189]. Other clinical symptoms include persistent high fever, anorexia, red body discolorations, blue ears, and hyperpnea and dyspnea. Studies from infected animals have detected virus in oral/pharyngeal fluids, blood, feces, urine, and semen[190,191]. The virus can be transmitted from infected to uninfected animals through direct or indirect contact through airborne or venereal routes. Inanimate fomites can also transmit the disease[192]. Virus may persist and replicate in the host for long periods after the initial infection. In an experimentally infected model, the virus has been detected 92 days post infection in semen samples[193]. In another study, the virus has been isolated from oropharygeal samples in experimentally infected pigs 157 days post infection[194]. The mechanism of persistence of the virus in the host animal is still unclear. The degree of persistence of the virus is found to vary between different studies and with different strains of the virus[195]. Eventually there is a decline in the replication rates of the virus and the virus gets cleared[195].

1.8: PRRSV genome organization and structural proteins:

The PRRSV virion is 50-65 nm in diameter. PRRSV has a central isometric nucleocapsid

30-35 nm in diameter, which consists of the positive single-stranded RNA genome and the nucleocapsid (N)protein. The nucleocapsid is surrounded by a lipid bilayer envelope[196]. The genome of the virus is approximately 15 kb, encoding at least nine different overlapping open reading frames (ORFs) – ORF1a, ORF1b, ORF2a, ORF2b, ORF3, ORF4, ORF5, ORF6 and ORF7, which are flanked by 5' and 3' untranslated regions (5' and 3'UTR) [196]. The structural organization of the sub-genomic RNAs in the genome resembles that of coronaviruses[179]. ORF1a and 1b comprise about 80% of the genome. The polypeptide generated from ORF1a and ORF1b is cleaved into smaller products and gives rise to at least twelve non-structural proteins of the virion, which function as the viral RNA replicase complex[197]. The structural proteins of the virion are encoded by ORF2 to ORF7. ORF2, ORF3, ORF4, and ORF5 encode the N-glycosylated structural proteins GP2, GP3, GP4, and GP5, respectively[198]. ORF6 encodes the membrane protein M. The N protein is encoded by ORF7[199]. The small envelope protein E is expressed from the overlapping region of ORF1 and ORF2. N, M and E are the non-glycosylated structural proteins; N, M and GP5 are the main structural proteins[200]. The M protein and GP5 are known to form heterodimers through disulfide linkages. ORF5 has the highest variability among the different PRRSV isolates and is often used for phylogenetic analyses. ORF 7 is well conserved among the two genotypes of the virus. Detection of the virus for diagnostic purposes by polymerase chain reaction (PCR) regularly uses primers against ORF7[201].

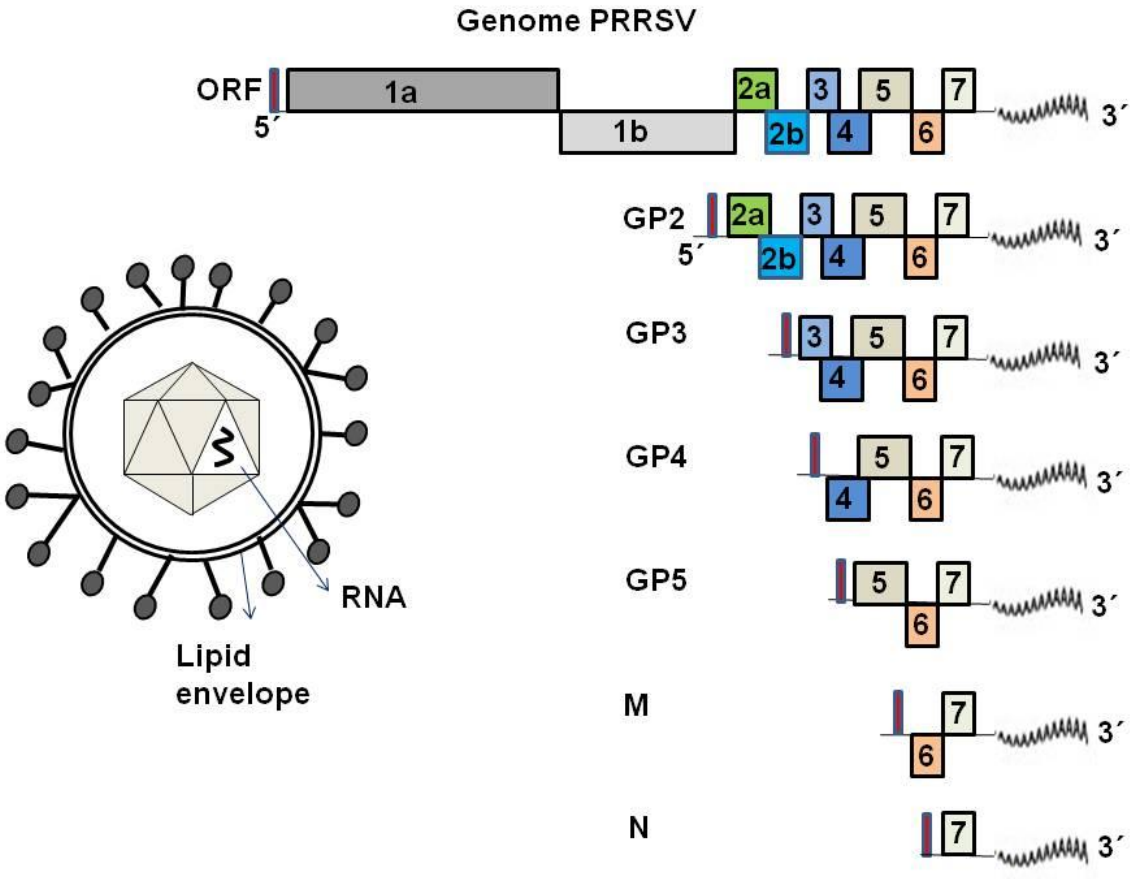

Figure 1.3: PRRSV genome structure adapted from [192]

1.9: PRRSV cell tropism:

During the course of infection, the virus invades and persists in organs like lungs, placenta, and various lymphoid organs including tonsils, Peyer's patches, thymus, spleen, and kidneys of the host[202,203]. The virus exhibits a narrow tropism and preferentially infects and replicates in well-differentiated cells of the monocyte/macrophage lineage[204] including porcine alveolar macrophages (PAM), pulmonary intravascular macrophages[205], subsets of macrophages in the lymph nodes, spleen, Peyer's patches, hepatic sinusoids, renal medullary interstitium[206,207], and intravascular macrophages of the placenta and umbilical cord. Circulating monocytes in the blood and bone marrow cells are resistant to PRRSV infection[202]. In experimentally-infected animals, PRRSV RNA and nucleocapsid protein have been isolatedfrom cells other than macrophages, including testicular germ cells, bronchiolar epithelial and arteriolar endothelial cells[208]. Current data however, do not clarify if the viral infection in these cells is productive or abortive. A productive infection leads to the production and release of a fully functional virion; abortive infection is characterized by initial stages of viral replication and production of viral transcription or translation products, but at some point viral replication is inhibited, resulting in the lack of release of fully functional virus particles.

In vitro, PRRSV can be cultured in porcine primary alveolar macrophages[172]. Primary lung dendritic cells have been found to be resistant to PRRSV infection[209] while bone marrow derived dendritic cells and freshly isolated blood monocytes and monocyte derived dendritic cells are permissive[210]. MARC 145 cells, derived as a homogeneous population of cell clones

from the African green monkey kidney epithelial cell line MA-104, is highly permissive to PRRSV infection and replication[211]. MARC-145 cells are extensively used for production of the virus. However, the mode of entry and infection of these cells by the virus is different from that of primary macrophages[212]. Since the virus needs to adapt to grow in this cell line, certain epitopes on the virus may be modified. CL2621, an established proprietary cell line of Boehringer Ingelheim Animal Health Inc., St Joseph, MO, USA, is also permissive to PRRSV replication[173]; however as a proprietary cell line, its availability to scientists is limited. Immortalized lung epithelial cells, the St-Jude porcine lung cell (SJPL) line, also support the infection and production of PRSSV[213]. Initially these cells were believed to have been derived from the porcine respiratory tract, but more recent genetic analyses and karyotyping studies suggest that these cells are more likely to be of simian origin[214]. Non-permissive cell lines, upon transfection with viral RNA, have been shown to support viral replication, thereby suggesting that the narrow cell tropism of PRRSV can be attributed to the presence or absence of cell surface receptors or other proteins that are required for virus entry[215]. Sialoadhesin (CD169), CD163 are the main molecules specific to monocyte/macrophage lineage that have so far been identified to mediate PRRSV entry into the host cell and in having a potential role in making non-permissive cell lines susceptible to PRRSV propagation[1]. Genetically modified cell lines permissive to PRRSV replication have been constructed such as immortalized PAM cells expressing CD163[216], porcine, feline, and baby hamster kidney cells expressing CD163[217], and BHK21 cells expressing CD151[218]. Co-expression of recombinant sialoadhesin and CD163 in non-permissive cell lines such as PK15, CHOK1 and BHK21 can result in the production of a higher

viral titre than expression of CD163 alone[219].

1.10: Entry of PRRSV into the host cell: PRRSV receptors

PRRSV enters the host cell through receptor mediated endocytosis:

PRRSV, like other arteriviruses, enters the host cell through clathrin-mediated endocytosis[220]. Studies have reported co-localization of PRRSV with clathrin-coated vesicles in porcine alveolar macrophages and in MARC145 cells[220,221]. Treatment of cells with endo/phagocytosis inhibitors such as cytochalasin or phenylarsine oxide can successfully block the entry of the virus[221]. Moreover, synthesis of viral RNA or production of infectious virus particles can be inhibited by treatment of the cells with inhibitors of endosomal acidification, suggesting PRRSV requires a low pH for entry[221]. In porcine alveolar macrophages, PRRSV co-localizes with early endosome markers (EEA1), in traces with CI-M6P which is an early to late endosome marker, but not with lysosomal marker Lamp1[222]. Endocytosis equips the entering virus with a number of advantages. Transportation in the endocytic vesicles helps the virus make its way through the overcrowded cytoplasmic matrix and especially the actin-dense cortical cytoskeleton which have been reported to provide hindrance to viral infection[223]. The virus can steal into the cell, minimizing the time spent on the cell membrane thereby avoiding or delaying detection by immune surveillance of the host. Also, minimal damage is caused to the host cell, thereby leaving the least possible cues for triggering immune responses of the host[224].

Receptors for PRRSV entry:

PRRSV entry into the host cell is mediated by its interaction with heparan sulfate, sialoadhesin and CD163[1]. CD151is also believed to play a role[218]. Heparan sulfate on host cell surface serves as a non-specific attachment factor for PRRSV, mediating its entry in its natural host cells as well as in cell lines such as MARC 145[225,226]. Sialoadhesin is a macrophage-restricted type I trans-membrane glycoprotein, expressed by tissue resident macrophages[227,228]. Sialoadhesin on the macrophage cell surface binds to sialic acids on the GP_5/M complex of PRRSV envelope and serves as an attachment and internalization factor[229]. In porcine alveolar macrophages, PRRSV has been reported to colocalize with sialoadhesin on the plasma membrane as well as just below it[230]. Sialoadhesin is not expressed in MARC 145 cells. In these cells, PRRSV binds to simian vimentin which serves a similar function[212]. Non-permissive cell lines expressing recombinant heparan sulfate and sialoadhesin have been found to internalize PRRSV but this did not result in a productive infection, suggesting the presence of other entry mediators[230]. CD163 was identified as a receptor for PRRSV in a functional screen of a cDNA expression library that conferred susceptibility to PRRSV infection when transfected into cells otherwise non-permissive to PRRSV[217]. CD163 binds to the structural proteins GP2 and GP4 of PRRSV envelope and facilitates its entry into the cell[231]. CD163 also play a role in uncoating and escape of the virus[219]. CD163 belongs to the scavenger receptor cysteine-rich (SRCR) superfamily and is best studied for its function of clearing hemoglobin-haptoglobin complexes from blood [232,233]. Other than PRRSV, African swine fever virus is also known to use CD163 for entering host cells[234]. CD163 is expressed on monocytes and macrophages, particularly in

differentiated tissue macrophages such as Kupffer cells, alveolar and interstitial macrophages in the lung, red pulp macrophages in the spleen, etc[235]. MARC 145 cells, although kidney epithelial cells, unexpectedly express CD163[217]. CD151 is a transmembrane glycoprotein belonging to the tetraspanin superfamily and is marked by the presence of four hydrophobic transmembrane domains[218]. It was identified as an entry mediator for PRRSV in a functional screen of a cDNA expression library constructed from MARC145 mRNA that conferred permissivity to PRRSV in otherwise non-permissive BHK21 cells. CD151 has been reported to bind to the 3'UTR of PRRSV[218]. RNA viruses have often been reported to use the secondary structures of their 5'UTR and 3'UTR to bind to host proteins to facilitate important viral replication mechanisms such as replication and transcription of viral RNA or transport of the viral genome[236,237]

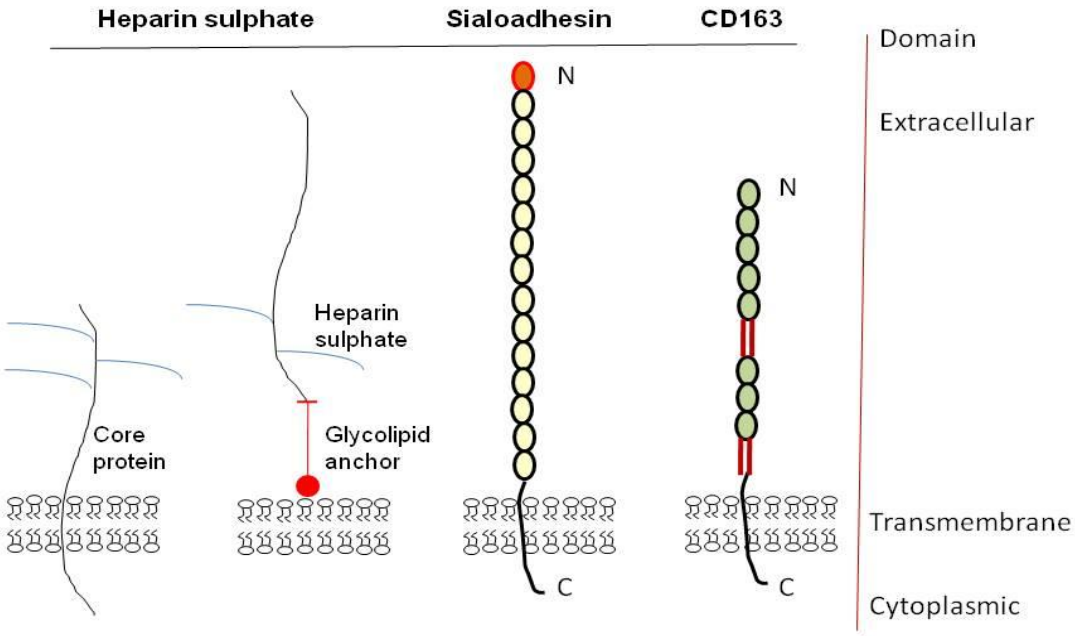

Figure 1.4: Entry mediators for PRRSV –diagram adapted from[1]

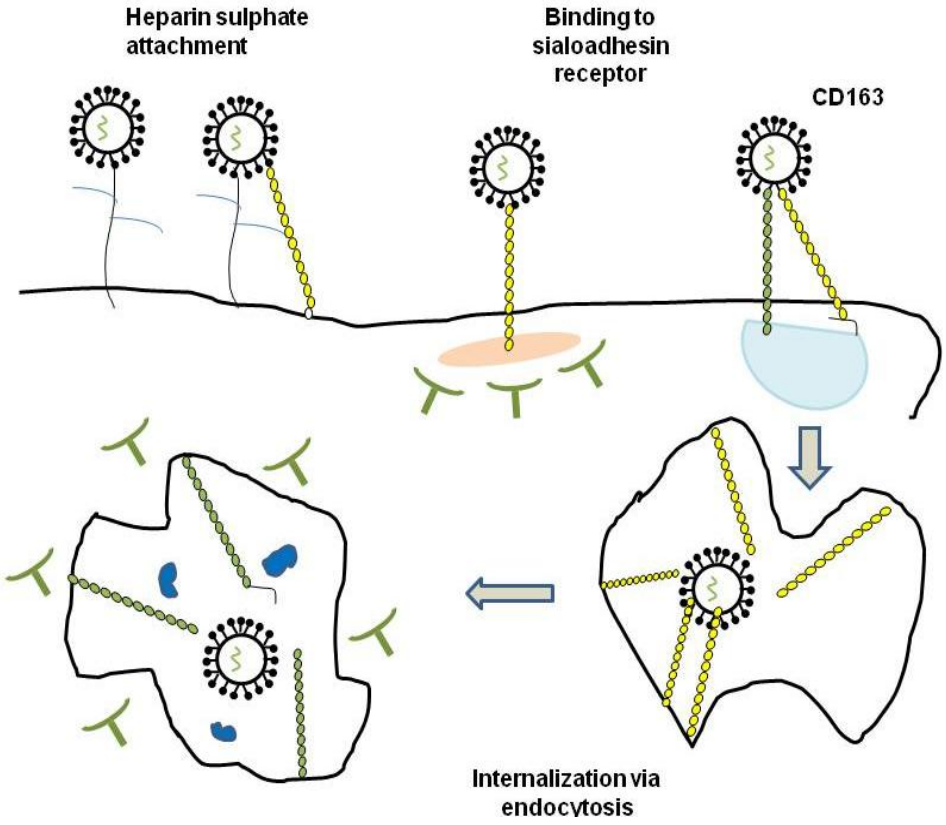

Figure 1.5: PRRSV internalization –adapted from [1]

1.11: Immune responses of the host animal to PRRSV:

PRRSV can modulate the host immune response in multiple ways. Infection with PRRSV leads to an overall state of immune-suppression in the host animal making the animal more susceptible to secondary infections. Susceptibility to secondary infections has been observed in farm animals sporadically infected with PRRSV as well as in experimental setups of PRRSV infection under in vitro or in vivo conditions[238,239]. Pneumonia, arthritis, eye infections, and meningitis have been commonly observed in animals with PRRSV infections[239,240]. In various field studies, infectious micro-organisms such as *Actinobacillus pleuropneumonia, Mycoplasma hyopneumoniae, Haemophilus parasuis, Actinomyces pyogenes, Streptococcus suis,* and swine influenza have been isolated from PRRSV-infected animals[238]. *Salmonella cholerasuis* infection also leads to respiratory disease in swine herds[241]. Clinical and experimental data suggest that *Salmonella cholerasuis* and PRRSV act in a synergistic fashion[242]. PRRSV-infected herds are more susceptible to salmonellosis and animals having salmonellosis are more likely to develop the respiratory symptoms of PRRS[242,243]. *In utero* infection of swine with PRRSV under laboratory conditions makes the host animals more susceptible to developing meningitis from co-infection from *Streptococcus suis*[244]. *In vitro* studies show that alveolar macrophages from pigs, when infected with PRRSV, are comparatively inefficient in killing pathogens like *Salmonella spp., Haemophilus parasuis, Staphylococcus aureus,* and *Candida albicans*[245-248]*.* However, results may be inconsistent depending on the pathogen used or the stage of infection. A deficiency in production of a respiratory burst has been suggested as a possible mechanism of susceptibility to secondary infections[248]. However, these studies are limited to measuring extracellular

reactive oxygen species using chemiluminescent methods. To date, the oxidative burst *inside* the phagosome in infected cells has not been compared to that in uninfected cells.

PRRSV can modulate cytokine production in the infected host. Typically in a virus infection, type I interferon production is induced as a host-defense strategy[249]. Type I interferons can stimulate a range of anti-viral responses in the host including induction of innate and adaptive immune responses[249]. PRRSV suppresses the first line of anti-viral defense mechanisms in the host by interfering with the interferon signaling pathway and inhibiting the production of type I interferons[250,251]. In contrast to other respiratory virus infection such as swine influenza virus, the levels of Interferon-α detected in pig lungs on PRRSV infection is very low[251]. Studies show that in the presence of type I interferons, PRRSV propagation in primary porcine alveolar macrophages (*in vitro*) and in the lungs of infected animals (*in vivo*) decreases significantly[252]. PRRSV infection can stimulate the production of IL10 in peripheral blood monocytes *in vitro*[253]. In infected animals higher levels of IL 10 can be detected in broncho-alveolar lavage samples[254]. IL 6 production is also induced in PRRSV infection[255]. Animals recovering from PRRSV infection have been reported to produce pro-inflammatory cytokines such as IFN- γ and IL2[256].

PRRSV infected animals can develop a rapid humoral immune response to the virus. In infected animals, circulating antibodies against PRRSV can be detected as early as 5-7 days post infection[257]. The early antibodies produced are, however, not neutralizing antibodies and do not correlate with protection. On the contrary, the early non-neutralizing antibodies produced can enhance virus replication in alveolar macrophages through antibody-dependent

enhancement[258]. Appearance of neutralizing antibodies in circulation is usually delayed and is detected around 28 days post-infection[259]. Neutralizing antibodies are mainly targeted against epitope B located in the N-terminal ectodomain of the GP5 protein of PRRSV[259]. GP4 and M proteins may also contain neutralization epitopes[260]. Lymphocyte proliferation has been detected in infected animals but occurs at least 4 weeks post infection, concurrently with the appearance of neutralising antibodies[261].

1.12: Hypothesis and Specific Aims:

PRRSV-infected animals are highly susceptible to secondary infections[241-243]. PRRSV primarily infects tissue macrophages which, under normal physiological conditions, are instrumental in clearing invading pathogens[204,206,207]. In the last two decades, studies have focused on investigating different aspects of PRRSV biology including viral pathogenesis, viral genomics and proteomics, host-virus interactions and vaccine development against the virus. However, nothing is known about how the phagosomal microenvironment may be altered in PRRSV-infected macrophages and how such alterations may dampen the microbicidal and degradative properties of the macrophage phagosome.

1.12.1: HYPOTHESIS:

The hypothesis of this thesis is that PRRSV infection changes the phagosomal microenvironment and phagosomal function in porcine macrophages and this in turn affects the function of the macrophage.

To address this hypothesis, this thesis has 3 specific aims.

1.12.2: SPECIFIC AIM I: To establish an in vitro system for studying PRRSV infection.

The field of PRRSV biology suffers from the lack of existence of a good *in vitro* system that can be used to study various aspects of PRRSV biology using a methodical reductionist approach. This thesis aims at establishing an *in vitro* system to study PRRSV infection. Conceptually this aim can be divided into 3 steps: (Figure 1a.1)

a) In vitro differentiation of porcine bone marrow cells into bone marrow derived macrophages (pBMMØ), followed by their microscopic and functional characterization.

b) Growing PRRSV (NVSL 97-7895) in MARC145 cells followed by quantitation of virus by titration.

c) Using virus from step (b), infecting pBMMØ and assessing if the infection is productive.

1.12.3: SPECIFIC AIM II: To study the effects of PRRSV infection in modulating the phagosomal lumenal properties in porcine bone marrow derived macrophages.

Using the established *in vitro* system, this study aims to investigate how PRRSV infection brings about a change in the phagosomal lumenal microenvironment and affects phagosome function in pBMMØ (Figure 1a.2). Phagocytic index, phagosomal proteolysis, phagosomal acidification, and phagosomal ROS production will be compared between pBMMØ infected *in vitro* with the virulent type II PRRSV strain NVSL 97-7895 and uninfected cells.

1.12.4: SPECIFIC AIM III: To characterize the functional alterations in the phagosomal lumenal microenvironment in porcine alveolar macrophages isolated from PRRSV-infected pregnant gilts.

This study also investigates how phagosomal microenvironment changes in porcine alveolar macrophages (PAM) isolated from PRRSV-infected pregnant gilts and uninfected animals (Figure 1a.3). This will include isolating PAM from bronchoalveolar lavage samples obtained from PRRSV-infected pregnant gilts and uninfected animals and comparing phagosome lumenal

properties such as proteolysis, phagocytic index and production of oxidative burst between them.

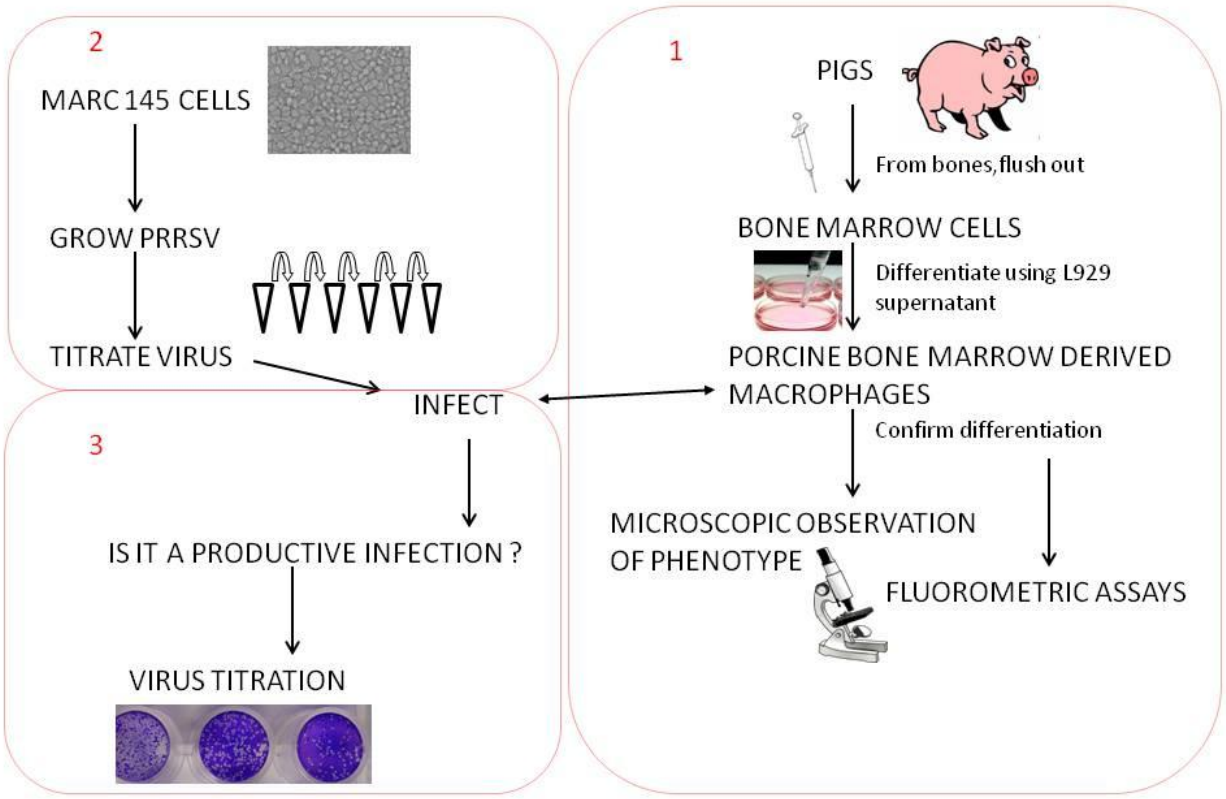

Figure 1a.1: Workflow for specific aim 1: The first specific aim of this thesis is to establish an *in vitro* system to study PRRSV infection. This will include isolation of porcine bone marrow cells and differentiating them in culture in presence of L929 cell supernatant into pBMMØ. To confirm differentiation, the cells will be examined microscopically and assessed for phagosomal functions using fluorometric assays. The PRRSV isolate NVSL 97-7895 will be grown and titrated on MARC 145 cells and will be subsequently used to infect pBMMØ. To determine if infection of pBMMØ is productive, culture supernatant from infected cells will be collected and titrated on MARC145 cells.

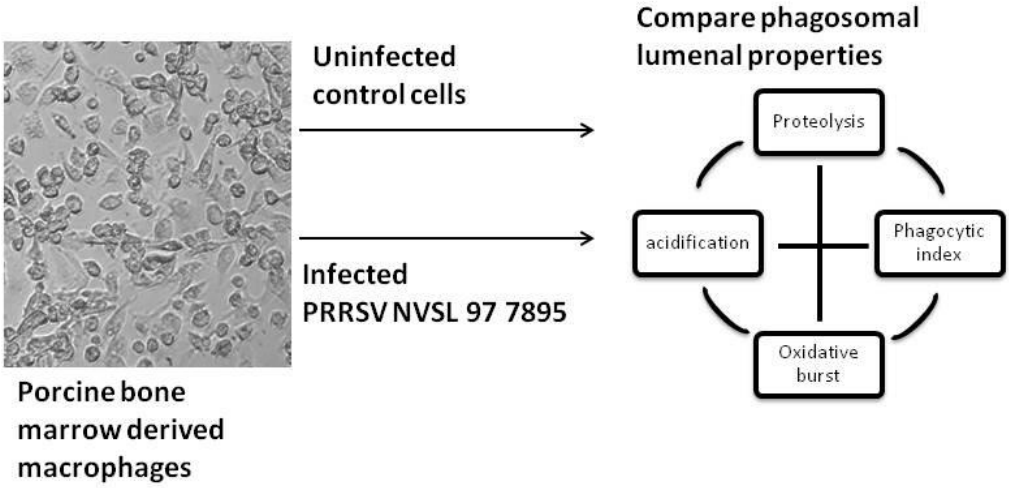

Figure 1a.2: Workflow for specific aim 2: The established *in vitro* system for PRRSV infection will be used to investigate how the phagosomal lumenal microenvironment changes on PRRSV infection in porcine macrophages. Phagosomal lumenal properties such as proteolysis, phagocytic index, acidification and oxidative burst will be compared. Since phagosomal chemistries are not independent functional parameters, but are rather interdependent on each other, it will also be investigated if one of the parameters is changing as a consequence of a change in another.

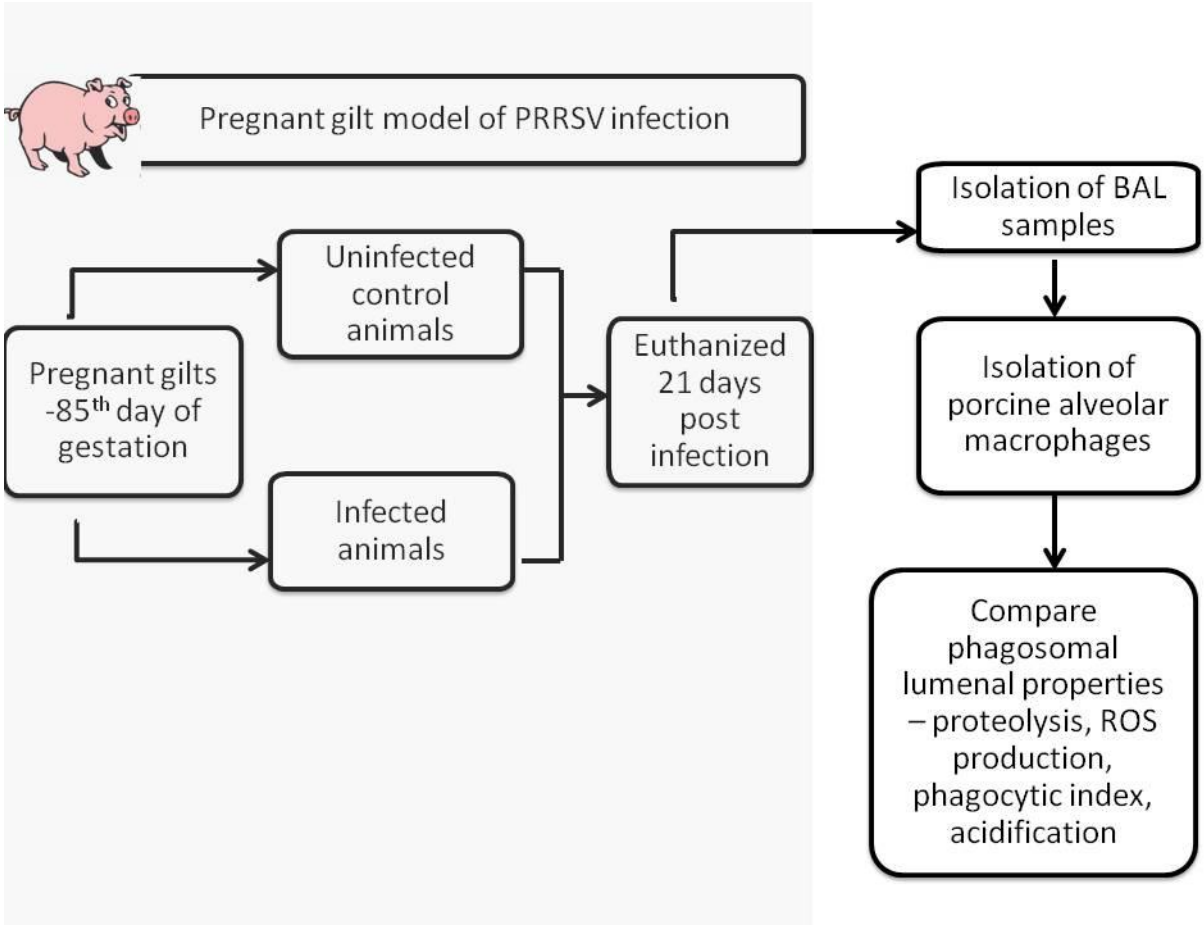

Figure 1a.3: Workflow for specific aim 3: Phagosomal lumenal properties will be compared between porcine alveolar macrophages isolated broncho-alveolar samples of PRRSV-infected pregnant gilts and uninfected animals. The pregnant gilt model of PRRSV infection will be used. Pregnant gilts will be infected with PRRSV NVSL 97-7895 on gestation day 85. 21 days post-infection, the infected animals and uninfected control animals will be humanely euthanized. Alveolar macrophages will be isolated from broncho-alveolar lavage samples collected from the infected and uninfected animals at necropsy. Phagosomal lumen properties such as proteolysis, oxidative burst, phagocytic index and acidification will be relatively assessed in the porcine alveolar macrophages isolated from infected and uninfected pregnant gilts.

CHAPTER 2: METHODS

2.1: Cell lines used:

2.1.1: MARC-145 cell line:

MARC-145 is an African green monkey (*Chlorocebus sabaeus*) kidney epithelial cell line derived from the MA-104 line as a homogeneous population of cells, highly permissive to PRRSV infection and replication[172,211]. MARC-145 cells were grown in tissue culture treated 75 cm^2 (T75) flasks (Greiner Bio-one) in MARC-145 growth media consisting of Dulbecco's Modified Eagle's Medium (DMEM) supplemented with 10% Fetal Calf Serum (FCS, Thermo Scientific), 2mM L-glutamine (Corning), 100 IU/mL penicillin and 100 µg/mL streptomycin (Corning). The cells were maintained at 37°C and 5% carbon dioxide (CO_2). Upon reaching confluency, the cells were detached from plates by treatment with prewarmed (37°C) trypsin–EDTA (ethylene diaminetetraacetic acid, Corning) for 5 minutes at 37°C, pipetted to disperse the monolayer, and seeded to fresh plates for subculturing at a ratio of 1:3. Growth medium was replenished once a week. For long term storage and future use, MARC-145 cells were trypsinized, washed in MARC-145 growth media, resuspended at a cell density of 3 x 10^7 cells /mL in freezing solution consisting of 90% FCS, 10% DMSO (dimethyl sulfoxide, Sigma) and stored at -150°C.

2.1.2: L929 cell line:

L929 is a mouse fibroblast cell line (ATCC CCL-1)[262]. The cells were grown in T75 flasks in D10 medium consisting of DMEM supplemented with 10% FCS, 2mM L-glutamine, 0.15% sodium bicarbonate (Corning), 100 IU/mL penicillin and 100 µg/mL streptomycin. The cells were maintained at 37°C and 5% CO_2. Upon reaching confluency, the cells were subcultured at a ratio of 1:4. For subculturing, the cells were incubated with ice-cold PBS for 10 minutes, detached by

scraping using a cell scraper (Greiner), pelleted down by centrifuging at 180 x g for 10 minutes at 4°C, resuspended in D10 growth medium and seeded in fresh T75 flasks at a ratio of 1:4. Growth medium was replenished once a week. For long term storage and future use, L929 cells were resuspended at a cell density of 3x10^{7} cells /ml in freezing solution and stored at-150°C.

2.2: Virus strain:

The porcine reproductive and respiratory syndrome virus (PRRSV) type II isolate NVSL 97-7895 (GenBank accession number AY545985.1) was used for all the studies. This particular isolate was originally obtained from a vaccinated swine herd that developed the infection in Iowa, USA and is one of the highly virulent PRRSV isolates[263] . The virus was provided as a kind gift by Dr. John Harding (University of Saskatchewan). Virus was divided into aliquots and stored frozen at -80°C. Before use, virus was thawed on ice.

2.3: Growing PRRSV isolate NVSL 97-7895 in MARC-145 cells:

The PRRSV isolate NVSL 97-7895 was grown and propagated in MARC-145 cells[211]. The virus was diluted in serum-free OptiMEM (SFM, Invitrogen) with no added supplements. MARC-145 cells grown to confluency in T75 flasks were trypisinized, resuspended in MARC-145 growth media at a density of 6 x 10^{5} cells/mL, and seeded on to 6-well dishes (Corning) at a concentration of 3 x 10^{5} cells/ well and were incubated overnight at 37°C and 5% CO_2 . The cells were grown to confluency and the growth medium replaced with SFM containing appropriate PRRSV NVSL 97-7895 dilutions. Infection was carried out at a multiplicity of infection (MOI) of

0.001. It was found that MARC-145 cells needed no adaptation to grow in SFM during virus infection and propagation. After infection, the cells were maintained at 37°C, 5% CO_2 and were carefully examined every day using light microscopy for the appearance of cytopathic effects (CPE). Four days post-infection, culture supernatant was collected (supernatant fraction) to obtain the secreted virus particles. To release intracellular viral particles, if any, cells were scraped up and subjected to 3 freeze-thaw cycles (freeze at -70°C for 30 minutes and thaw at room temperature). The titre of the virus was determined by plaque assay (see section 2.4 below), before further use[264].

2.4: Titration of virus by plaque assay:

PRRSV previously grown in pBMMØ or in MARC-145 cells was titrated using plaque assay on MARC-145 cells. MARC-145 cells, grown to confluency on tissue culture treated T75 flasks, were trypisinized and resuspended in MARC-145 growth media at a density of 6 x 10^5 cells /mL. The cells were seeded on to tissue culture-treated 12-well dishes (Corning) at a concentration of 1 x 10^5 cells/ well and were incubated overnight at 37°C and 5% CO_2 . Following overnight incubation, the MARC-145 cells grew to 90% confluency and were ready to be used for plaque titration. The virus was serially diluted in SFM. The dilutions were mixed by gentle vortexing to ensure proper mixing of the virus. Pipette tips were changed between dilutions. The growth medium on MARC-145 cells was removed; the cells were washed with PBS to remove any overgrown cell monolayers and infected with serially diluted virus. The infection for each virus dilution was carried out in triplicate. The following dilutions of the virus

were used for infection: 10^{-1}, 10^{-2}, 10^{-3}, 10^{-4}, 10^{-5} and 10^{-6}. 400 µl of inoculum was used per well. The cells were infected for one hour at 37°C and 5% CO_2. Sterile 2% agarose (Amresco) in water was quickly resuspended in equal volumes of plaquing medium (2X DMEM supplemented with 20%FCS, 4mM L-glutamine and 15% sodium bicarbonate) to obtain a final solution of 1% agarose in 1X DMEM/10% FCS, 2mM L-glutamine, 7.5% sodium bicarbonate. The plaquing medium was pre-equilibrated at room temperature and the motlen agarose at 56°C before mixing. Following the 1 hour infection, the inoculum was removed and the cells overlaid with 1% agarose/1X DMEM prepared as described above. Care was taken to ensure that the temperature of the overlaying agarose was in the range of 37°C to 42°C. Overlaying agarose if at higher temperature can kill the cells. The cells were incubated at 37°C, 5% CO_2 for 48 hours, after which the cells were fixed with 4% formalin (v/v), 0.9% NaCl (w/v) (formal saline) overnight at room temperature. The agarose plugs were then gently washed off under slowly running tap water. The cell monolayer was stained with 1-2 drops of crystal violet using a transfer pipette (VWR). The plaques showed up as clear zones against the dark violet background of cell monolayer. The number of plaques was manually counted from whichever dilution numbered between 10 to 100 plaques. To determine virus titre, PFU (plaque forming unit)/ml was calculated as number of plaques formed x dilution x volume factor (amount of inoculum)[264,265]. Figure 2.1 shows a schematic protocol for the plaque assay.

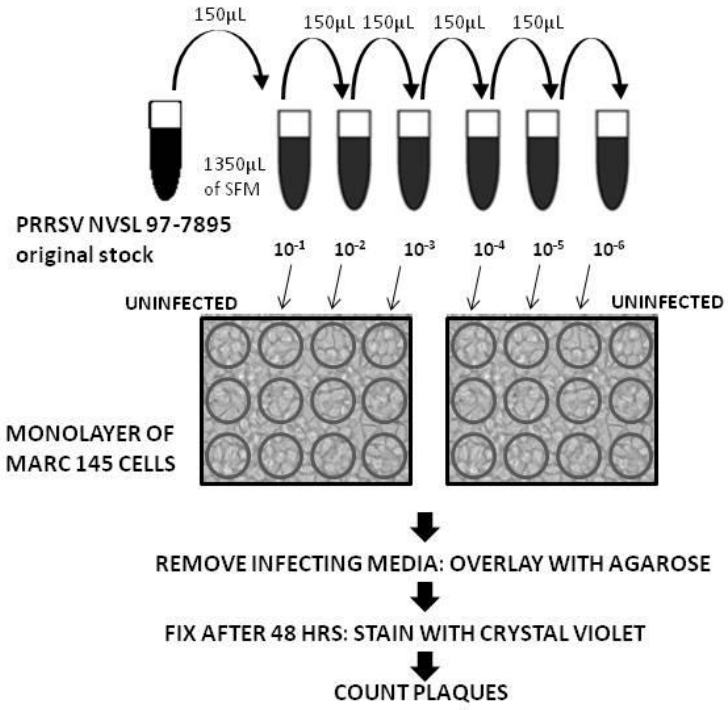

Figure 2.1: Schematic diagram for quantitation of PRRSV titre by plaque assay on MARC-145 cells.

2.5: Cultivation of L929 supernatant:

L929 cell supernatant was harvested as a source of murine macrophage colony stimulating factor (M-CSF or CSF1) [266]. L929 cells were grown in 25cm^2 (T25) and 75 cm^2 (T75) tissue culture flasks (Greiner Bio-one) for 3 days in 5% CO_2, 37^oC until they reached confluency. On day 4, cells were scraped, combined together and seeded in ten 150 cm^2 (T150) flasks (Greiner Bio-one) and grown to confluency. On Day 9, the cells were again scraped, combined together and seeded in 32 triple-layered tissue culture flasks (Nunc). Care was taken to seed equal amounts of initial cell inoculum into each layer of a triple layered flask using a sterile fine tip Pasteur pipette (VWR). Also, all the flasks were seeded with equal volume of initial inoculum to synchronize cell growth such that they become ready for harvest at the same time. The cells were grown to confluency. The cells were observed every day by light microscopy to monitor general cell health and detect contamination if any. The flasks were also monitored daily to ensure that the medium was evenly distributed between layers. Each triple-layer flask contained 96 mL medium. Just before the cells started to show appearance of granules and/or detach from the flask surface, the culture supernatant was harvested (batch A). This first harvest was usually done in 17- 19 days. The cells were replenished with fresh medium and allowed to grow for another 3-5 days. Just before the cells showed signs of starting to detach from the flask surface, the supernatant was harvested for the second and final time (batch B). The harvested supernatants were tested and optimized for their efficiency of differentiating mice bone marrow cells (C57Bl/6 mice purchased from Charles River Laboratories and maintained according to the guidelines set by University of Calgary animal use and care

committee) into bone marrow derived macrophages before use, using standard protocols[65,267]. L929 cell supernatant was stored at -70°C for future use. Figure 2.2 outlines the important timelines during cultivation of L929 supernatant.

2.6 : *In vitro* differentiation of porcine bone marrow cells into porcine bone marrow derived macrophages:

Mid-thoracic costal (rib) bones were aseptically collected (by our collaborators in the labs of Dr. Soren Boysen or Dr. John Tyberg at the University of Calgary) from freshly euthanized 6-8 weeks old pigs without any previous records of infections. We obtained and used the costal bones from our collaborators according to the regulations set by the protocol for secondary usage of animal parts by University of Calgary animal use and care committee. The outer surfaces of the bones were cleaned by removing any remnant flesh and were flame-sterilized by dipping in 100% ethanol and then burning off the ethanol by passing through a flame. Both ends of the bone were then trimmed with sterile shears and the bone marrow was flushed into a sterile 50 mL conical tube (BD Falcon) with PBS (Phosphate Buffer Saline – 137mM sodium chloride, 2.7 mM potassium chloride, 8.1 mM disodium hydrogen phosphate 1.47mM potassium dihydrogen phosphate) containing 1% heparin (Organon Canada Ltd). Heparin (100U/ml) was included to prevent clotting. A 20 mL syringe (BD Biosciences) fitted with an 18 gauge needle (BD Biosciences) was used to flush out the bone marrow. The cells were washed twice in PBS by centrifuging at 180 x g for 10 minutes at 4°C. Following the two washes, the cell pellet was vigorously resuspended in 10mL of BMMØ medium (DMEM

supplemented with 10% FCS, 2mM L-glutamine, 1 mM Na-pyruvate, 1% penicillin-streptomycin (100 units/mL) and 20% L929 conditioned culture supernatant, as a source of M-CSF). The resuspended cells were allowed to stand for 5 minutes at room temperature to let any contaminating flesh or debris to settle down to the bottom of the tube. The cells were pipetted up without disturbing the settled debris and plated on untreated sterile plastic Petri dishes (100 mm x 15 mm, Fisher Scientific). The cells were cultured in a total volume of 10 mL media. Otherwise, the bone marrow cells were frozen down for future use as described in section 2.7. The cells were maintained at 37°C, 7% CO_2. After 3 days, the cells were replenished with 10 mL of fresh pre-warmed (37°C) BMMØ medium. The cells differentiated into macrophages in 10 days (generation P_0). The cells were checked regularly by microscopy to monitor cell health and risk of contamination. To passage cells, the differentiated macrophages were incubated with ice cold PBS for 10 minutes at 4°C and then scraped from the plates and subcultured at a ratio of 1:2 (generation P_1). Figure 2.3 outlines the important steps in the differentiation of porcine bone marrow cells into macrophages.

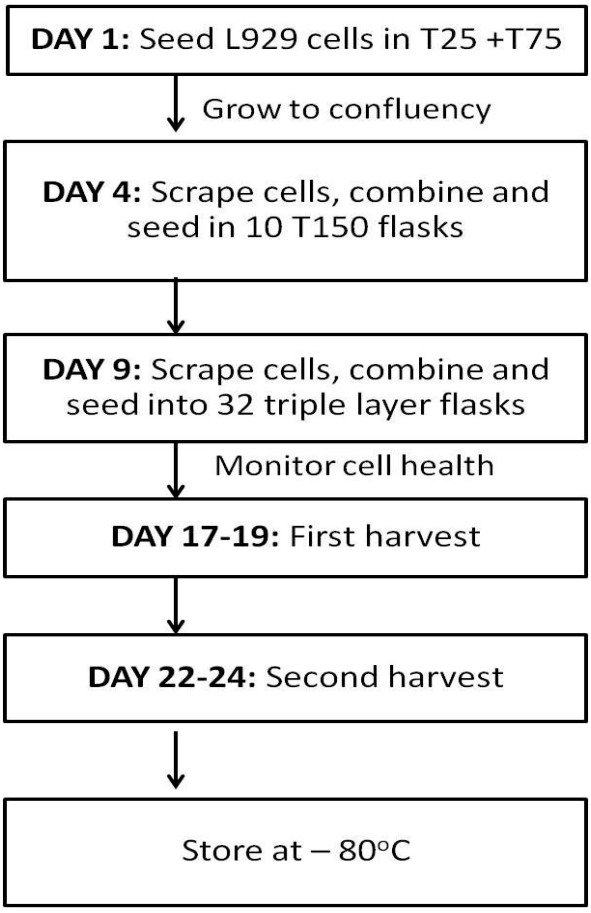

Figure 2.2: Important timelines in cultivation and harvest of L929 cell

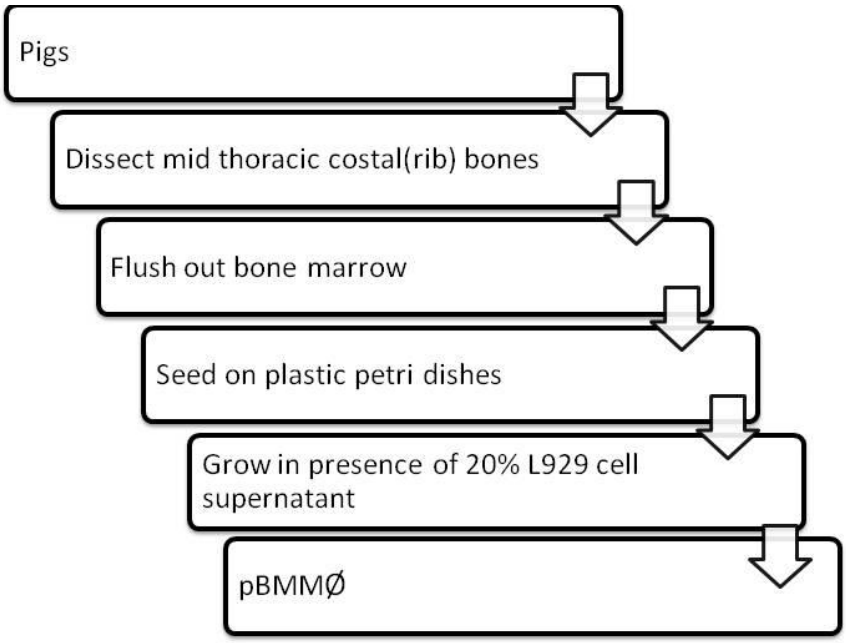

Figure 2.3: A simplified protocol highlighting the most important steps in differentiation of porcine bone marrow cells into macrophages.

2.7: Freezing and thawing of porcine bone marrow cells:

In order to cryopreserve the pBMMØs, the porcine bone marrow cells were centrifuged at 180 x g for 10 minutes. The pelleted cells were resuspended carefully in pre-chilled freezing solution and transferred to a pre-chilled cryo-vial (VWR). Cells were frozen overnight at -80°C and then transferred to liquid nitrogen or -150°C for long term storage. While thawing, the cells from liquid nitrogen were directly incubated in a 37°C water bath. Cells were warmed until all frozen liquid was nearly thawed. Using a pipette, the cells were aspirated and resuspended gently into 8 mL of DMEM and centrifuged at 180 x g for 5 minutes. The pellet was resuspended in BMMØ medium and seeded in untreated plastic Petri dishes (100 mm x 15 mm, Fisher Scientific).

2.8: Infection of pBMMØ:

Fully differentiated pBMMØ were grown to confluency in a 12-well plate (Corning) or a 96-well tissue culture treated assay plate (Greiner Bio-One µClear). PRRSV was diluted in OptiMEM. For infection, the growth medium of pBMMØ was replaced with virus diluted in OptiMEM. pBMMØ were infected at a MOI of 0.1. Following infection, the cells were incubated at 37°C, 5% CO_2 for 24 hours before performing the fluorometric assays. For virus propagation, pBMMØ were infected at a MOI of 0.001 with PRRSV isolate NVSL 97-7895 and incubated at 37°C, 5% CO_2 for 96 hours before harvesting the virus.

2.9: Maintenance and infection of pregnant gilts:

Pregnant gilt challenge model:

The pregnant gilt model of PRRSV infection exploited in this study was set up by our collaborators led by Dr. John Harding at the University of Saskatchewan. Studies were performed with F1 pregnant gilts selected from commercially breed herds, free from specific pathogens such as *Salmonella*, Porcine Circovirus 2 and PRRSV. Gilts confirmed pregnant were housed in Intervac L2 isolation rooms (University of Sasktachewan) in batches of 10, every second week. Pregnant gilts (n=120) were infected through the intranasal route with PRRSV isolate NVSL 97-7895 on gestation day 85. As a control, age-matched pregnant gilts (n=19) were sham inoculated on gestation day 85. 21 days post-infection, on the 105th day of gestation, the infected pregnant gilts and uninfected control animals were humanely euthanized. At necropsy, bronchoalveolar lavage (BAL) samples were prepared from the animals as follows: One lung was dissected from the euthanized animal, the trachea was cut open using a scalpel and 750 mL of PBS containing 250 µg/mL Amphotericin B was poured into the lung. The lung was massaged and BAL fluid was removed, centrifuged and resuspended in DMEM containing 10% FCS, 2mM L-glutamine and 0.1% penicillin-streptomycin (100 units/mL). Samples were then shipped by overnight courier to Calgary on ice packs. Alveolar macrophages were isolated from the BAL samples upon receipt the following morning as described in section 2.10.

2.10: Isolation of porcine alveolar macrophages (PAM) from BAL samples by density gradient centrifugation:

BAL samples are frequently used as a source of alveolar macrophages[93]. Under normal physiological conditions, BAL samples consist of >95% alveolar macrophages[93,268] . All steps of alveolar macrophage isolation were performed on ice or at 4°C. BAL samples from infected and uninfected animals were centrifuged at 180 x g for 10 minutes, the pellet washed with 10 mL of HBSS buffer (Hanks' Balanced Salt Solution – 5.33mM potassium chloride, 0.441 mM potassium dihydrogen phosphate, 4.17mM sodium bicarbonate, 137 mM sodium chloride, 0.338 mM sodium dihydrogen phosphate and 5.56 mM glucose, Sigma), and resuspended in 15 mL pre-chilled HBSS buffer. The cells were then very gently layered onto a 10 mL Ficoll-Hypaque 1077 (Sigma-Aldrich) gradient, without disturbing the interface, and centrifuged at 660 x g for 30 minutes at 4°C with the lowest acceleration and brake setting on the centrifuge. Macrophages/monocytes sedimented at the Ficoll-Hypaque/HBSS interface while the contaminating erythrocytes pelleted down to the bottom of the column[269]. The cells at the interface were transferred to a sterile 50mL conical centrifuge tube using sterile transfer pipettes (VWR). The volume was made up to 30 mL with HBSS to remove residual Ficoll-Hypaque solution; samples were then centrifuged at 180 x g for 10 minutes at 4°C. Erythrocytes were lysed by resuspension of cell pellet in 3 mL of hypotonic RBC lysis buffer (155 mM ammonium chloride, 0.1mM EDTA, 10mM potassium bicarbonate, pH 7.4) followed by a 5 minute incubation on ice. The tonicity of the solution was restored by diluting with 25 mL of PBS. The cells were then centrifuged at 180 x g for 10 minutes. The pellet was washed with 10

mL PBS and resuspended in 5 mL of DMEM supplemented with 10% FCS, 2mM L-glutamine, 1% penicillin-streptomycin (100units/mL), gentamycin (final concentration of 150 µg/mL). The gentamycin-containing media was removed after 15 minutes. The cells were washed and resuspended in DMEM supplemented with 10% FCS, 2mM L-glutamine, 1% penicillin-streptomycin Pen-Strep (100units/mL). A small aliquot of the cells was stained with 0.01% Trypan blue (EMD Chemicals) in PBS. The number of live cells, which did not take up the vital dye, was counted using a hemocytometer. The yield of viable cells in the BAL samples sent to us was approximately 3 x 10^7 cells. Approximately 10^7 cells were seeded in a 100 x 15 mm petri dish. Medium was replaced 8-12 hours after plating to eliminate dead cells or any other contaminating non-adherent cells isolated from the BAL, such that only adherent cells were used to carry out the phagosomal assays. Figure 2.4 represents the workflow for isolating PAM from BAL fluid.

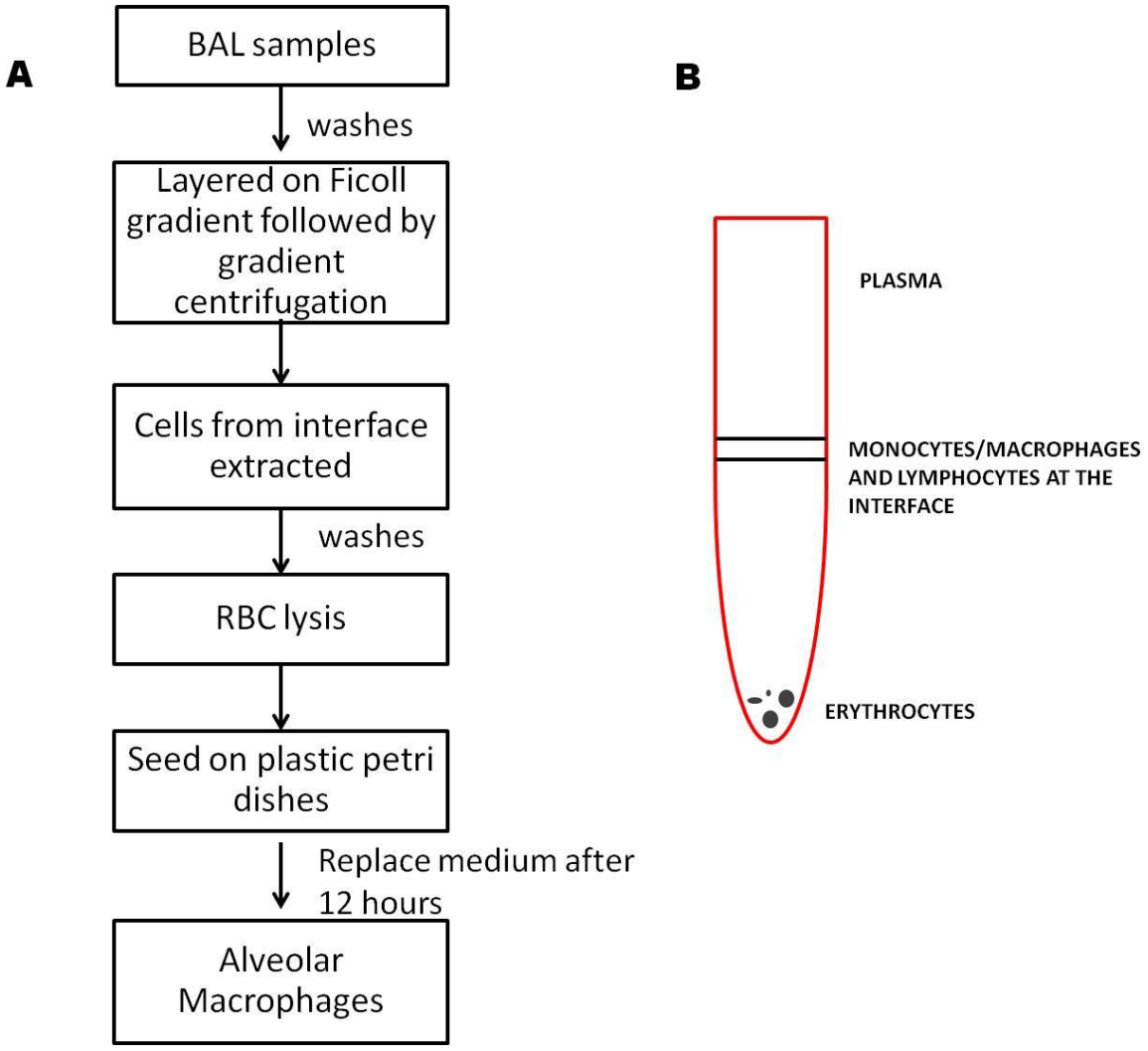

Figure 2.4: (A): Schematic representation of the most important steps in the isolation of alveolar macrophages from BAL samples. **(B):** BAL samples contaminated with blood after Ficoll-gradient centrifugation has cells of monocyte/macrophage lineage and other lymphocytes deposit at the interface. RBC settle down at the bottom of the gradient while the plasma and plasma proteins occupy the topmost part of the gradient.

2.11: Assays for studying phagosomal lumenal properties:

A bank of assays developed for use in murine BMMØ was used for studying phagosomal microenvironment. These assays rely on phagocytic uptake of different experimental particles. Typically the experimental particles consisted of 3 µm carboxylate-modified silica beads conjugated to a phagocytic receptor ligand, a calibration fluor and a reporter fluorophore. As the phagosome matures, the fluorescence intensity from the reporter fluorophore changes while the calibration fluor remains constant. A ratio of the fluorescence intensity from the reporter fluor to the fluorescence intensity of the calibration fluor over time gives a measure of the changes in the particular phagosomal maturation parameter being investigated. A ratiometric measurement approach reduces errors that may stem from uneven distribution of the fluorophores on the experimental particles or random noise generated in the imaging setup including bleaching, change in focus of the instrument, variations in excitation intensity, etc. These assays are designed in a flexible manner so that they can be adapted to multiple different technical platforms such as plate-readers, microscopes and flow cytometers according to the nature and aim of the assay[270-272].

2.11.1: Preparation of experimental particles:

2.11.1.1: Preparation of experimental particles for phagocytic index calculation:

50 mg of 3 µm carboxylate-modified silica beads (5% solution, Kisker Biotech) were washed twice in PBS by vortexing and briefly centrifuging using a tabletop centrifuge. The beads were resuspended in PBS containing freshly dissolved cyanamide (Sigma) at a concentration of

25mg/ml and rotated at room temperature for 15 minutes. The cyanamide acts as a heterobifunctional crosslinker. Excess cyanamide was removed by washing twice with borate buffer (0.1 M sodium borate in PBS pH 8). The beads were then resuspended in 500 µL of borate buffer with 0.1 mg human IgG (Sigma) and rotated at room temperature for at least 3 hours. This step was to add Fc receptor ligand to the beads to facilitate their opsonisation. The beads were then washed twice with borate buffer and resuspended in 200 µL of borate buffer containing 0.5 µL of 2 mg/mL Alexa Fluor 594 succinimidyl ester (Invitrogen) and rotated at room temperature for 15 minutes. The succinimidyl ester (SE) is amine-reactive. Alternatively Alexa Fluor 555SE (Invitrogen) or Alexa Fluor 488SE (Invitrogen) was used to fluorescently label the beads. The beads were finally washed twice in storage buffer (25mM glycine in PBS). For longer storage, 10 µl of 2% sodium azide (Sigma) (2% solution in distilled water) was added and samples were stored at 4°C for future use.

2.11.1.2: Preparation of proteolysis reporter experimental particles:

Bulk proteolysis reporter experimental particles were prepared similarly to the procedure described in section 2.12.1.1 with the difference that beads after being coupled to human IgG, were cross-linked to DQgreen BSA (Invitrogen) and for the calibration fluor, either Alexa Fluor 594SE (Invitrogen) or Alexa Flour 633SE (Invitrogen) was used. Where mentioned, 1.5 µm carboxylate modified silica beads were used instead of 3 µm beads.

2.11.1.3: Preparation of oxidation-sensitive experimental particles:

The oxidation-sensitive experimental particles were prepared similarly to the procedure described above in section 2.12.1.1. All solutions used were degassed before starting to remove

any dissolved oxygen. After coupling with human IgG, the 3 µm carboxylate modified silica beads were conjugated to OxyBURST Green H2HFF BSA (Invitrogen) and calibration fluor Alexa Fluor 594 (Invitrogen).

2.11.1.4: Preparation of pH-sensitive experimental particles:

pH-sensitive experimental particles were prepared similarly to the procedure described above in section 2.12.1.1. After coupling with human IgG, the 3 µm carboxylate modified silica beads were conjugated to NHS-carboxyfluorescein (Invitrogen).

2.11.1.5: Preparation of fluorescent latex beads with or without Fc receptor ligand:

500 µL of carboxylate modified 2 µm yellow green (505|515 nm) fluorescent latex microspheres (Invitrogen) were washed in PBS by vigorously vortexing and briefly centrifuging using a tabletop centrifuge. The beads were then resuspended in 500 µL of 25 mg/mL cyanamide in PBS and nutated at room temperature for 15 minutes to crosslink the beads to cyanamide. The beads are then washed in PBS and resuspended in borate buffer containing 10 mg of defatted BSA and nutated for 45 minutes at room temperature. The beads were washed in PBS and resuspended in 200 µL of borate buffer. To 100 µL of the beads, 10 µL of anti-BSA antibody (Rockland) was added and nutated for 3 hours at room temperature. To the other 100 µL of the beads, 10 µL of dissolved defatted BSA was added and nutated at room temperature for 3 hours. The beads were then washed and resuspended in storage buffer and counted using a hemocytometer.

2.11.1.6: Preparation of serum-opsonised zymosan:

14 mg of zymosan (Sigma) was suspended in 1 mL PBS and boiled for 30 minutes in a 100°C dry bath. The particles were spun down and resuspended in 1 mL PBS and an equal volume (1mL) of endotoxin -free FCS and incubated at 37°C for 30 minutes. The particles were washed in PBS 3 times and finally pelleted by centrifugation at 11000 x g for 5 minutes and resuspended in PBS at a concentration of 10mg/ml. This was used as a 200X stock of zymosan.

2.11.2: Measuring phagocytic index:

2.11.2.1: Measuring phagocytic index by microscopy:

A small volume of experimental particles were washed thrice with sterile PBS to remove all traces of sodium azide, and the beads were resuspended in PBS such that the bead concentration was approximately 10^{7} beads/mL. The pBMMØ or porcine alveolar macrophages were seeded on a 96-well assay plate (Grenier Bio-One µClear) and grown to confluency. The experimental particles were added to a confluent monolayer of cells at a MOI of 2-3 beads/cell in gel reaction buffer (an assay buffer containing PBS supplemented with 1mM Calcium chloride, 2.7mM Potassium chloride, 0.5mM Magnesium chloride, 5mM dextrose and 0.25% gelatin). The cells were incubated with the experimental particles for 30 minutes at 37°C and then stained with 0.01% Trypan blue (in PBS) to effectively quench fluorescence from the extracellular particles. Using an Olympus IX70 inverted fluorescent microscope equipped with a 20X (air), NA=0.75 objective, three fields of view were imaged for each sample using brightfield illumination, and epifluorescence using the appropriate filter. Each experimental group had 3

replicates. Phagocytic index was calculated as the percentage of beads inside the cell. Experimental groups were compared by Student's t-test using GraphPad Prism software.

2.11.2.2: Measuring phagocytic index using flow cytometry:

A small volume of experimental particles were washed thrice with sterile PBS to remove all traces of sodium azide, and the beads were resuspended in PBS such that the bead concentration was approximately 10^7 beads/ml. The pBMMØ or porcine alveolar macrophages were seeded on a 96-well assay plate (Grenier Bio-One μClear) and grown to confluency. The experimental particles were added to a confluent monolayer of cells at a MOI of 2-3 beads/cell in gel reaction buffer. The cells were incubated with the experimental particles for 30 minutes at 37°C. After incubation, the cells were harvested by scraping, pelleted by centrifugation at 300 x g for 5 minutes. The pellet was resuspended in FACS buffer consisting of PBS supplemented with 1% FCS and assayed using a flow cytometer. Cells not incubated with beads were first run to adjust the voltage on the cytometer such that the signals from this negative population of cells were restricted to the first decade of the axis, thereby allowing a dynamic range for acquiring the positive signal. Data acquisition was performed using Cell Lab Quanta Collection Software. Additional data analysis on the data files exported in listmode data (lmd) format was performed using Flow Jo software (Tree Star Inc). The phagocytic index was calculated as the percentage of cells containing beads.

2.11.3: Measuring phagosomal proteolysis:

Fluorometric measurements of phagosomal proteolysis in real time:

A small volume of the proteolysis reporter beads were washed thrice with sterile PBS to remove all traces of sodium azide and the beads were resuspended in PBS such that the bead concentration was approximately 10^7 beads/ml. The pBMMØ or porcine alveolar macrophages were seeded on a 96-well assay plate (Grenier Bio-One µClear) and grown to confluency. The experimental particles were added to a monolayer of cells at a MOI of 2-3 beads/cell in gel reaction buffer. Measurements were performed using a microplate reader (FLUOstar OPTIMA fluorescent plate-reader, BMG Labtech, or Perkin Elmer Envision 2104 Multilabel Reader). Fluorescence intensities were measured at 594|620 nm and 490|515 nm (excitation λ| emission λ). The fluorescence of the calibration fluor Alexa Fluor 594 (594|620 nm) remained constant throughout the assay, while the fluorescence intensity of the reporter fluor BODIPY FL increased with progressive proteolysis of DQ-BSA substrate following phagocytosis of the experimental particles. Figure 2.5 schematically represents the principle behind the assay. Data was collected over 120 minutes starting at time t=0 which corresponds to addition of the experimental particles to cells. Where mentioned, cells were treated with 100nM of the v ATPase inhibitor concanamycin A (Sigma) (conAv-ATPase inhibitor) for 10 minutes before addition of experimental particles. Treatment with concanamycin A prevents phagosomal acidification and thereby inhibits the protease activity of phago-lysosomal proteases. Background fluorescence measurements (594|620 nm and 490|515 nm) were recorded for cells alone without beads. Background values were deducted from the data. The ratio of

substrate fluorescence to calibration fluorescence which denotes the relative fluorescence intensity (RFU) was plotted against time. The slope of the linear portion of the curve was calculated (as defined by the equation y=mx+c where y=RFU, m=slope and x=time) and compared amongst samples. It signifies the overall proteolysis in the phagosomal lumen of the cell population over a defined time period. Proteolysis in different experimental groups was compared by Student's t-test using GraphPad Prism software.

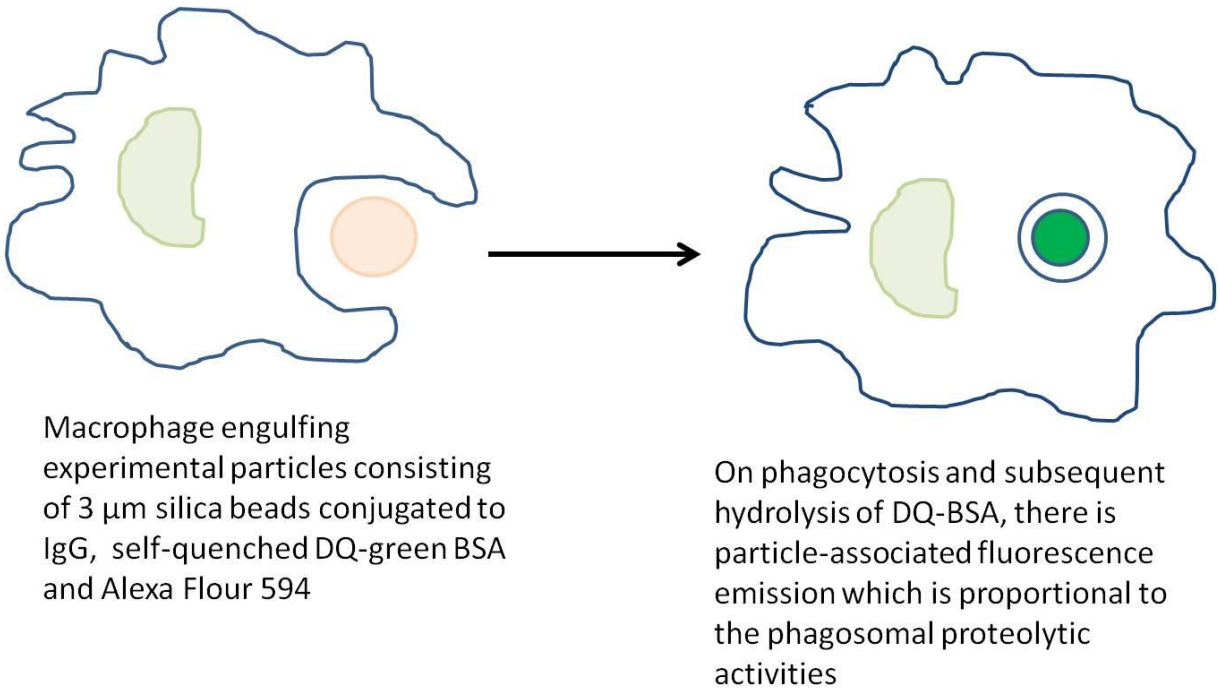

Figure 2.5: Schematic representation of how proteolytic reporter experimental particles are used to assay phagosomal proteolysis

2.11.4: Measuring intra-phagosomal oxidative burst through phagocytosis of oxidation-sensitive experimental particles:

The pBMMØ or porcine alveolar macrophages were seeded on a 96-well assay plate (Grenier Bio-One µClear) and grown to confluency. The oxidation-sensitive experimental particles were added to a monolayer of cells at a MOI of 3-4 beads/cell in gel reaction buffer. Measurements were performed using a microplate reader (FLUOstar OPTIMA fluorescent plate-reader, BMG Labtech, or Perkin Elmer Envision 2104 Multilabel Reader). Fluorescence intensities were measured at 594|620 nm and 490|515 nm (excitation λ| emission λ). The fluorescence of the calibration fluor Alexa Fluor 594 (594 nm|620 nm) remains unchanged throughout the assay while the fluorescence intensity of the reporter fluor dihydro-2',4,5,6,7,7'-hexafluorofluorescein (H2HFF) (490|515 nm) increases upon oxidation following phagocytosis of the beads. Data was collected over 120 minutes starting at time t=0 which corresponds to addition of experimental particles to the cells. Background fluorescence measurements (594|620 nm and 490|515 nm) were recorded for the cells alone without addition of particles. Background values were deducted from the data. The ratio of substrate fluorescence to calibration fluorescence, which denotes the relative fluorescence intensity (RFU), was plotted against time. The slope of the linear portion of the curve was calculated (as defined by the equation y=mx+c where y=RFU, m=slope and x=time) and compared amongst samples. It signifies the overall ROS production in the phagosomal lumen of the cell population over a certain time period.

2.11.5: Extracellular detection of phagosomal ROS by amplex red assay:

This assay was used to measure phagosomal ROS (hydrogen peroxide in particular) that has leaked out into the extracellular milieu. Amplex Red (Invitrogen) is a fluorogenic substrate which, in its non-oxidized form, is non fluorescent. Amplex red reacts with hydrogen peroxide in a stoichiometric ratio of 1:1 in presence of HRP to get converted to its oxidized form which is highly fluorescent in the red spectrum (excitation|emission maxima: 570|585 nm). The pBMMØ or porcine alveolar macrophages were seeded on a 96-well assay plate (Grenier Bio-One µClear) and grown to confluency. The cells were activated by incubating with serum-opsonised zymosan (0.5 mg/mL) for 1 hour at 37°C and 7% CO_2. Following the incubation period, 1U of HRP (Sigma) and 1mM amplex red (final concentration) were added per well and incubated at room temperature in the dark for 30 minutes. The absolute fluorescence intensity values were recorded at 615 nm after excitation at 550nm using a fluorescent plate reader (Perkin Elmer Envision 2104 Multilabel Reader). Untreated cells (not activated by treating with serum opsonised zymosan) were used as controls to calculate the background fluorescence resulting from detection of non-phagosomally produced ROS.

2.11.6: Fluorometric measurement of phagosomal acidification in real time:

A small volume of pH-sensitive experimental particles were washed thrice with sterile PBS to remove all traces of sodium azide and the beads were resuspended in PBS such that the bead concentration was approximately 10^7 beads/ml. The pBMMØ or porcine alveolar macrophages were seeded on a 96-well assay plate (Grenier Bio-One µClear) and grown to

confluency. The pH-sensitive experimental particles were added to a monolayer of cells at a MOI of 2-3 beads/cell in gel reaction buffer. Measurements were performed using a microplate reader (FLUOstar OPTIMA fluorescent plate-reader BMG Labtech or Perkin Elmer Envision 2104 Multilabel Reader). Fluorescence intensities were measured at 450|520 nm and 490|520 nm (excitation λ| emission λ). The fluorescence from carboxyfluorescein at 520 nm is sensitive to decreasing pH when excited at 490 nm but not when excited at 450 nm. Data was collected over 60-90 minutes as indicated starting at time t=0 which corresponds to addition of experimental particles to the cells. Background fluorescence measurements (450|520 nm and 490|520 nm) were recorded for the cells alone, incubated without experimental particles. Background values were deducted from the data. 490/450 nm fluorescence was calculated and the values were converted to corresponding pH by regressing to a third-order polynomial standard curve. The polynomial pH standard curve is generated as follows. pH-sensitive experimental particles were suspended in pH standard buffer from pH 4 to pH 7.5 and the fluorescence intensities were measured at 520 nm after alternating excitation at 450 nm and 490 nm. The background values were obtained from fluorescence intensity measurements at 520 nm from the pH standard buffers alone after alternating excitation at 450 nm and 490 nm. The average ratio of fluorescence intensity for excitation ratio of 490/450 nm was calculated for the experimental particles in each standard pH buffer after deduction of the background values. The normalized 490/450 nm excitation values were plotted against pH values and the polynomial equation that best fits the curve was calculated. To compare the average pH amongst samples at any particular time point, the slope of the curve at that particular time

point was calculated from the equation y=mx+c, where m is the slope, y is the 490/450 nm excitation fluorescence intensity ratio, and x is the time in minutes.

2.12: Statistical analysis:

Numerical values have been represented as mean ± standard error of the mean (SEM). Data was analysed using Graph Pad Prism Software (version 5, Graphpad Software Inc). To compare statistical significance of experimental outcomes between two experimental groups, P value was calculated using one-way ANOVA with Tukey's post test or by Student's t-test, whichever appropriate. Statistical significance was considered to be established if observed P value was less than 0.05.

2.13: Imaging:

All samples were imaged using Olympus IX70 epifluorescence microscope in the brightfield or in the epifluorescence illumination mode (EPI) using the appropriate fluorescence filter. The microscope is equipped with 10X (NA=0.45), 20X (NA=0.75) and 40X (NA=0.95) objectives, a choice of four different fluorescent filter sets (DAPI, FITC, TRITC and TEXAS-RED) and a CCD camera. Images were acquired and analyzed using Q-capture Pro 7 Image and Analysis software (Olympus).

CHAPTER 3: RESULTS

3.1: *In vitro* differentiation of porcine bone marrow cells into porcine bone marrow derived macrophages (pBMMØ) using L929 cell supernatant:

L929 is a murine fibroblast cell line known to secrete Macrophage Colony Stimulating Factor (M-CSF or CSF1)[273]. L929 cell supernatant is therefore a rich source of M-CSF and is frequently used for *in vitro* differentiation of murine bone marrow cells into bone marrow derived macrophages[65,76]. L929 cell supernatant has been reported to differentiate bone marrow cells into macrophages in species other than mouse[274]. In pigs, L929 cell supernatant has been used to differentiate peripheral blood mononuclear cells into macrophages[275]. Also porcine bone marrow cells have been differentiated into macrophages by growing in the presence of recombinant human M-CSF[276]. These studies suggest that the binding of M-CSF to its receptor CSF-1R to initiate the signaling pathways leading to macrophage differentiation is not strictly species-specific. In addition, sequence analysis show that porcine M-CSF has 85% identity with murine M-CSF at the nucleotide level and 77% at the protein level. In addition to the existing studies, sequence analysis provided preliminary incentive that L929 cell supernatant can be used to differentiate porcine bone marrow cells into macrophages. With the aim of establishing a primary culture of porcine bone marrow derived macrophages, porcine bone marrow cells flushed out of mid-thoracic costal (rib) bones were grown in the presence of L929 cell supernatant on sterile bacteriological plasticware. When examined using light microscopy, on day 1 the bone marrow cells in culture were non-adherent and had a round-cell morphology – consistent with hematopoietic stem cells (Figure 3.1A). Gradually the cells showed development of a macrophage-like appearance (Figure 3.1B, 3.1C and 3.1D). The

heterogeneous mixture of cell types was gradually transformed into a homogeneous population of macrophages. By day 10, the cells have a typical macrophage-like appearance, forming large cells with extensive cytoplasm, numerous vacuoles, and an almost indistinguishable cell membrane. The cells strongly adhered to the plastic surface, formed a monolayer and had proliferative capacity. The cells lack the multiple long dendrites typical of dendritic cells (Figure 3.1E). On day 10, the cells when incubated with IgG opsonized experimental particles exhibited enhanced phagocytosis (Figure 3.1F).

Figure 3.1: Porcine bone marrow cells isolated from mid-costal (rib) bones can be differentiated *in vitro* by culturing in the presence of L929 cell supernatant containing murine M-CSF. The cells were imaged using brightfield microscopy on an Olympus IX70 fluorescence microscope equipped with a 20×, NA= 0.75 objective. **(A):** On Day 1, bone marrow cells were non adherent and had round-cell morphology consistent with hematopoietic stem cells. **(B**,**C,D):** Representative images of cells consisting of a heterogeneous mixture of undifferentiated and partially differentiated cells on Day 4, Day 5 and Day 6 respectively. The cells gradually developed a macrophage-like appearance. **(E):** On Day 10, the culture contained a homogeneous population of cells. The cells have a typical macrophage-like appearance, forming large cells with extensive cytoplasm and almost indistinguishable plasma membrane. **(F):** On Day 10, the cells exhibited phagocytosis of opsonised experimental particles. The experimental particles consisted of yellow-green fluorescently labelled 2 µm latex beads (Molecular Probes) covalently coupled to BSA and anti-BSA. Cells were imaged using Olympus IX70 fluorescence microscope equipped with a 20×, NA= 0.75 objective, using the FITC filter.

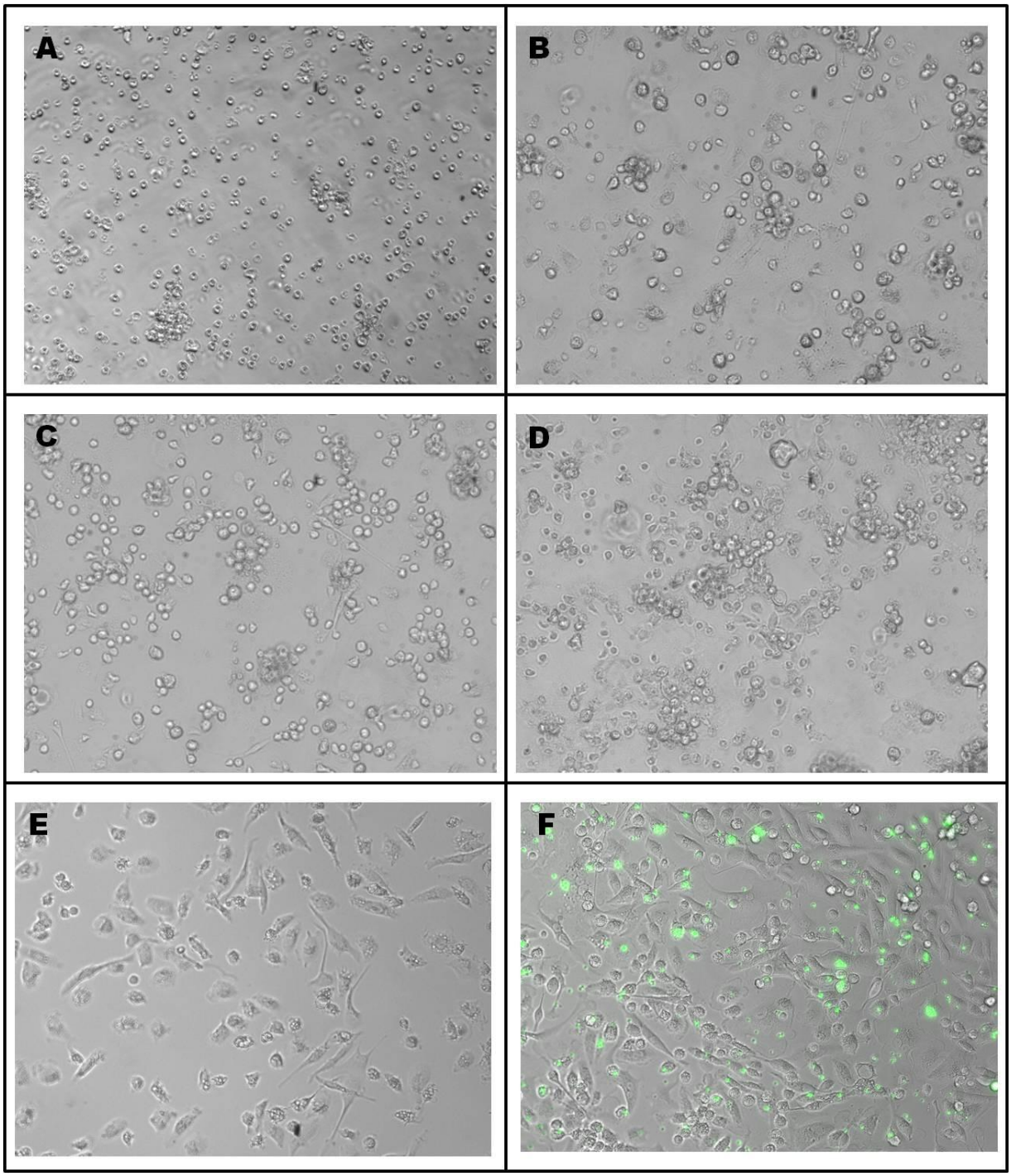
A
B
C
D
E
F

3.2: *In vitro* differentiated pBMMØ exhibit FcγR-mediated phagocytosis of experimental particles:

To test if pBMMØ exhibited higher levels of uptake of IgG-opsonized phagocytic targets than non-opsonized targets, the phagocytic efficiences of the cells in ingesting opsonized and non-opsonised experimental particles were compared. Macrophages recognize and internalize IgG-opsonized experimental particles through FcγR-mediated phagocytosis[277]. Non-opsonized particle recognition may occur through the mannose receptor or through engagement of one or more of the scavenger receptors[278]. Since FcγR -mediated phagocytosis is typically more efficient than the other pathways, to determine whether our pBMMØ expressed FcγR and the associated signaling components, we compared rates of phagocytosis of opsonized and non-opsonized particles. pBMMØ were incubated for 30 minutes at 37°C, 7% CO_2, with experimental particles consisting of carboxylate-modified 2 µm yellow-green (505| 515 nm) fluorescent latex beads covalently conjugated to BSA, with or without prior incubation with rabbit anti-BSA IgG. To serve as a negative control for the experiment, pBMMØ were treated with 5 µM cytochalasin D (cytD) for 10 minutes prior to being incubated with beads. To assess phagocytic efficiency, cells were stained post-incubation with 0.01% trypan blue (for quenching extracellular experimental particles). Each sample was imaged for three fields of view. The brightfield and fluorescent images were overlapped and analyzed. The number of extracellular and intracellular experimental particles was manually counted. Each experimental group had three replicates. pBMMØ exhibited significantly higher levels of internalization of IgG-opsonized

experimental particles, suggesting that the pBMMØ express FcR and exhibit FcR-mediated phagocytosis (Figure 3.2).

3.3: *In vitro* differentiated pBMMØ show characteristic phagosomal acidification:

A newly formed macrophage phagosome is relatively neutral with a pH of around 7-7.5[158,159]. As the phagosome matures, it becomes progressively acidic, with the phagolysosome becoming as acidic as pH 4.5 – pH 5.5[159]. Proper phagosomal acidification is indicative of, as well as essential for, maturation of the phagosome and phagosome-lysosome fusion[159]. Acidification also contributes to the microbicidal and degradative capacities of the phagosome as most phagolysosomal hydrolases have optimum activity at acidic pH[279]. To test if the cells from the established primary culture of *in vitro* differentiated pBMMØ showed characteristic acidification patterns, phagosomal pH was measured using a real-time acidification assay[271]. This *in vitro* assay measures the dynamics of acidification of phagosomes in live, undisturbed cells, by ratiometric fluorometry measurements. This is a highly robust and extensively validated assay which utilizes uptake of pH-sensitive experimental particles by live cells[271]. pH-sensitive experimental particles consisting of silica beads covalently coupled to human IgG and the pH-sensitive fluorophore, carboxyfluorescein were added to a confluent monolayer of pBMMØ. Using a fluorescence plate reader, fluorescence emission was recorded at 520 nm after fluorescence excitation successively at 480 nm and 450 nm. The fluorescence emission from carboxyfluorescein is sensitive to pH change when excited at 490 nm but not when excited at 450 nm. The ratio of fluorescence intensities at these two wavelengths was

calculated. The ratiometric fluorescence intensity measurements from the experimental particles were converted to pH by extrapolation to a previously standardized third order polynomial standard curve by regression analysis. The phagosomal pH in untreated pBMMØ was found to change from pH 7.5 to pH 5 within 30 minutes of particle internalization consistent with acidification profiles recorded in murine BMMØ[271,280]. In pBMMØ pre-treated with 100nM concanamycin A (conA), a v-ATPase inhibitor[160], for 10 minutes prior to addition of experimental particles which serve as negative controls for the experiment, the phagosomal pH remained relatively constant over time. Phagosomal lumenal pH at 45 minutes in untreated pBMMØ was found to be significantly lower than that in 100 nM conA-treated pBMMØ. In pBMMØ after 30 to 45 minutes, the pH reached a final acidic value which remained constant and was not found to change during the remaining assay period (total duration of 80 minutes) (Figure 3.3).

3.4: *In vitro* differentiated pBMMØ show characteristic phagosomal proteolysis:

Phagosomal proteolysis in macrophages is the pre-requisite for many of the cell's functions including generation and preservation of peptide antigens. Phagosomal proteolysis was measured in pBMMØ using a real time fluorometric assay. The assay relies on phagocytic uptake of experimental particles consisting of 3 µm silica beads conjugated to IgG, a calibration fluor (Alexa Fluor 594), and DQ-BSA (which consists of BSA conjugated to BODIPY FL in such high quantities that it is self-quenched) by pBMMØ. Following phagocytosis, DQ-BSA is hydrolyzed, resulting in dequenching of the substrate and bright fluorescence from the

individual digested fragments. The fragments emit fluorescence at 515 nm when excited at 505 nm. The fluorescence from the calibration fluor remains constant over time. Measures of the level of proteolysis are obtained from by calculating the ratio of the fluorescence from the dequenched BODIPY substrate fluor to the calibration fluor. This is a robust and well-validated assay for studying phagosomal proteolysis in real time[271]. Untreated pBMMØ show increasing levels of proteolysis over a period of 120 minutes indicating that proteases are active in the pBMMØ phagosome (Figure 3.4). pBMMØ treated with 100 nM conA were used as negative controls. To quantify proteolytic activity of each experimental group, the slope of the linear portion of the graph depicting real time phagosomal proteolytic traces was calculated. The average slope was calculated and compared from three independent experiments. Untreated pBMMØ exhibited significantly higher levels of proteolysis relative to conA-treated samples. These findings correspond with previous findings in murine BMMØs assayed using the same technique[76,280,281] .

Figure 3.2: pBMMØ showed significantly higher levels of phagocytosis of opsonised experimental particles than non-opsonized particles. Cells were incubated with experimental particles consisting of fluorescent latex beads covalently coupled to BSA only or to both BSA and anti-BSA for 30 minutes at 37°C. In order to distinguish between ingested and extracellular (quenched) experimental particles, cells were stained with Trypan blue (0.01% v/v in PBS). Phagocytic index was calculated as the ratio of the number of experimental particles ingested to the number of extracellular particles. Phagocytic index was assessed by fluorescence microscopy 30 minutes after particle uptake. Cells pre-treated with cytochalasin D (cytD, 5µM) were negative controls for the experiment. Data represent the average percentage of beads phagocytosed from three independent experiments. Error bars represent SEM. P values were calculated using one-way ANOVA. *** represents $P<0.001$.

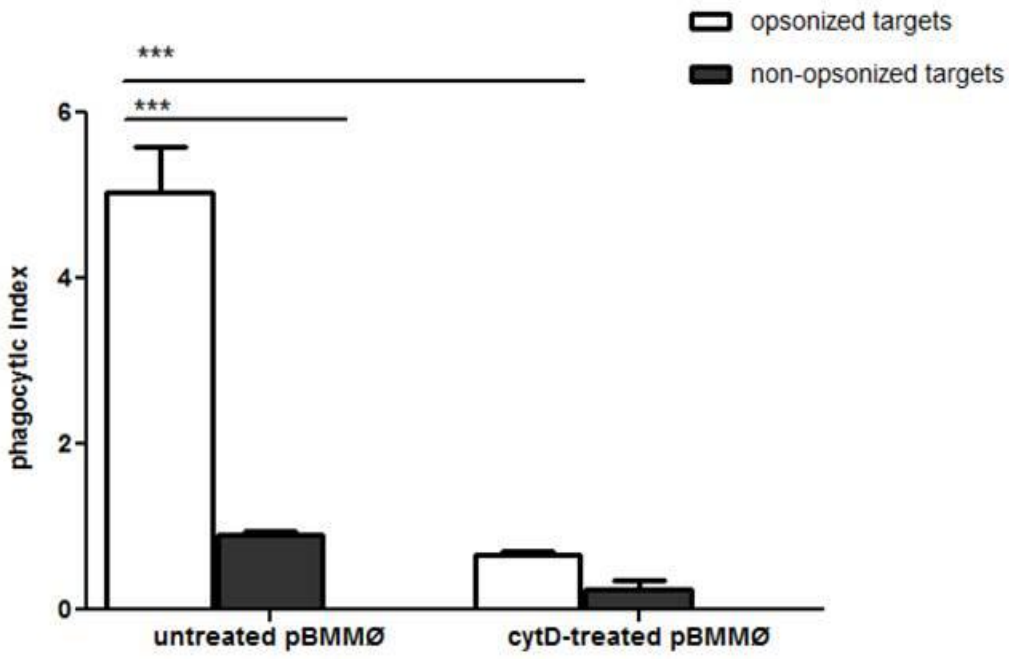
opsonized targets
non-opsonized targets
***
***
6
4
2
0
phagocytic index
untreated pBMMØ
cytD-treated pBMMØ

Figure 3.3: Phagosomes formed by *in vitro* differentiated pBMMØ, upon ingestion of experimental particles, showed characteristic acidification. Acidification profiles were generated in untreated and concanamycin A (conA, 100nM)-treated pBMMØ. Cells were incubated with IgG-coupled 3 µm silica particles labeled with the pH-sensitive fluor CFSE (λex_1 485 nm, λex_2 450nm; λem 520 nm) for 90 minutes. Acidification was measured in real time by reading the fluorescence change in CFSE, and extrapolated to a standard curve by linear regression in order to determine pH. **(A):** Representative real-time phagosomal acidification profiles over a time period of 80 minutes **(B):** Lumenal pH at 45 minutes after internalization of experimental particles. Graph represents averaged data from three independent experiments. Error bars represent SEM. P values were determined using Student's t-test in GraphPad Prism. * represents P<0.0.5.

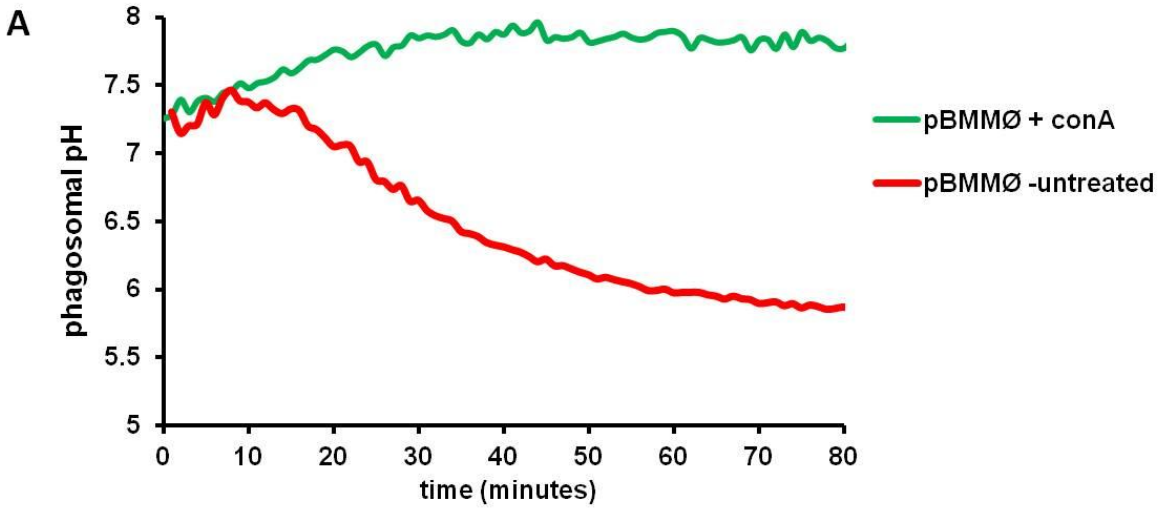
A
8
7.5
7
6.5
6
5.5
5
phagosomal pH
0
10
20
30
40
50
60
70
80
time (minutes)
pBMMØ + conA
pBMMØ -untreated

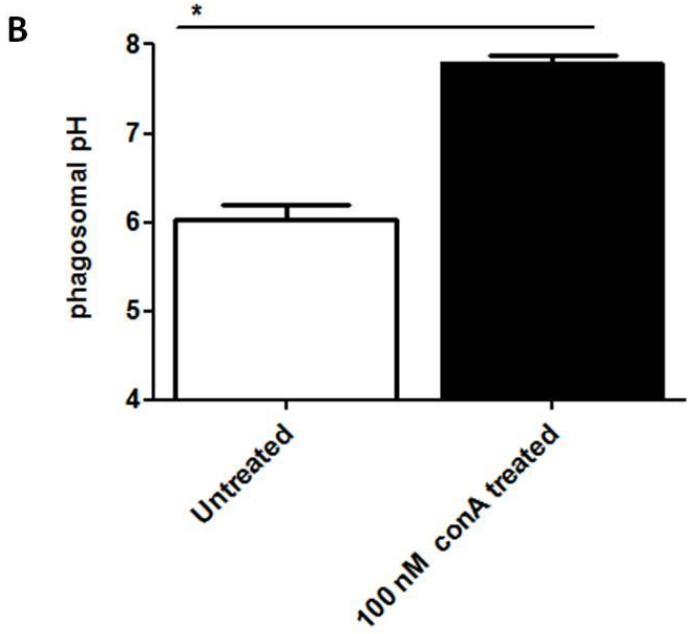
B
*
8
7
6
5
4
phagosomal pH
Untreated
100 nM conA treated

Figure 3.4: In vitro differentiated pBMMØ showed characteristic phagosomal proteolysis. Following incubation of pBMMØ at 37°C with proteolysis reporter experimental particles consisting of 3µm silica beads conjugated to self-quenched DQ-BSA, calibration fluor Alexa Fluor 594, and IgG, the proteolytic efficiencies of phagosomes were assessed in real time by measuring the amount of fluorescence liberated from hydrolysis of particle-associated DQ-BSA substrate, relative to the calibration fluor Alexa Fluor 594. **(A):** Representative real-time traces of phagosomal proteolysis. ConA-treated pBMMØ represent a negative control. **(B):** Averaged proteolytic activities of conA-treated samples relative to untreated samples from six different experiments. To quantify proteolytic activity, the slope of the linear portion of the real-time trace was calculated (from the equation y=mx+c, where y=relative fluorescence, m=slope and x=time) and expressed relative to untreated samples. Error bars represent SEM. P values were calculated using Student's t-test. *** represents $P<0.001$.

A

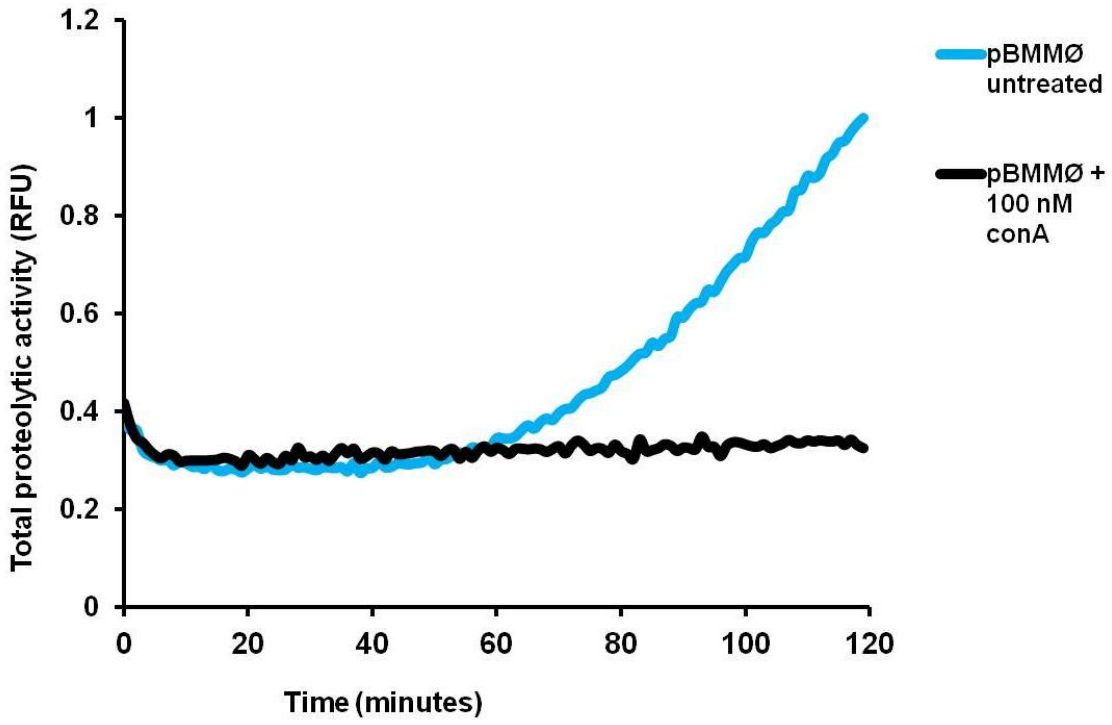
1.2
1
0.8
0.6
0.4
0.2
0
Total proteolytic activity (RFU)
0
20
40
60
80
100
120
Time (minutes)
pBMMØ untreated
pBMMØ + 100 nM conA

B

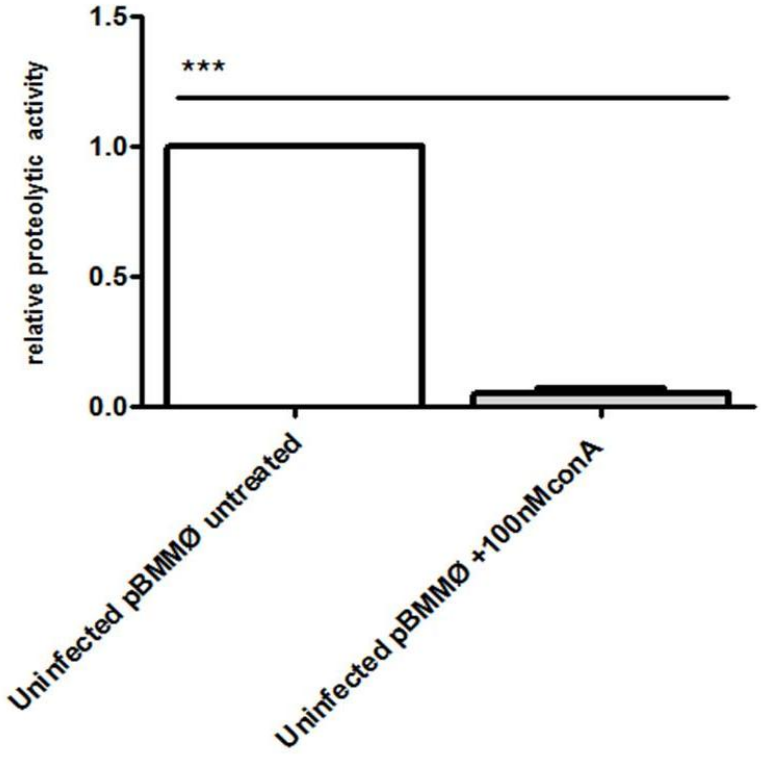
1.5
1.0
0.5
0.0
relative proteolytic activity
***
Uninfected pBMMØ untreated
Uninfected pBMMØ +100nMconA

3.5: PRRSV isolate NVSL 97-7895 was propagated in MARC-145 cells:

The PRRSV isolate NVSL 97-7895 was grown and propagated in MARC-145 cells. A confluent monolayer of MARC-145 cells was infected with the PRRSV isolate NVSL 97-7895 at a MOI of 0.001 in SFM. When examined using light microscopy 4 days post-infection, infected cells showed clear cytopathology such as shrinkage and rounding up of cells, presence of granularity, and detachment from substrate. Uninfected control cells showed no change in phenotype (Figure 3.5). To quantify the virus produced, culture supernatant was harvested 4 days post-infection for secreted virus. The virus was quantified by plaque assay on MARC-145 cells. The virus thus grown was found to form plaques. The titre of the virus produced was 7.06 x 10^4 PFU/mL (average from three independent experiments). This signifies a 19% increase in virus titre on propagation (Figure 3.5).

3.6: *In vitro* infection of pBMMØ is productive:

A productive virus infection of a host cell is marked by the production of functional virions after infection. In contrast, in an abortive infection, the virus infects the host cell but no viable virions are produced; virus replication is hindered at some time point. In order to examine if PRRSV infection of pBMMØ was productive, pBMMØ were infected with PRRSV isolate NVSL 97-7895, grown as described in section 3.5 above, at a MOI of 0.001 in SFM and infected cells and uninfected control cells were incubated at 37°C for 72-96 hours. Secreted virus was harvested by collecting culture supernatant and titrated by plaque assay on MARC-145 cells. The plaques were counted from dilutions that showed between 10-100 plaques. The

titre of the virus produced was 4.67 x 10^3 PFU/mL (average from three independent experiments) (Figure 3.6). This signifies an increase in virus titre on propagation (Figure 3.6).

Figure 3.5: PRRSV isolate NVSL-97-7895 was propagated in MARC-145 cells. Infection of MARC-145 cells with PRRSV isolate NVSL-97-7895 results in cytopathology. Monolayers of MARC-145 cells were grown to confluency and infected with PRRSV isolate NVSL-97-7895 at a MOI of 0.001. Infected and uninfected control cells were incubated at 37°C post infection. Four days post-infection, culture supernatant containing secreted virus was collected and the infected and uninfected cells were imaged using an Olympus IX70 fluorescence microscope equipped with a 20×, NA= 0.75 objective at a magnification of 20X. Secreted virus in supernatant was quantified by plaque assay titration using MARC-145 cells. **(A):** Micrograph of uninfected control cells. The monolayer of uninfected cells remains unaffected. **(B):** Micrograph of infected cells. Infected cells show clear cyotpathology at 4 days post-infection. **(C):** Virus titres of inoculum vs yield. There is a 19% increase in virus titre. Graph represents titre from three independent plaque assay experiments. Error bar represents SEM.

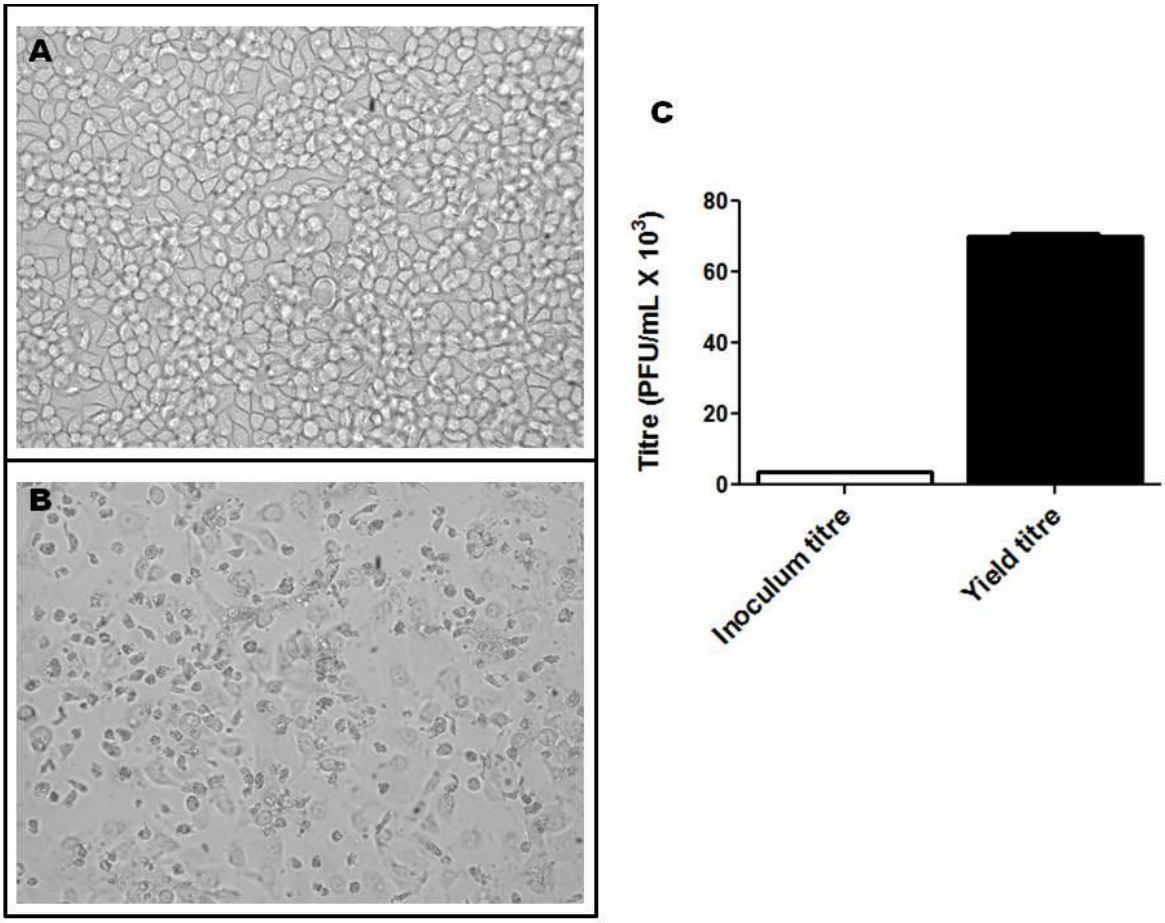
A
B
C
Titre (PFU/mL X 10^3)
80
60
40
20
0
Inoculum titre
Yield titre

Figure 3.6: Infection of pBMMØ with PRRSV isolate NVSL-97-7895 is productive. Confluent monolayers of pBMMØ were infected with PRRSV isolate NVSL-97-7895 at a MOI of 0.001. Infected and uninfected control cells were incubated at 37°C post infection. Four days post-infection, supernatant containing secreted virus was collected and titrated by plaque assay on MARC-145 cells. There is an increase in the virus titre. Graph represents titre from three independent experiments. Error bar represents SEM.

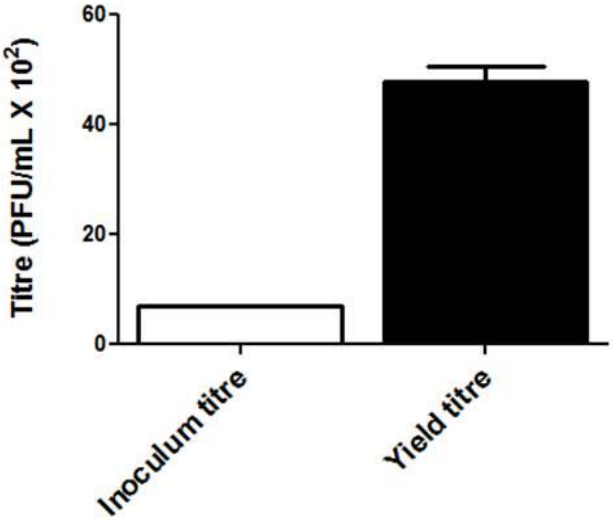
Titre (PFU/mL X 10^2)
60
40
20
0
Inoculum titre
Yield titre

3.7: pBMMØ samples infected *in vitro* with PRRSV isolate NVSL 97-7895 did not show cell death 24 hours post-infection:

A confluent monolayer of pBMMØ was infected with PRRSV at a MOI of 0.1 in SFM. In order to test if PRRSV infection of pBMMØ at a MOI of 0.1 led to cell death 24 hours post-infection, infected and uninfected cells were trypsinized, resuspended in PBS and stained with 0.01% trypan blue and counted using a hemocytometer. No significant difference was observed between the ratio of live to dead cells in infected and uninfected samples (Figure 3.7). Preliminary results also show that there is no significant difference in the number of cells undergoing apoptosis between infected and uninfected pBMMØ samples (data not shown).

Figure 3.7: Infection of pBMMØ with PRRSV isolate NVSL-97-7895 does not result in significant cell death 24 hours post-infection. Confluent monolayers of pBMMØ were infected with PRRSV isolate NVSL-97-7895 at a MOI of 0.1. Infected and uninfected control cells were incubated at 37°C post-infection. 24 hours post-infection, the infected and uninfected cells were stained with vital dye Trypan blue (0.01% v/v in PBS), counted using a hemocytometer and the percentage of dead cells were calculated. There is no significant difference in the percentage of dead cells between infected and uninfected samples. Graph represents average from three independent experiments. Error bars represent SEM. P values were calculated using Student's t-test.

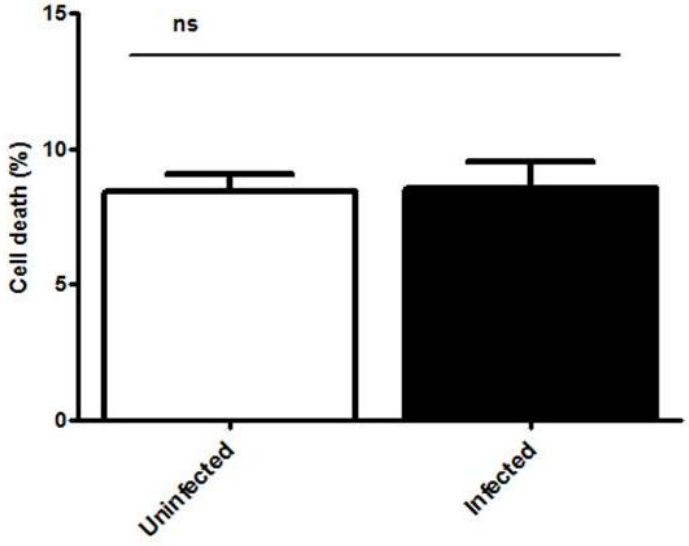
ns
15
10
5
0
Cell death (%)
Uninfected
Infected

3.8: pBMMØ infected *in vitro* with PRRSV isolate NVSL 97-7895 exhibited significantly lower levels of phagosomal proteolysis than uninfected cells:

Phagosomal proteolysis is fundamental to macrophage function including for antigen processing and presentation[282]. To investigate if PRRSV infection brought about changes in the levels of phagosomal proteolysis, proteolysis was assessed in real time in pBMMØ infected with PRRSV isolate NVSL 97-7895 at a MOI of 0.1, 24 hours post-infection, and in uninfected control cells. Proteolytic activities in the experimental groups were assayed using the experimental particle uptake assay as described in section 3.4. The cells were checked microscopically before and after addition of experimental particles to ensure that the cells were a confluent monolayer and that the experimental particles were added at an MOI of 2-3 beads/cell. No cytopathic effect was observed in the pBMMØ samples infected with PRRSV before or immediately after the assay. Cells pretreated with 100 nM conA for 10 minutes prior to the addition of experimental particles served as negative control for the experiment. pBMMØ samples infected with PRRSV showed significantly lower levels of proteolysis than uninfected control cells (Figure 3.8). Both infected and uninfected experimental groups showed onset of proteolysis at the same time. However, the overall proteolytic activities of the infected pBMMØ were reduced by about 4-fold relative to the uninfected untreated pBMMØ. As anticipated, the conA-treated samples showed little increase in proteolytic activity over time.

3.9: pBMMØ infected *in vitro* with PRRSV isolate NVSL 97-7895 show no significant difference in phagocytic efficiency compared to uninfected cells:

To test if the differences in phagosomal proteolysis were a consequence of differential uptake of experimental particles by infected and uninfected samples of pBMMØ, phagocytic efficiencies in the cells were assessed microscopically. The assay was carried out 24 hours post-infection. At this time point, the infected pBMMØ showed no visible cytopathology. Experimental particles consisting of carboxylated silica beads conjugated to human IgG and Alexa Fluor 555 were added to a confluent monolayer of pBMMØ. The cells were incubated for 30 minutes before staining with 0.01% trypan blue to quench extracellular experimental paticles, and imaged. The numbers of ingested and extracellular experimental particles were counted manually. Phagocytic index was calculated as the ratio of extracellular experimental particles to the number of experimental particles phagocytosed. Infected samples showed no significant difference in uptake of experimental particles compared to uninfected cells (Figure 3.9). pBMMØ pretreated with cytochalasin D (5 μM) prior to addition of experimental particles (which inhibits internalization but not binding of experimental particles) show significantly lower levels of phagocytic efficiency and are a negative control for the experiment. These results suggest that differences observed in proteolytic capacity between infected and uninfected experimental groups (Figure 3.9) is not due to differential uptake of experimental particles.

3.10: pBMMØ infected *in vitro* with PRRSV isolate NVSL 97-7895 show no significant difference in acidification pattern from uninfected cells:

Phagosomal proteases have optimal activity in acidic pH[282]. Inhibition of acidification of the phagosome will thus lead to lower phagosomal proteolysis, and will signify defects in phagosome maturation and phagosome-lysosome fusion[279]. To investigate if PRRSV-infected cells had defects in phagosomal acidification, phagosomal pH was measured in real time in infected and uninfected pBMMØ. The assay was carried out 24 hours post-infection. At this stage, the infected samples showed no cytopathic effects. pH-sensitive experimental particles consisting of silica beads conjugated to human IgG and carboxyflourescein (succimidyl ester, CFSE) were added to a confluent monolayer of cells. Using a fluorescence microplate reader, fluorescence intensities were recorded at 520 nm after excitation at 450 nm and 490 nm. The ratio of fluorescence intensities at these two wavelengths was calculated. The ratiometric fluorescence intensity measurements from the experimental particles were converted to pH by extrapolation to a previously standardized third-order polynomial standard curve by regression analysis. Samples pretreated with conA 10 minutes before addition of experimental particles were used as negative controls for the experiment. Infected samples showed similar acidification patterns as uninfected cells (Figure 3.11). Phagosomal pH at 45 minutes were compared between infected and uninfected experimental groups and were found to be not significantly different. This implies that reduced proteolysis in infected cells is not due to defects in phagosomal acidification.

3.11: pBMMØ infected *in vitro* with PRRSV isolate NVSL 97-7895, produce significantly lower levels of phagosomal ROS than uninfected cells:

Phagosomal proteases are known to be controlled by phagosomal redox conditions[281]. Decreased NOX2-dependent ROS production has been associated with higher levels of proteolysis by redox-mediated activation of cathepsins[76]. To investigate if lower levels of proteolysis in the PRRSV-infected pBMMØ correspond to higher ROS production, levels of membrane permeable phagosomal ROS were measured extracellularly using Amplex Red. Amplex Red is a non-fluorescent substrate, which in the presence of horseradish peroxidase (HRP), reacts with hydrogen peroxide in a stoichiometric ratio of 1:1 to form the fluorescent oxidation product resorufin which emits a red fluorescence at 585 nm when excited at 571 nm. ROS production was determined in pBMMØ 24 hours post-infection with PRRSV isolate NVSL 97-7895, infected at a MOI of 0.1. The cells were activated by pre-treatment with serum-opsonised zymosan for 1 hour, prior to addition of Amplex Red and HRP. Untreated, non-activated cells were used as internal controls for every experiment, in addition to cells treated with 0.5 µM diphenyleneiodonium (DPI), an inhibitor of NOX2, as a negative control. ROS production is directly proportional to the fluorescence from Amplex Red. ROS production from infected pBMMØ was expressed relative to uninfected cells. pBMMØ infected *in vitro* with PRRSV were found to produce significantly lower levels of phagosomal ROS than uninfected cells (Figure 3.10) suggesting that the reduced level of proteolysis observed in infected cells is not controlled by redox parameters such as phagosomal ROS production.

Figure 3.8: pBMMØ infected *in vitro* with PRRSV showed significantly lower levels of phagosomal proteolysis than uninfected cells. pBMMØ infected with PRRSV isolate NVSL 97-7895 at a MOI of 0.1 for 24 hours, and uninfected control cells, were incubated at 37°C with proteolytic reporter experimental particles consisting of IgG-conjugated 3µm silica beads, also conjugated to DQ-BSA and calibration fluor Alexa Fluor 594 in order to quantitate proteolysis. Proteolytic efficiencies of the phagosomes were assessed in real time by measuring the amount of fluorescence liberated from hydrolysis of particle-associated DQ-BSA substrate relative to the calibration fluor Alexa Fluor 594 following phagocytosis. **(A):** Representative real-time traces of phagosomal proteolysis. RFU values are proportional to the degree of proteolysis of the substrate **(B):** Averaged proteolytic activities of infected pBMMØ and conA-treated pBMMØ, relative to untreated, uninfected samples. Data represent results from six independent experiments. To determine the proteolytic activities, the slope of the linear portion of the real-time trace was calculated (from the equation y=mx+c, where y=relative fluorescence, m=slope and x=time) and expressed relative to untreated samples. Error bars represent SEM. P values were calculated using one-way ANOVA. *** represents P<0.001.

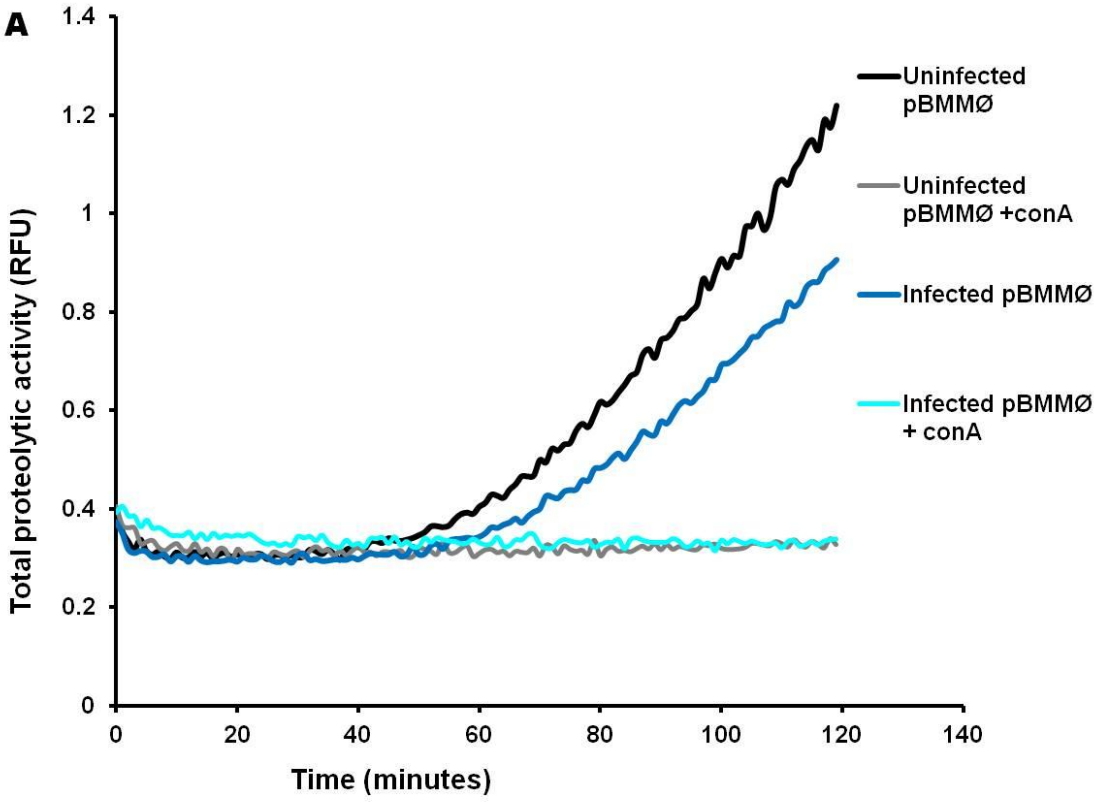
A
Total proteolytic activity (RFU)
Time (minutes)
Uninfected pBMMØ
Uninfected pBMMØ +conA
Infected pBMMØ
Infected pBMMØ + conA

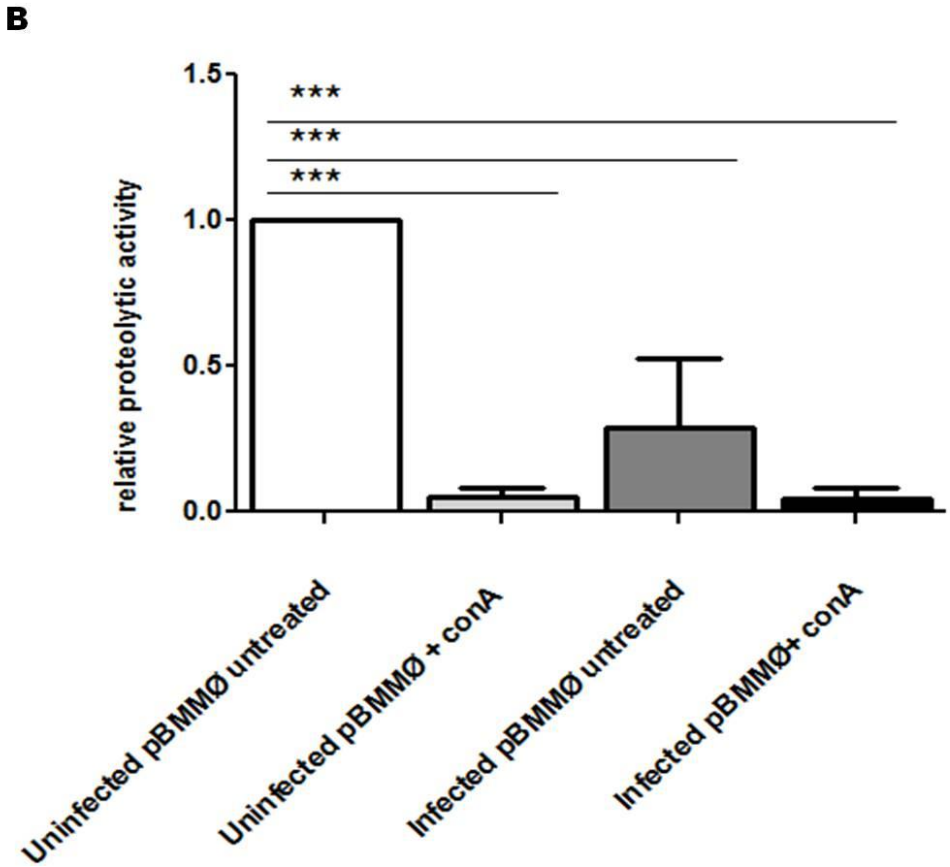
B
relative proteolytic activity
***
***
***
Uninfected pBMMØ untreated
Uninfected pBMMØ + conA
Infected pBMMØ untreated
Infected pBMMØ+ conA

Figure 3.9: pBMMØ infected with PRRSV (NVSL-97-7895) at a MOI of 0.1 showed no significant differences in efficiency of phagocytic uptake than uninfected cells. Cells were incubated 30 minutes at 37°C with experimental particles consisting of 3µm silica beads covalently coupled to human IgG and Alexa Fluor 555, and then assayed for phagocytic index by counting using fluorescence microscopy. To distinguish between ingested and extracellular experimental particles, cells and particles were stained with the vital dye Trypan blue (0.01% v/v in PBS) which quenches fluorescence in extracellular particles. Phagocytic index was calculated as the ratio of the number of experimental particles ingested to the number of extracellular particles. CytochalasinD (5 µM, cytD)-treated cells were used as negative control for the experiment. **(A,B,C,D):** Representative micrographs of untreated uninfected pBMMØ, cytD-treated uninfected cells, untreated infected cells and cytD-treated infected cells, respectively. **(E):** Data represent the average percentage of beads phagocytosed from three independent experiments. Error bars represent SEM. P values were calculated using one-way ANOVA.

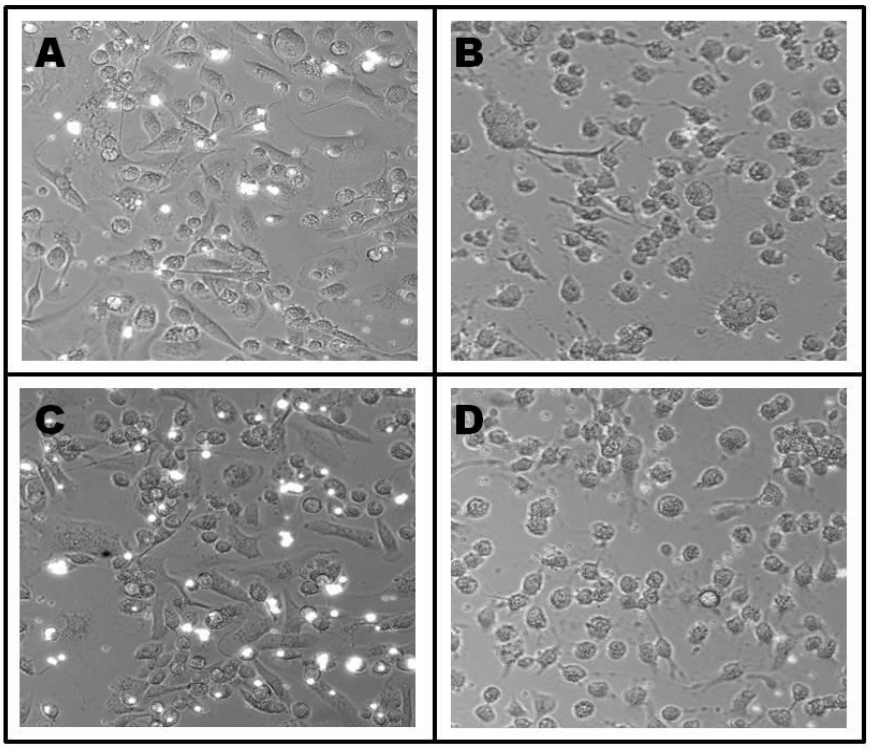
A
B
C
D

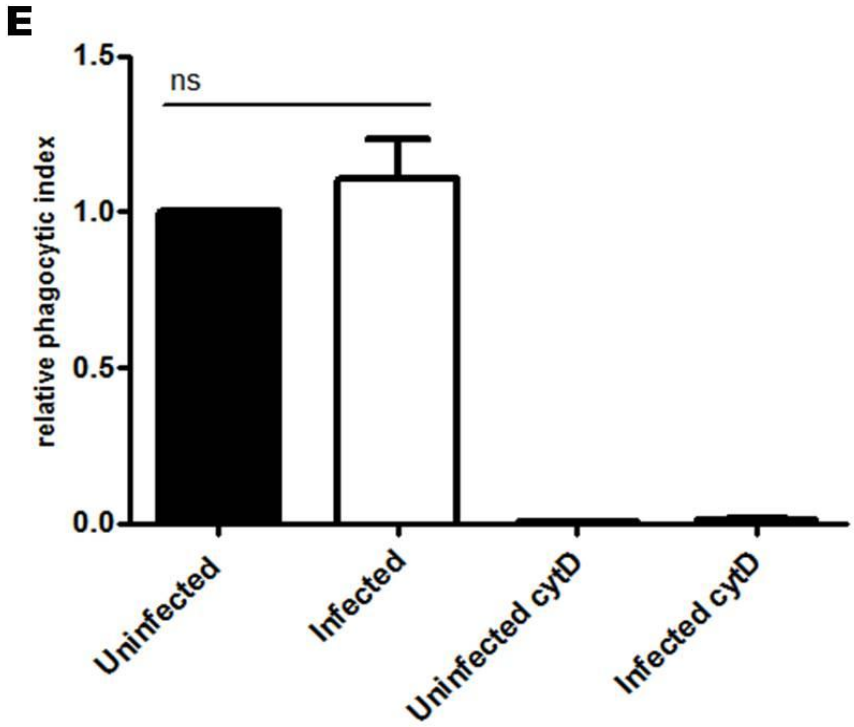
E
1.5
1.0
0.5
0.0
ns
relative phagocytic index
Uninfected
Infected
Uninfected cytD
Infected cytD

Figure 3.10: There is no significant difference in the phagosomal pH between uninfected and PRRSV-infected pBMMØ. Cells were incubated at 37°C with 3 µm silica beads conjugated to IgG and labelled with the pH-sensitive fluor CFSE (λex_1 485 nm, λex_2 450nm; λem 520 nm). Acidification in phagosomes was measured in real time by fluorometric measurement of the CFSE, and calculated using extrapolation to a standard pH curve by linear regression to a third-order polynomial standard curve **(A):** Representative real-time phagosomal acidification profiles. **(B):** Lumenal pH at 45 minutes after internalization of experimental particles. Data represent results from three independent experiments. Error bars represent SEM. P values were determined using one-way ANOVA. *** represents P<0.001.

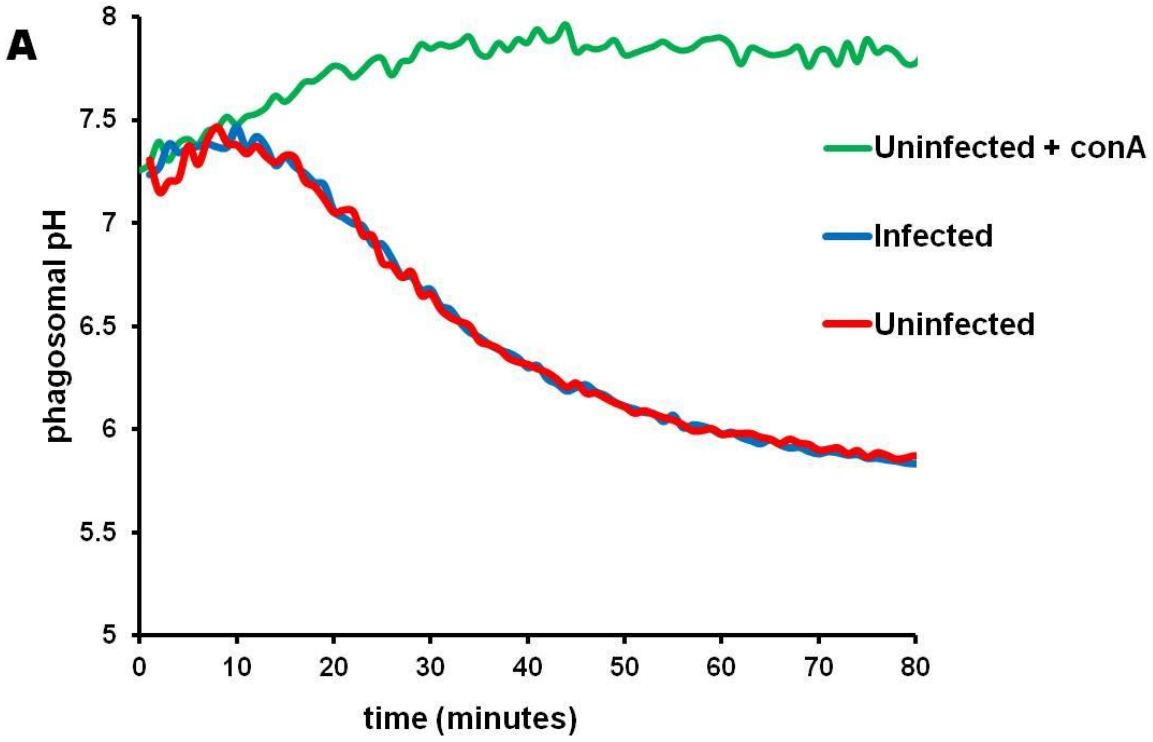
A
8
7.5
7
6.5
6
5.5
5
phagosomal pH
0
10
20
30
40
50
60
70
80
time (minutes)
Uninfected + conA
Infected
Uninfected

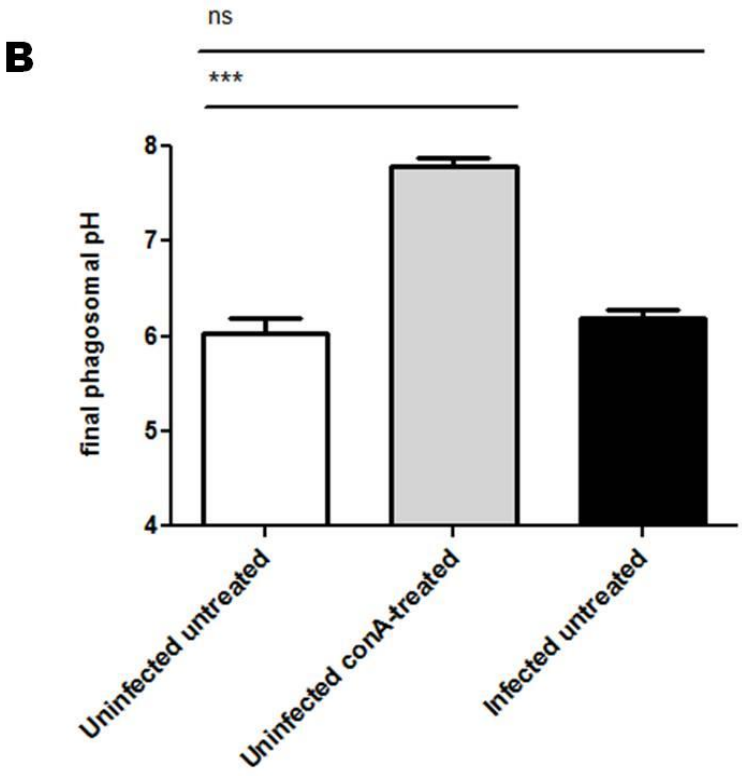
B
ns
***
8
7
6
5
4
final phagosomal pH
Uninfected untreated
Uninfected conA-treated
Infected untreated

Figure 3.11: pBMMØ infected *in vitro* with PRRSV isolate NVSL 97-7895 exhibit significantly lower levels of phagosomal ROS production than uninfected control cells. pBMMØ infected at a MOI of 0.1 for 24 hours, or uninfected controls, were activated by serum-opsonized zymosan at 37°C for one hour, followed by 30 minutes incubation at room temperature with Amplex Red and HRP in the dark. Phagosomal ROS production levels were assayed by measuring the fluorescence intensity (λ_{ex} 550 nm|λ_{em} 615 nm) of extracellular ROS-reacted Amplex Red reagent. Data represent results from three independent experiments. Error bars represent SEM. P values were generated using Student's t-test. * represents P<0.05.

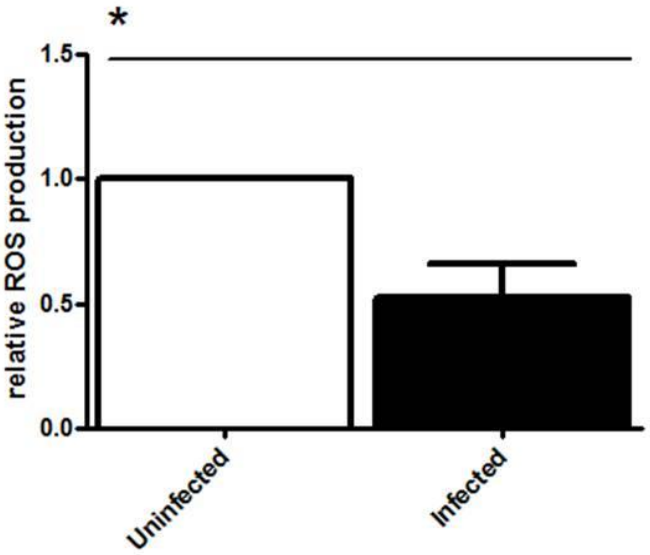
*
1.5
1.0
0.5
0.0
relative ROS production
Uninfected
Infected

3.12: Alveolar macrophages isolated *ex-vivo* from PRRSV-infected gilts exhibit significantly higher levels of proteolysis than alveolar macrophages from uninfected animals:

pBMMØ infected *in vitro* with PRRSV show significantly lower levels of phagosomal proteolysis than uninfected control cells. We wished to determine if porcine alveolar macrophages (PAM), primary targets of PRRSV replication *in vivo,* from PRRSV-infected pregnant gilts have a similar trend of decreased proteolytic capacity in the phagosome. To study this, we utilized the pregnant gilt model of PRRSV infection set up and used by our collaborators at the University of Saskatchewan (Dr. John Harding and colleagues). Pregnant gilts were infected with PRRSV NVSL 97-7895 on gestation day 85. On gestation day 105, 21 days post-infection, the animals were humanely euthanized by cranial captive bolt along with uninfected age-matched control animals (sham-inoculated pregnant gilts). Broncho-alveolar lavage (BAL) samples were extracted from the infected and uninfected animals and shipped to us on ice. The BAL samples were subjected to Ficoll gradient centrifugation and cells deposited at the interface (macrophage/ monocytes/ lymphocyte layer) were isolated, with some cells stained with trypan blue for enumeration, and plated on bacteriological plastic Petri dishes (Figure 2.4). After overnight incubation, only the adherent cells were used for carrying out phagosome lumenal assays. The adherent cells, when examined by light microscopy, exhibited macrophage-like appearance and upon incubation with experimental particles conjugated to IgG, showed enhanced phagocytosis. Since the cells we were observing were isolated from the interface in a density gradient centrifugation of BAL samples, had a macrophage-like

appearance, attached to a plastic surface, and exhibited enhanced phagocytosis of IgG-conjugated experimental particles, we anticipated them to be PAM.

Phagosomal proteolysis was assessed in PAM from infected and uninfected animals using a real-time fluorometric assay based on uptake of proteolytic reporter experimental particles as described in section 3.4. The experimental particles were added to a confluent monolayer of cells at a MOI of 2-3 beads/cell. Cells pretreated with 100 nM conA 10 minutes prior to addition of the beads were used as negative controls for the experiment. Phagosomal proteolysis was found to be significantly higher in PAM isolated from infected animals than those from uninfected control animals (Figure 3.12). Both experimental groups showed the onset of proteolysis at the same time. But the overall proteolytic activities in the PAM isolated from infected pregnant gilts showed a 3-fold increase. This phenotype was ablated to a similar level in infected and uninfected samples by conA treatment. PAM isolated from infected pregnant gilts when pretreated with conA 10 minutes prior to addition of experimental particles showed significantly reduced proteolytic activities compared to untreated PAM from the same animals (Figure 3.12). Over a period of 120 minutes the conA-treated samples barely showed an increase in proteolytic level (Figure 3.12). When pretreated with conA, PAM from infected and uninfected pregnant gilts showed no significant difference in overall proteolytic activities (Figure 3.12).

3.13: Alveolar macrophages from PRRSV-infected gilts show no significant difference in phagocytic index than alveolar macrophages from uninfected animals:

The difference observed in the proteolytic capacity of the PAM between infected and uninfected animals may be due to differential uptake of experimental particles by the cells. To investigate if this is the case, the phagocytic index was calculated in PAM isolated from PRRSV-infected pregnant gilts and compared to those from uninfected control animals. PAM were incubated with experimental particles consisting of 3 µm silica particles conjugated to IgG and Alexa Fluor 633. Phagocytic index was assessed by flow cytometry. Acquisition parameters on the flow cytometer were adjusted such that unstained cells which were not incubated with labelled particles were clustered in the first decade of the histogram thus leaving enough space to identify cells which had phagocytosed beads. Gates were set in an EV-SS (Electronic voltage-Side scatter) plot to include only cells with similar dimensions to macrophages, in order to exclude extracellular beads and cell debris from the analysis. The number of fluorescent experimental particles taken up by a population of cells is given by the percentage of fluorescent events which denotes percentage of cells with ingested beads. PAM from PRRSV-infected pregnant gilts show no significant differences compared to PAM from uninfected control animals in phagocytic uptake of experimental particles (Figure 3.13) suggesting that the difference in proteolysis between the experimental groups is not due to differential particle uptake. Cells treated with cytochalasin D (5 µM) were used as negative controls for the experiment.

3.14: ROS production in alveolar macrophages from PRRSV-infected gilts was not significantly different than from alveolar macrophages from uninfected animals:

High amounts of ROS can lead to inactivation of phagosomal cathepsins, thereby resulting in lower levels of proteolysis[76]. Higher levels of proteolysis can therefore correlate with lower levels of ROS production. To investigate if this is the case, intra-phagosomal ROS production was assayed in PAM isolated from infected pregnant gilts and uninfected control animals. This assay relies on the phagocytic uptake of experimental particles consisting of 3 µm silica beads conjugated to Oxyburst Green H2HFF-BSA (BSA coupled to dihydro-2`,4,5,6,7,7`-hexafluorofluorescein, a oxidation-sensitive fluor), AF594 as a calibration fluor, and IgG for phagocytic uptake, by PAM. Upon phagocytosis and subsequent oxidation, the substrate is converted to a green fluorescent fluorescein product with emission at 530 nm when excited at 488 nm. The calibration fluor remains constant over time. ROS production is proportional to the ratio of the green fluorescence from the oxidized substrate over the red fluorescence from the calibration fluor. Relative ROS production is determined by calculating the slope of the linear portion of the real-time trace. Using this assay, ROS production in PAM from 3 uninfected and 11 PRRSV-infected animals were compared. No statistically significant difference was found between ROS production in these two experimental groups (Figure 3.14). PAM treated with 0.5 µM DPI 10 minutes prior to incubation with experimental particles were used as negative control for the experiment. DPI-treated PAM showed a significant decrease in ROS production than corresponding untreated samples (Figure 3.14). Phagosomal ROS production was also detected in the extracellular milieu in PAM from infected pregnant gilts and uninfected animals

by using Amplex Red reagent. The cells were activated by pre-treatment with serum-opsonised zymosan for 1 hour, prior to addition of Amplex Red and HRP. Untreated, non-activated cells were used as internal controls for every experiment, in addition to cells treated with DPI as a negative control to account for non-phagosomal ROS production. PAM from PRRSV-infected gilts showed no significant difference in ROS production compared to PAM from uninfected animals (Figure 3.14).

Figure 3.12: Porcine alveolar macrophages (PAM) isolated from pregnant gilts infected with PRRSV (isolate NVSL 97-7895) show significantly higher phagosomal proteolysis than PAM from uninfected control animals. Alveolar macrophages were isolated from BAL samples extracted from the pregnant gilts post euthanization. PAM were incubated with experimental proteolysis reporter particles consisting of 3µm silica beads conjugated to self-quenched DQ-BSA, calibration fluor Alexa Fluor 594 and IgG in order to quantify proteolysis. The efficiency of phagosomal proteolysis was assayed in real time by measuring the amount of fluorescence liberated from hydrolysis of particle-associated DQ-BSA substrate relative to the calibration fluor Alexa Fluor 594. **(A):** Representative real-time traces of phagosomal proteolysis in PAM from one experiment consisting of five infected animals and two uninfected animals. RFU values are directly proportional to substrate hydrolysis. **(B):** Proteolytic activities in PAM from infected and uninfected animals can be ablated to a similar degree by conA treatment. Representative real-time traces of phagosomal proteolysis with or without conA treatment in porcine alveolar macrophages isolated from infected and uninfected animals. **(C):** Averaged proteolytic activities of alveolar macrophages isolated from infected animals relative to uninfected control animals from six different experiments (representing 26 infected and 12 uninfected animals). Data represented as a scatter-plot and shows the heterogeneity in proteolysis levels in the infected group. **(D):** Averaged proteolytic activities of alveolar macrophages isolated from infected animals relative to uninfected control animals from six different experiments (representing 26 infected and 12 uninfected animals).To determine bulk proteolytic activities, the slope of the linear portion of the real time trace was calculated (from the equation y=mx+c, where y=relative fluorescence, m=slope and x=time) and expressed relative to untreated samples. Error bars represent SEM. P values were calculated using one-way ANOVA. * represents $P<0.05$.

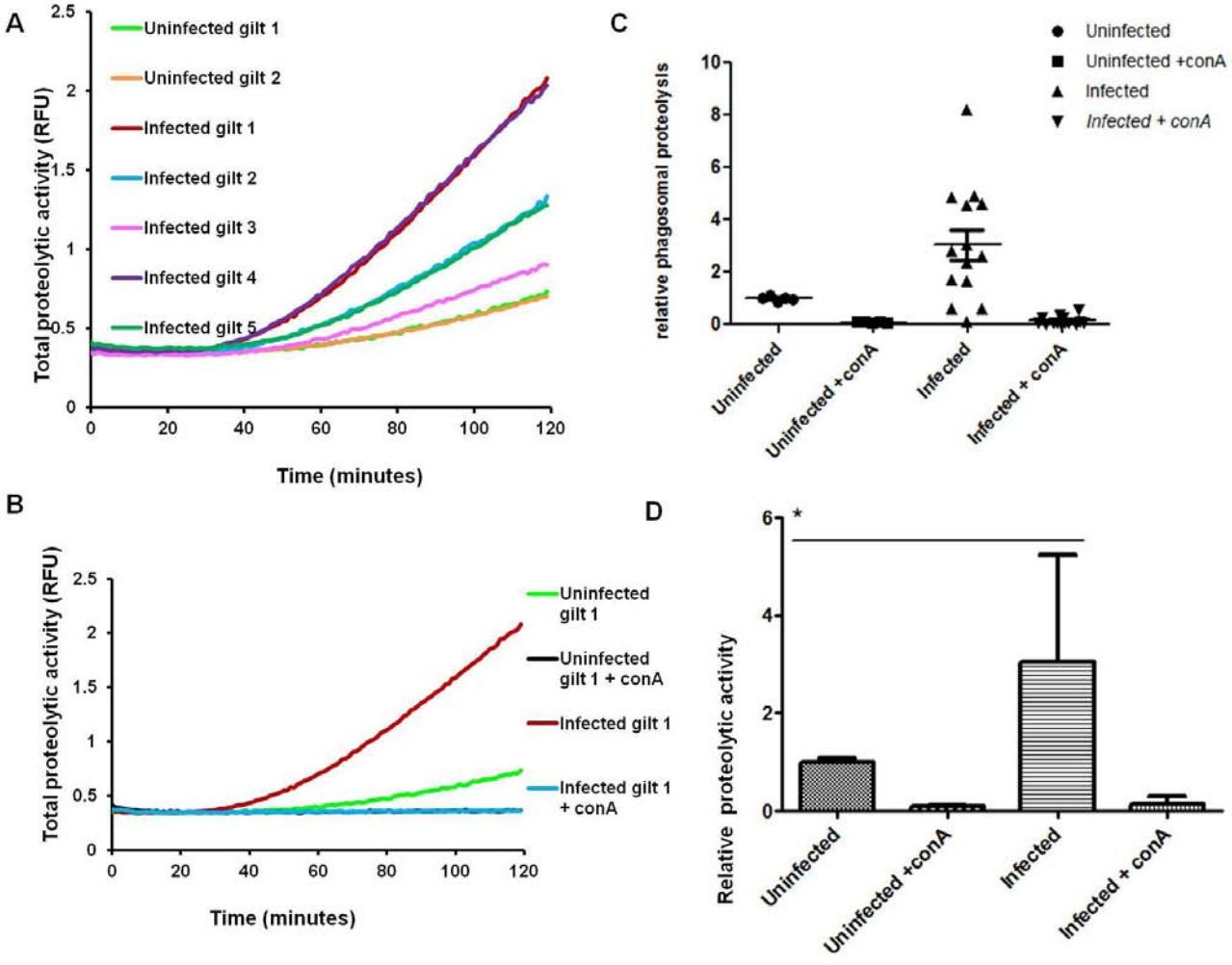
A
Uninfected gilt 1
Uninfected gilt 2
Infected gilt 1
Infected gilt 2
Infected gilt 3
Infected gilt 4
Infected gilt 5
Total proteolytic activity (RFU)
Time (minutes)
C
Uninfected
Uninfected +conA
Infected
Infected + conA
relative phagosomal proteolysis
B
Uninfected gilt 1
Uninfected gilt 1 + conA
Infected gilt 1
Infected gilt 1 + conA
Total proteolytic activity (RFU)
Time (minutes)
D
Relative proteolytic activity
Uninfected
Uninfected +conA
Infected
Infected + conA

Figure 3.13: There is no significant difference in the phagocytic index between alveolar macrophages isolated from PRRSV-infected and uninfected pregnant gilts. Cells were incubated with 3 µm silica beads conjugated to IgG, and labelled with Alexa Fluor 633. Phagocytic index was assessed by flow cytometry. Graph represents percentage of cells exhibiting phagocytosis of experimental particles. Data represent results from three independent experiments. Error bars represent SEM. P values were determined using Student`s t-test.

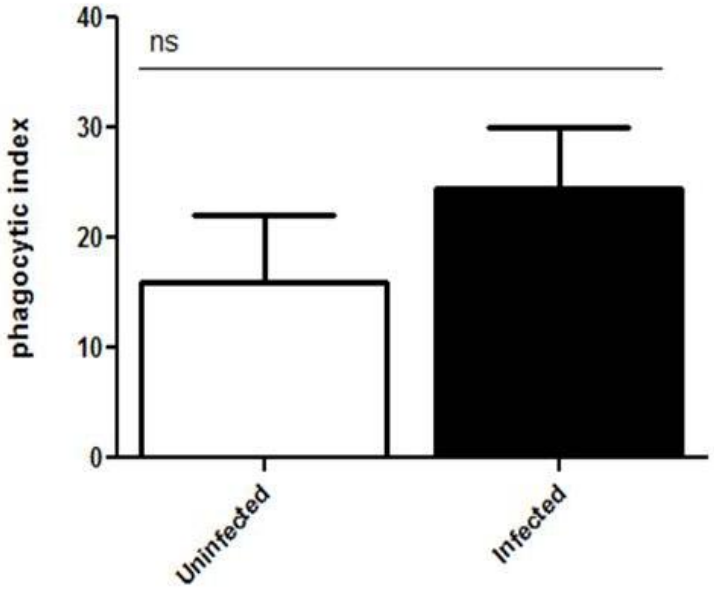
40
30
20
10
0
ns
phagocytic index
Uninfected
Infected

Figure 3.14: Alveolar macrophages isolated from PRRSV-infected pregnant gilts and uninfected control animals showed no significant difference in phagosomal ROS production. **(A):** Phagosomal ROS production was assessed in real-time by measuring the amount of fluorescence liberated from oxidation of particle-associated H2HFF Oxyburst substrate relative to Alexa Fluor 594 after phagocytosis of oxidation-sensitive experimental particles by PAM. Data represent average phagosomal ROS production in PAM isolated from 3 uninfected and 11 infected animals. Error bars represent SEM. P values were calculated using one-way ANOVA. **(B):** Phagosomal ROS in the extracellular milieu was assayed by using Amplex Red reagent. Alveolar macrophages, isolated from PRRSV-infected pregnant gilts, or uninfected controls, were activated by serum-opsonized zymosan at 37°C for one hour, followed by incubation with Amplex Red and HRP. Phagosomal ROS production levels were assayed by measuring the fluorescence intensity (λ_{ex} 550 nm$|\lambda_{em}$ 615 nm) of extracellular ROS-reacted Amplex Red reagent. Data represent average ROS production from 14 infected and 6 uninfected animals. Error bars represent SEM. P values were generated using Student's t-test. * represents P<0.05.

A

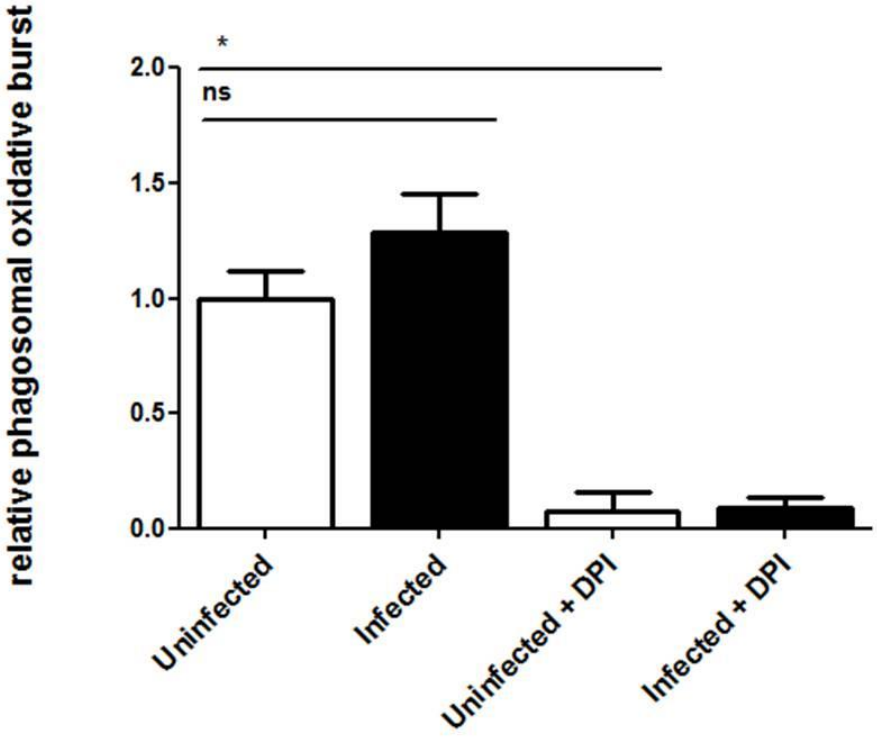
relative phagosomal oxidative burst
*
ns
2.0
1.5
1.0
0.5
0.0
Uninfected
Infected
Uninfected + DPI
Infected + DPI

B

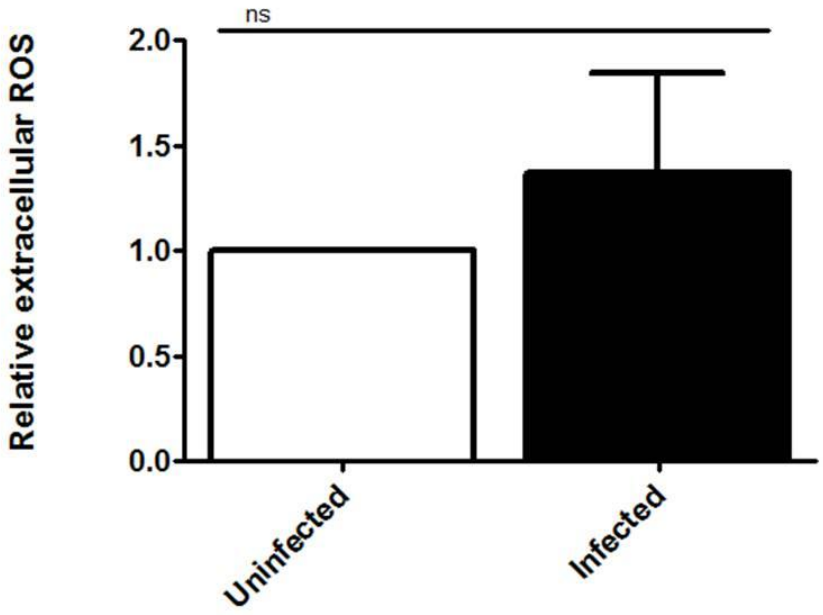
Relative extracellular ROS
ns
2.0
1.5
1.0
0.5
0.0
Uninfected
Infected

CHAPTER 4: DISCUSSIONS

PRRS emerged as a major and devastating disease of the swine industry more than two decades ago[172,173]. Since then, studies have elucidated different aspects of PRRSV biology. However, research in this field still suffers from the lack of a good *in vitro* system that can be used to study the biology of PRRSV infection using a methodical reductionist approach. This thesis addresses this deficit in the field and establishes a new *in vitro* system to study PRRSV infection. Using this newly established *in vitro* system, this study investigates how PRRSV infection alters the phagosomal microenvironment in porcine bone marrow derived macrophages (pBMMØ). This study also investigates how the phagosomal microenvironment changes in *ex-vivo* porcine alveolar macrophages (PAM) isolated from PRRSV-infected pregnant gilts.

4.1: Establishment of a novel *in vitro* system to study PRRSV infection:

4.1.1: Advantages of the established system over the existing systems:

PPRSV, like other Arteriviruses, infects cells of the monocyte/macrophage lineage[180]. In the host animal, PRRSV primarily infects tissue macrophages including alveolar macrophages, pulmonary intravascular macrophages, placental macrophages, and splenic macrophages[202,203,205] . For *in vitro* studies, primary porcine alveolar macrophages, MARC- 145 cells, or genetically modified cell lines are primarily used[209-211,216,217]. Currently, the MARC- 145 cell line is the most popular system for studying PRRSV biology including different aspects of the virus replication cycle. PRRSV is also grown and propagated in MARC- 145 cells for production of live attenuated or killed vaccines[283,284]. MARC- 145 is a kidney epithelial cell line,

and thus not a phagocyte nor a derivative of the monocyte/macrophage lineage[211]. In addition, it is derived from the African green monkey (*Chlorocebus sabaeus),* which is not the natural host of the virus. Hence this system neither represents the host cell type nor the host species of PRRSV. PRRSV uses different receptors for entering MARC- 145 cells than PAM suggesting that the virus may need to adapt to grow in MARC- 145 and this may lead to epitope modification on the virus[1]. Upon PRRSV infection, the cellular proteome of MARC- 145 and PAM are altered differently, suggesting that PRRSV may induce different signaling pathways in these cells[285]. In response to infections and other stress conditions, macrophages secrete or stimulate the secretion of cytokines[60,286]. However, infection of MARC- 145 cells will not result in such an immune response[285]. Overall these properties suggest that infection and replication of PRRSV in MARC- 145 cells is very different from that in natural host cells of the virus and is not ideal for PRRSV propagation; however the low cost, ease of infection and high yields of the virus in these cells make it an attractive option. Various studies have attempted to genetically modify cell lines to make them susceptible to PRRSV infection and replication. Such systems suffer from being derived from mammals different than that of the host species of PRRSV[217,287]. To date, a macrophage cell line such as RAW 267.4 has not been used[288]. Making non-permissive cell lines permissive to PRRSV infection can be a prolonged process requiring a number of cloning and selection steps. Porcine alveolar macrophages, although naturally tropic for the virus, are difficult to isolate, cannot be proliferated in culture, and are susceptible to batch variation and the risk of contaminating pathogens[196,238]. When the host animal is pre-exposed to allergens or pathogens, the population of alveolar macrophages may be partially or totally polarized to a

particular macrophage activation state (classical activation M1, alternative activation M2)[68]. The field of PRRSV biology thus suffers from the dearth of a good *in vitro* system for the study of the virus. In this thesis, a novel *in vitro* system for studying PRRSV biology is established which utilizes productive infection of pBMMØ by PRRSV. Unlike MARC-145 cells, pBMMØ represent the host species of PRRSV and belong to the monocyte/macrophage lineage of cells. Unlike alveolar macrophages, pBMMØ are homogeneous, have proliferative capacity, are relatively easy to isolate and grow, and are less susceptible to batch variations as they are differentiated *in vitro* from hematopoietic stem cells. Under appropriate culture conditions, bone marrow derived macrophages do not exhibit any skews towards M1 or M2 activation[68]. Secreted virus collected from pBMMØ can form plaques on MARC-145 cells indicating that the infection of pBMMØ is productive leading to formation of functional virions. We found PRRSV can be propagated in pBMMØ and there is approximately a 40-fold increase in the yield titre of the virus relative to the inoculum titre (Figure 3.6).

4.1.2: L929 cell supernatant can differentiate porcine bone marrow cells into bone marrow derived macrophages:

pBMMØ are differentiated from bone marrow cells *in vitro*. Unlike for mice, procuring porcine-specific antibodies and reagents can be challenging as their commercial availability is limited. Conditioned supernatant from L929 cell culture which contains murine M-CSF[273] is regularly used to differentiate murine bone marrow cells into macrophages *in vitro*[65]. In various studies L929 cell supernatant has been used to differentiate bone marrow cells into bone marrow derived macrophages in species other than mouse[274]. In pigs, L929 cell supernatant has

been used to differentiate peripheral blood mononuclear cells into macrophages[275]. Human recombinant M-CSF has been used to differentiate porcine bone marrow cells into bone marrow derived macrophages[276]. In addition to sequence analysis indicating 77% identity between porcine and murine M-CSF at the amino acid level, these studies provided us the preliminary incentive to use L929 cell supernatant to differentiate porcine bone marrow cells into macrophages. The complex series of reactions leading to differentiation of macrophages from precursor monocytes is initiated when M-CSF binds to its receptor CSF -1R[289]. Crystal structure analysis of murine and human M-CSF indicates that it bind to CSF-1R through its N-terminal receptor binding domain[290-292]. That M-CSF from one specific species can successfully differentiate bone marrow cells of a different species suggests that M-CSF can also bind to CSF-1R of different but related species.

4.1.3: Fluorometric analysis of phagosomal microenvironment can be used as functional assays to identify macrophages:

Macrophages have been traditionally distinguished from other immune cells of the monocyte/macrophage lineage by the cell surface molecules they express. However, cells of the monocyte/macrophage lineage often express overlapping cell surface markers. For example, in mice CD11b is expressed by both macrophages and dendritic cells, CD14 is a marker of monocytes but is also expressed by macrophages[27]. In mice, macrophage populations are commonly distinguished by their expression of F4/80[25]. Various studies have developed monoclonal antibodies against porcine monocytes and macrophages[293]. However their availability and specificity to macrophages remains doubtful. Some of these monoclonal

antibodies designed to detect macrophages have shown high specificity to a particular subset of tissue macrophages and fail to detect macrophages from other tissues[294]. Given the paucity in the availability of reagents suitable for detection of known surface markers of porcine macrophages, we decided to use an arsenal of fluorometric assays to functionally characterize the established primary culture of porcine bone marrow derived macrophages in addition to observation of cell morphology using a microscope. These assays are designed to quantify different aspects of the phagosomal microenvironment such as proteolysis, ROS production, acidification, etc[270-272]. Using these assays, we found that porcine bone marrow derived macrophages exhibited FcR-mediated phagocytosis, had a higher rate of phagocytosis of opsonised experimental particles relative to non-opsonised particles (Figure 3.2). pBMMØ showed regular patterns of phagosomal acidification and phagosomal proteolysis on phagocytosis of experimental particles. Acidification and proteolysis could be controlled in pBMMØ using v-ATPase inhibitor, a finding consistent with that in murine BMMØ[65,271].

4.1.4: Future directions Aim 1:

In this study PRRSV isolate NVSL 97-7895 was successfully propagated in pBMMØ. It can be anticipated that PRRSV infection in pBMMØ closely resembles that in PAM, especially with regard to receptors used and immune responses generated. However, for pBMMØ to be accepted across the scientific community as a model system for propagation and study of PRRSV, it is essential to test several properties of the system. MARC-145 cells and PAM are susceptible to both North American and European genotypes of PRRSV including all field isolates of PRRSV tested so far[295,296]. Different field isolates of PRRSV are regularly isolated

using PAM. The susceptibility of pBMMØ to different PRRSV isolates needs to be tested. In addition to NVSL 97-7895 which represents a highly virulent type II genotype, a prototype of type I isolate needs to be tested for its ability to propagate in pBMMØ. Duplication time of PRRSV in different cells is found to vary between 36-48 hours[297,298]. Replication dynamics and duplication time of PRRSV in pBMMØ will serve as useful information for using this model. This can be tested by collecting cell-associated and secreted virus from PRRSV-infected pBMMØ at different time points and titrating the virus on MARC--145 cells. Titer assays may include $TCID_{50}$ and/or plaque assays. In this study, we use plaque assay to titrate PRRSV production. Though $TCID_{50}$ assays are becoming increasingly popular, quantification of virus by $TCID_{50}$ is comparatively more subjective and prone to user-error[299]. Plaque assays provide a more easily quantitated and consistent method of virus titration.

Recent studies have revealed that innate immune responses to various stimuli in humans, particularly in human macrophages, are more closely related to that in pigs compared to mice. In human macrophages, unlike in mice, iNOS is not induced in response to LPS; similarly, in pigs, iNOS-dependent nitric oxide production is not observed in LPS stimulation, even with IFN-γ priming[276,300]. In humans, expression and activation of TLRs, particularly TLR9, in response to viral infection has been found to be different from mice and similar to pigs[300] . A simple protocol for differentiating, growing, and characterizing porcine bone marrow derived macrophages as described in this thesis may be very useful to the growing number of studies which are using porcine macrophages to study the basics of macrophage biology.

4.2: pBMMØ when infected in vitro with PRRSV show different phagosomal lumen properties:

4.2.1: PRRSV-infected pBMMØ exhibit significantly lower levels of phagosomal proteolysis:

In this study we show that pBMMØ, when infected *in vitro* with PRRSV at a MOI of 0.1, show significantly lower levels of phagosomal proteolysis than uninfected cells (Figure 3.8). Phagosomal proteolysis in infected cells was controllable by conA suggesting that the levels of phagosomal prtoteolysis in these cells were lower but not absent (Figure 3.8).The first question we asked was if the infected macrophages are undergoing apoptosis and/or necrosis and are thereby shutting down most of their cellular functions including phagosomal proteolysis. This question was further stimulated by the finding that the PRRSV-infected pBMMØ also exhibited significantly lower levels of phagosomal ROS production (Figure 3.11). Host immune responses against virus infection are known to trigger apoptosis in host cells as a mechanism of eliminating the virus[301-303]. Viruses, on the other hand, have evolved various strategies to prevent apoptosis of their target cells[304]. In this study we found no significant difference between the number of cells undergoing apoptosis, necrosis, or both in infected and uninfected population of cells, 24 hours post infection. Various studies have detected apoptosis in cells infected *in vitro* with PRRSV and also in tissues derived from PRRSV-infected animals. The results vary depending on the cell type and the time point of assessment[305-307]. Host cells have been reported to undergo apoptosis during later stages of virus infection. The findings in this thesis are in accordance with previous reports which show that during early stages of PRRSV

infection, apoptosis of the host cells is prevented[308]. In porcine alveolar macrophages PRRSV infection has been shown to protect against drug-induced apoptosis[308]. During PRRSV infection, bystander cells have been reported to undergo apoptosis thereby contributing to the presence of apoptotic cells in infected tissues[308]. MARC- 145 cells, when infected with PRRSV, have been reported to undergo necrosis rather than apoptosis[308]. In this study, no significant cell death could be detected 24 hours post-infection in PRRSV-infected pBMMØ. All phagosomal assays were carried out at this time point, indicating that apoptosis or necrosis of host cells is not responsible for any of the observed phenotypes.

Several virus infections have been known to affect the efficiencies of phagocytic uptake in infected macrophages thereby directly reducing microbicidal capacities of the infected macrophages[309,310]. In PRRSV infection decreased phagocytic uptake in infected macrophages would directly explain susceptibility of the macrophages and hence the infected animals to secondary pathogens. In this study, we sought to determine if decreased phagocytic uptake was a cause of decreased phagosomal proteolysis in infected cells. We found no significant difference in the phagocytic index of infected and uninfected pBMMØ suggesting that the decreased proteolysis is not due to differential particle uptake (Figure 3.9). These findings indicate that the reduced phagosomal proteolysis observed is likely to be resulting from reduced phago-lysosomal protease expression or activity, rather than inability of the macrophage to phagocytose experimental particles.

Expression of phagosomal proteases is controlled at various levels including transcriptional, translational, post-translational modifications including pro-domain removal,

interactions with regulatory proteins such as cystatin, or activation or inhibition through modulation of the phagosomal microenvironment including acidification and redox conditions[76,281]. Phago-lysosomal and endosomal proteases require an acidic pH for optimal activity[281]. Defects in regular phagosomal acidification patterns can lead to protease inactivity. In this study we found no significant difference in the final phagosomal pH (45 minutes after experimental particle phagocytosis) between infected and uninfected pBMMØ (Figure 3.10). Infected pBMMØ also show regular patterns of acidification suggesting that it is highly unlikely that they have a defect in phagosomal maturation. This finding thereby suggests that decreased proteolysis is not due to pH-mediated inactivation of phagosomal proteases. PRRSV is known to enter host cells through clathrin-mediated endocytosis[220,221]. Acidification of the endo-phagolysosomal system is anticipated to provide one of the triggers for the escape of the virus from the endosomal system into the cell in a CD163-dependent fashion[217,220,221]. Hence it is highly unlikely that the virus infection would prevent acidification, as in case of such an event, it would prevent its own escape and propagation. Hence our findings support the previous reports which suggest (through the use of inhibitors and drugs) that low pH is required for the virus escape and uncoating[220]. However, no study has previously directly measured the endosomal or phagosomal pH in real time in PRRSV-infected cells.

Viral infections are known to polarize macrophages to classical activation particularly by inducing expression of IFNγ. Classically activated macrophages are distinguished by their high respiratory burst[68]. NOX2-dependent ROS production has been reported to negatively regulate the expression of cysteine cathepsins in the phagosomes through redox-mediated control[76,281].

In this study we found that infected cells have significantly lower levels of ROS production which if anything should correspond to an increase and not a decrease in phagosomal proteolysis. Hence phagosomal proteases are not negatively regulated by increased ROS production in PRRSV-infected pBMMØ. Lower ROS production in macrophages is one of the possible explanations as to why macrophages in PRRSV-infected animals exhibit poor microbicidal abilities, making these animals susceptible to secondary infections.

4.2.2: Future directions Aim 2:

This study describes how phagosomal proteolysis decreases on PRRSV infection. Also in this study, we can rule out apoptosis, differential particle uptake, inhibition of phagosomal acidification and respiratory burst-mediated control of phagosomal proteolysis in PRRSV-infected samples. Cathepsins (cysteine and aspartic) are the most important group of phago-lysosomal proteases. Using specific cathepsin substrates conjugated to experimental particle and fluorescent reporters, specific activities of the cathepsins can be compared between PRRSV-infected and uninfected experimental groups[270-272]. In the absence of well-standardized monoclonal antibodies against porcine cathepsins, their expression levels can be compared at the mRNA level between infected and uninfected pBMMØ using Q-PCR.

Proteolysis of three-dimensionally folded protein essentially involves two steps – reduction of its disulfide bonds to convert the protein into a linear peptide and cleavage of the linear peptide into smaller peptides by proteases. The two processes are not necessarily sequential and may occur simultaneously[76,281]. Proteases act on specific amino acid substrates. If due to three-dimensional folding, such substrates are not exposed to reduction by lumenal

reductases, and this situation may lead to reduced proteolysis levels. It will be interesting to compare the levels of disulfide reduction in real time between PRRSV-infected and uninfected pBMMØ.

As the phagosome matures, it recruits proteases from the endo-lysosomal system with which it continually undergoes a series of fission and fusion reactions. Defects or delay in phagosome-lysosome fusion lead to defects in protease acquisition by the phagosome. Hence this will lead to decreased phagosomal proteolysis. Using a well-standardized FRET-based fluorometric assays[271] it will be interesting to compare the dynamics of phagosome-lysosome fusion in PRRSV-infected and uninfected pBMMØ.

Phagosomal proteolysis is one of the major functions of macrophages and is fundamental to the cell's ability to process and present antigens in complex with MHC class II molecules to CD4+ T cells[168]. In addition, macrophages can also present peptides via the MHC class I pathway to CD4+ T cells[168]. Not all peptides are presented. How proteins are degraded at preferred sites and which peptides get presented has been a topic of intense research[168]. Antigen processing leading to the generation and presentation of immunodominant peptides is controlled at various levels. One of the factors contributing to the control of antigen processing is the level of phagosomal proteolysis. Lower phagosomal proteolysis can imply defects in antigen processing and antigen presentation by macrophages. At the same time, higher phagosomal proteolysis can lead to destruction of immunodominant epitopes. It will be interesting to investigate how PRRSV-infected macrophages process standard peptide antigens and if a defect in phagosomal proteolysis correlates to a defect in antigen processing and

presentation by these cells. In addition to macrophages, dendritic cells are the main antigen presenting cells in the body. Dendritic cells are also the main cells responsible for triggering T-cell proliferation. PRRSV-infected animals have been reported to show a delayed T-lymphocyte proliferation which may co-relate with defects in antigen processing and presentation by dendritic cells. It will therefore be interesting to investigate antigen processing and presentation by dendritic cells in PRRSV infection.

Virus infections have been known to skew macrophage populations to their deactivating subset – characterized by production of high levels of IL10, TGF-β and low levels of phagosomal ROS and low levels of MHC II expression[68]. PRRSV infection has been correlated to high levels of IL10 production suggesting that the macrophages may have been polarized to their deactivating subsets[253,254]. IL10 is known to have an inhibitory effect on ROS production in macrophages[56,311]. However, no study has looked into phagosomal parameters such as phagosomal proteolysis and phagosomal acidification in deactivating IL10-stimulated macrophages. This will be an interesting research question to pursue in the future.

4.3 : Porcine alveolar macrophages (PAM) isolated from PRRSV-infected pregnant gilts showed significantly higher levels of phagosomal proteolysis than cells isolated from healthy animals:

PAM isolated from PRRSV-infected pregnant gilts showed significantly higher levels of phagosomal proteolysis than porcine alveolar macrophages isolated from healthy animals (Figure 3.12). We found no significant difference in the ability of infected and uninfected PAM

to phagocytose experimental particles, suggesting that higher levels of proteolysis in PAM from infected animals is not due to increased phagocytic uptake (Figure 3.13). We also found no significant difference in ROS production between PAM from infected and uninfected animals suggesting that higher proteolysis is not mediated by a decrease in NOX2-dependent ROS production which facilitates a reductive environment, leading to activation of cysteine cathepsins (Figure 3.14). Preliminary results suggest that PAM from infected and uninfected animals showed regular acidification patterns. Also it is theoretically unlikely that PRRSV-infected PAM will exhibit defects in phagosomal acidification as the virus needs an acidic pH for uncoating and escape.

Tissue macrophages in a particular tissue may exhibit certain specialized functions. Alveolar macrophages are body's first line of defense in clearing invading pathogens and foreign debris entering through the airway. Alveolar macrophages also are among the first immune cells to trigger antiviral responses against respiratory viruses[312]. No study has however, directly quantified phagosomal proteolysis in alveolar macrophages in response to viral infections. To see if higher phagosomal proteolysis is an inherent characteristic of alveolar macrophages, alveolar macrophages isolated from the uninfected control pregnant gilts used for this study was infected *in vitro* using various PRRSV titres. The phagosomal proteolysis was compared in uninfected and *in vitro* infected PAM. *In vitro*-infected PAM showed lower levels of phagosomal proteolysis (data not shown), and thus resembled *in vitro* infection of pBMMØ by PRRSV. This indicates direct infection of PAM by PRRSV is not responsible for the observed increased proteolysis. Also on comparison of levels of proteolysis between PAM from

uninfected pregnant gilts and pBMMØ, PAM showed lower proteolysis levels (data not shown), thereby indicating that higher proteolysis is not a tissue-specific property of alveolar macrophages.

The observed levels of higher proteolysis in PAM isolated from infected pregnant gilts is apparently in contrast to the results obtained with *in vitro* PRRSV infection, where PRRSV-infected pBMMØ showed lower levels of proteolysis (Figure 3.8). A number of factors can be contributing to this apparent discrepancy in data, including heterogeneity of the two macrophage population, cytokine milieu and activation states of the macrophages and presence of infiltrating phagocytes. pBMMØ and PAM are heterogeneous in aspects of origin, receptors expressed and ambient cytokine milieu[27]. Bone marrow cells differentiated *in vitro* in culture resembles macrophages derived from circulating monocytes in the body. Alveolar macrophages, on the other hand, are known to be derived from circulating monocytes as well as through local proliferation[40,88,91]. In adults, hematopoiesis is restricted to bone marrow. However, hematopoiesis also occurs in embryonic yolk sac and fetal liver before birth[27]. The origin of alveolar macrophages can be traced to hematopoietic cells in adult bone marrow as well as to that in embryonic sac and fetal liver. Alveolar macrophages are also known to express a wide range of PRRs compared to other tissue macrophages[40,88,91]. To avoid generation of proinflammatory responses to inhaled particulate matter, alveolar macrophages are continuously bathed in a deactivating cytokine mileu consisting of IL 10 and TGFβ[57]. The differences in proteolysis levels may just stem from the heterogeneity of pBMMØ and PAM. However, preliminary findings show that PAM infected *in vitro* with PRRSV show lower levels of

phagosomal proteolysis (data not shown) suggesting that something more than heterogeneity of the two macrophage population is contributing to the observed phenotype. PRRSV infection in pBMMØ may more closely resemble infection of one of the other tissue macrophages (such as splenic or placental) by PRRSV. In response to a proinflammatory conditions such as a virus infection, phagocytes may infiltrate into the alveolar tissues and may contribute to differences observed in phagosomal proteolysis (discussed in 4.3.1). The cytokine milieu and activation state of the macrophages may also contribute to the differences observed in phagosomal proteolysis (discussed in 4.3.1). Overall, we are looking at two different systems. The *in vitro* model of PRRSV infection is useful to study different aspects of the infection using a methodical and reductionist approach. Whereas the pregnant gilt infection model is a complex system. Studying both the systems is important as without a rudimentary knowledge about what is happening in a reductionist system, it is difficult to study a holistic complex system. More experiments (as discussed in 4.3.1) have to be performed to fit in different parts of the puzzle together.

4.3.1: Future directions Aim 3:

Virus infections are primarily pro-inflammatory and can recruit various immune cells to the site of inflammation. So is the observed phenotype of higher phagosomal proteolysis contributed by a different cell type such as dendritic cells, or circulating monocytes. It is highly unlikely that we are looking at a dendritic cell or neutrophil population as only cells that adhered to bacteriological plastic overnight were used for the assay. Adherence to

bacteriological plastic ware is a property of macrophages which has been frequently exploited for its purification from other cells[313,314]. Lung diseases have been often associated with high levels of infiltrating macrophages into the lungs. Infiltrating macrophages may be polarized to an alternatively activated state[68]. Alternatively activated macrophages have been known to exhibit higher phagosomal proteolysis[76]. PRRSV infection in later stages induces apoptosis in the host cells as well as in bystander cells in the infected issue[308]. Presence of apoptotic and necrotic cells in the infected tissue may be compared to a later stage of an inflammatory reaction. To prevent excessive and unneccessary tissue damage, a severe inflammatory immune response is usually followed by infiltration of alternatively activated macrophages to the inflamed site[68]. Alternatively activated macrophages are in particular known for their functions of tissue repair and healing[68]. It will be interesting to investigate if we are looking at an M2-skewed macrophage population. This may be determined by testing for expression of arginase mRNA which is a hallmark of M2 macrophages. Macrophages are known to exhibit a considerable amount of plasticity of activation states. In various disease states, tissue macrophages have been reported to exhibit features common to more than one activation state. Also it will be interesting to test what percentage of the cells present in the BAL sample from the infected pregnant gilt is actually infected by PRRSV. This will indicate if the observed phenotype is due to PRRSV-infected cells or potentially bystander or infiltrating cells. This can be achieved by staining with fluorescently conjugated SDOW17 anti-PRRSV antibody and analyzing the samples by flow cytometry.

4.4: Overall future directions:

In this thesis, with PRRSV infection of alveolar macrophages as a model, we attempted to study what functional changes occur in the phagosomal lumen under proinflammatory conditions mediated by a virus infection. Many viruses including HIV are macrophage-tropic and exploit the endo/phagolysosmal system of the host cell for infection and propagation purposes. Influenza virus causing outbreaks and significant morbitidy and mortality worldwide infects alveolar macrophages. As in PRRSV-infected animals, humans infected with influenza virus exhibit immunosuppression and susceptibility to secondary bacterial infections. Other macrophage-tropic viruses that impair macrophage function and cause significant morbidity include Ebola, Dengue, and Chikungunya viruses[315], among others[316]. No study has previously investigated changes in phagosomal function in a macrophage during a virus infection. Using PRRSV infection as a model we showed that the phagosomal microenvironment is considerably modified in a virus infection. In the future, it will be interesting to investigate if in other virus infections, the phagosomal microenvironment is altered in a similar fashion, which can contribute significantly to study of the pathogenesis of these diseases. Similar analysis of these basic research problems will generate useful information and will contribute to the global understanding of virus infections in the macrophage.

1 Van Breedam, W. *et al.* Porcine reproductive and respiratory syndrome virus entry into the porcine macrophage. *J Gen Virol* **91**, 1659-1667, doi:10.1099/vir.0.020503-0 vir.0.020503-0 [pii] (2010).
2 Tauber, A. I. Metchnikoff and the phagocytosis theory. *Nat Rev Mol Cell Biol* **4**, 897-901, doi:10.1038/nrm1244nrm1244 [pii] (2003).
3 Solomon, J. M., Rupper, A., Cardelli, J. A. & Isberg, R. R. Intracellular growth of Legionella pneumophila in Dictyostelium discoideum, a system for genetic analysis of host-pathogen interactions. *Infect Immun* **68**, 2939-2947 (2000).
4 Lichanska, A. M. & Hume, D. A. Origins and functions of phagocytes in the embryo. *Exp Hematol* **28**, 601-611, doi:S0301-472X(00)00157-0 [pii] (2000).
5 Elrod-Erickson, M., Mishra, S. & Schneider, D. Interactions between the cellular and humoral immune responses in Drosophila. *Curr Biol* **10**, 781-784, doi:S09609822(00)00569-8 [pii] (2000).
6 Sansonetti, P. Phagocytosis of bacterial pathogens: implications in the host response. *Semin Immunol* **13**, 381-390, doi:10.1006/smim.2001.0335 S1044-5323(01)90335-5 [pii] (2001).
7 Vyas, J. M., Van der Veen, A. G. & Ploegh, H. L. The known unknowns of antigen processing and presentation. *Nat Rev Immunol* **8**, 607-618, doi:10.1038/nri2368 nri2368 [pii] (2008).
8 Tam, M. A., Rydstrom, A., Sundquist, M. & Wick, M. J. Early cellular responses to Salmonella infection: dendritic cells, monocytes, and more. *Immunol Rev* **225**, 140-162, doi:10.1111/j.1600-065X.2008.00679.x IMR679 [pii] (2008).
9 Erwig, L. P. & Henson, P. M. Clearance of apoptotic cells by phagocytes. *Cell Death Differ* **15**, 243-250, doi:4402184 [pii] 10.1038/sj.cdd.4402184 (2008).
10 Ricardo, S. D., van Goor, H. & Eddy, A. A. Macrophage diversity in renal injury and repair. *J Clin Invest* **118**, 3522-3530, doi:10.1172/JCI36150 (2008).
11 Rappolee, D. A., Mark, D., Banda, M. J. & Werb, Z. Wound macrophages express TGF-alpha and other growth factors in vivo: analysis by mRNA phenotyping. *Science* **241**, 708-712 (1988).
12 Rabinovitch, M. Professional and non-professional phagocytes: an introduction. *Trends Cell Biol* **5**, 85-87, doi:S0962892400889552 [pii] (1995).
13 Wakefield, J. S. & Hicks, R. M. Erythrophagocytosis by the epithelial cells of the bladder. *J Cell Sci* **15**, 555-573 (1974).
14 Banchereau, J. & Steinman, R. M. Dendritic cells and the control of immunity. *Nature* **392**, 245-252, doi:10.1038/32588 (1998).
15 Phillipson, M. & Kubes, P. The neutrophil in vascular inflammation. *Nat Med* **17**, 1381-1390, doi:10.1038/nm.2514 nm.2514 [pii] (2011).
16 Ley, K., Laudanna, C., Cybulsky, M. I. & Nourshargh, S. Getting to the site of inflammation: the leukocyte adhesion cascade updated. *Nat Rev Immunol* **7**, 678-689, doi:nri2156 [pii] 10.1038/nri2156 (2007).

17 Dahlgren, C. & Karlsson, A. Respiratory burst in human neutrophils. *J Immunol Methods* **232**, 3-14, doi:S0022-1759(99)00146-5 [pii] (1999).
18 Steinman, R. M. Decisions about dendritic cells: past, present, and future. *Annu Rev Immunol* **30**, 1-22, doi:10.1146/annurev-immunol-100311-102839 (2012).
19 Therrien, D., St-Pierre, Y. & Dea, S. Preliminary characterization of protein binding factor for porcine reproductive and respiratory syndrome virus on the surface of permissive and non-permissive cells. *Arch Virol* **145**, 1099-1116 (2000).
20 Hume, D. A. *et al.* The mononuclear phagocyte system revisited. *J Leukoc Biol* **72**, 621-627 (2002).
21 Alexander, P. The role of macrophages in tumour immunity. *J Clin Pathol Suppl (R Coll Pathol)* **7**, 77-82 (1974).
22 Wynn, T. A., Chawla, A. & Pollard, J. W. Macrophage biology in development, homeostasis and disease. *Nature* **496**, 445-455, doi:10.1038/nature12034 nature12034 [pii] (2013).
23 Murray, P. J. & Wynn, T. A. Protective and pathogenic functions of macrophage subsets. *Nat Rev Immunol* **11**, 723-737, doi:10.1038/nri3073 nri3073 [pii] (2011).
24 Wynn, T. A. & Barron, L. Macrophages: master regulators of inflammation and fibrosis. *Semin Liver Dis* **30**, 245-257, doi:10.1055/s-0030-1255354 (2010).
25 Austyn, J. M. & Gordon, S. F4/80, a monoclonal antibody directed specifically against the mouse macrophage. *Eur J Immunol* **11**, 805-815, doi:10.1002/eji.1830111013 (1981).
26 Dijkstra, C. D., Van Vliet, E., Dopp, E. A., van der Lelij, A. A. & Kraal, G. Marginal zone macrophages identified by a monoclonal antibody: characterization of immuno- and enzyme-histochemical properties and functional capacities. *Immunology* **55**, 23-30 (1985).
27 Gordon, S. & Taylor, P. R. Monocyte and macrophage heterogeneity. *Nat Rev Immunol* **5**, 953-964, doi:10.1038/nri1733 (2005).
28 Shioi, A., Ross, F. P. & Teitelbaum, S. L. Enrichment of generated murine osteoclasts. *Calcif Tissue Int* **55**, 387-394 (1994).
29 Teitelbaum, S. L., Tondravi, M. M. & Ross, F. P. Osteoclasts, macrophages, and the molecular mechanisms of bone resorption. *J Leukoc Biol* **61**, 381-388 (1997).
30 Naito, M., Hasegawa, G., Ebe, Y. & Yamamoto, T. Differentiation and function of Kupffer cells. *Med Electron Microsc* **37**, 16-28, doi:10.1007/s00795-003-0228-x (2004).
31 Tremblay, M. E. *et al.* The role of microglia in the healthy brain. *J Neurosci* **31**, 16064-16069, doi:31/45/16064 [pii] 10.1523/JNEUROSCI.4158-11.2011 (2011).
32 Smythies, L. E. *et al.* Human intestinal macrophages display profound inflammatory anergy despite avid phagocytic and bacteriocidal activity. *J Clin Invest* **115**, 66-75, doi:10.1172/JCI19229 (2005).
33 Barnes, M. J. & Powrie, F. Regulatory T cells reinforce intestinal homeostasis. *Immunity* **31**, 401-411, doi:10.1016/j.immuni.2009.08.011 S1074-7613(09)00369-0 [pii] (2009).
34 Wood, G. W. Macrophages in the thymus. *Surv Immunol Res* **4**, 179-191 (1985).

35 Esashi, E., Sekiguchi, T., Ito, H., Koyasu, S. & Miyajima, A. Cutting Edge: A possible role for CD4+ thymic macrophages as professional scavengers of apoptotic thymocytes. *J Immunol* **171**, 2773-2777 (2003).
36 den Haan, J. M. & Kraal, G. Innate immune functions of macrophage subpopulations in the spleen. *J Innate Immun* **4**, 437-445, doi:10.1159/000335216 000335216 [pii] (2012).
37 McGaha, T. L., Chen, Y., Ravishankar, B., van Rooijen, N. & Karlsson, M. C. Marginal zone macrophages suppress innate and adaptive immunity to apoptotic cells in the spleen. *Blood* **117**, 5403-5412, doi:10.1182/blood-2010-11-320028 blood-2010-11-320028 [pii] (2011).
38 Eloranta, M. L. & Alm, G. V. Splenic marginal metallophilic macrophages and marginal zone macrophages are the major interferon-alpha/beta producers in mice upon intravenous challenge with herpes simplex virus. *Scand J Immunol* **49**, 391-394 (1999).
39 Baumann, I. *et al.* Impaired uptake of apoptotic cells into tingible body macrophages in germinal centers of patients with systemic lupus erythematosus. *Arthritis Rheum* **46**, 191-201, doi:10.1002/1529-0131(200201)46:1<191::AID-ART10027>3.0.CO;2-K (2002).
40 Bowden, D. H. The alveolar macrophage. *Curr Top Pathol* **55**, 1-36 (1971).
41 Naito, M. *et al.* Development, differentiation, and phenotypic heterogeneity of murine tissue macrophages. *J Leukoc Biol* **59**, 133-138 (1996).
42 van Furth, R. & Cohn, Z. A. The origin and kinetics of mononuclear phagocytes. *J Exp Med* **128**, 415-435 (1968).
43 Serbina, N. V., Jia, T., Hohl, T. M. & Pamer, E. G. Monocyte-mediated defense against microbial pathogens. *Annu Rev Immunol* **26**, 421-452, doi:10.1146/annurev.immunol.26.021607.090326 (2008).
44 Serbina, N. V., Hohl, T. M., Cherny, M. & Pamer, E. G. Selective expansion of the monocytic lineage directed by bacterial infection. *J Immunol* **183**, 1900-1910, doi:10.4049/jimmunol.0900612 jimmunol.0900612 [pii] (2009).
45 Strauss-Ayali, D., Conrad, S. M. & Mosser, D. M. Monocyte subpopulations and their differentiation patterns during infection. *J Leukoc Biol* **82**, 244-252, doi:jlb.0307191 [pii] 10.1189/jlb.0307191 (2007).
46 Mohty, M. *et al.* IFN-alpha skews monocyte differentiation into Toll-like receptor 7-expressing dendritic cells with potent functional activities. *J Immunol* **171**, 3385-3393 (2003).
47 Nahrendorf, M. & Swirski, F. K. Monocyte and macrophage heterogeneity in the heart. *Circ Res* **112**, 1624-1633, doi:10.1161/CIRCRESAHA.113.300890 112/12/1624 [pii] (2013).
48 Khan, B., Rangasamy, S., McGuire, P. G. & Howdieshell, T. R. The role of monocyte subsets in myocutaneous revascularization. *J Surg Res* **183**, 963-975, doi:10.1016/j.jss.2013.02.019 S0022-4804(13)00104-2 [pii] (2013).
49 Zawada, A. M. *et al.* Monocyte heterogeneity in human cardiovascular disease. *Immunobiology* **217**, 1273-1284, doi:10.1016/j.imbio.2012.07.001

S0171-2985(12)00155-6 [pii] (2012).
50 Nahrendorf, M. *et al.* The healing myocardium sequentially mobilizes two monocyte subsets with divergent and complementary functions. *J Exp Med* **204**, 3037-3047, doi:jem.20070885 [pii]
10.1084/jem.20070885 (2007).
51 Sawyer, R. T., Strausbauch, P. H. & Volkman, A. Resident macrophage proliferation in mice depleted of blood monocytes by strontium-89. *Lab Invest* **46**, 165-170 (1982).
52 de Groot, C. J., Huppes, W., Sminia, T., Kraal, G. & Dijkstra, C. D. Determination of the origin and nature of brain macrophages and microglial cells in mouse central nervous system, using non-radioactive in situ hybridization and immunoperoxidase techniques. *Glia* **6**, 301-309, doi:10.1002/glia.440060408 (1992).
53 Lawson, L. J., Perry, V. H. & Gordon, S. Turnover of resident microglia in the normal adult mouse brain. *Neuroscience* **48**, 405-415, doi:0306-4522(92)90500-2 [pii] (1992).
54 Naito, M., Hasegawa, G. & Takahashi, K. Development, differentiation, and maturation of Kupffer cells. *Microsc Res Tech* **39**, 350-364, doi:10.1002/(SICI)1097-0029(19971115)39:4<350::AID-JEMT5>3.0.CO;2-L [pii]
10.1002/(SICI)1097-0029(19971115)39:4<350::AID-JEMT5>3.0.CO;2-L (1997).
55 Mosser, D. M. The many faces of macrophage activation. *J Leukoc Biol* **73**, 209-212 (2003).
56 Mosser, D. M. & Edwards, J. P. Exploring the full spectrum of macrophage activation. *Nat Rev Immunol* **8**, 958-969, doi:10.1038/nri2448 (2008).
57 Sica, A. & Mantovani, A. Macrophage plasticity and polarization: in vivo veritas. *J Clin Invest* **122**, 787-795, doi:10.1172/JCI5964359643 [pii] (2012).
58 Biswas, S. K. *et al.* A distinct and unique transcriptional program expressed by tumor-associated macrophages (defective NF-kappaB and enhanced IRF-3/STAT1 activation). *Blood* **107**, 2112-2122, doi:2005-01-0428 [pii]10.1182/blood-2005-01-0428 (2006).
59 Mackaness, G. B. The Immunological Basis of Acquired Cellular Resistance. *J Exp Med* **120**, 105-120 (1964).
60 Biswas, S. K. & Mantovani, A. Macrophage plasticity and interaction with lymphocyte subsets: cancer as a paradigm. *Nat Immunol* **11**, 889-896, doi:10.1038/ni.1937 ni.1937 [pii] (2010).
61 Kubota, K. Innate IFN-gamma production by subsets of natural killer cells, natural killer T cells and gammadelta T cells in response to dying bacterial-infected macrophages. *Scand J Immunol* **71**, 199-209, doi:10.1111/j.1365-3083.2009.02366.x SJI2366 [pii] (2010).
62 Mills, C. D., Kincaid, K., Alt, J. M., Heilman, M. J. & Hill, A. M. M-1/M-2 macrophages and the Th1/Th2 paradigm. *J Immunol* **164**, 6166-6173, doi:ji_v164n12p6166 [pii] (2000).
63 Kawai, T. *et al.* Lipopolysaccharide stimulates the MyD88-independent pathway and results in activation of IFN-regulatory factor 3 and the expression of a subset of lipopolysaccharide-inducible genes. *J Immunol* **167**, 5887-5894 (2001).
64 MacMicking, J., Xie, Q. W. & Nathan, C. Nitric oxide and macrophage function. *Annu Rev Immunol* **15**, 323-350, doi:10.1146/annurev.immunol.15.1.323 (1997).

65 Yates, R. M., Hermetter, A., Taylor, G. A. & Russell, D. G. Macrophage activation downregulates the degradative capacity of the phagosome. *Traffic* **8**, 241-250, doi:10.1111/j.1600-0854.2006.00528.x (2007).
66 Krausgruber, T. *et al.* IRF5 promotes inflammatory macrophage polarization and TH1-TH17 responses. *Nat Immunol* **12**, 231-238, doi:10.1038/ni.1990 ni.1990 [pii] (2011).
67 Cao, H., Wolff, R. G., Meltzer, M. S. & Crawford, R. M. Differential regulation of class II MHC determinants on macrophages by IFN-gamma and IL-4. *J Immunol* **143**, 3524-3531 (1989).
68 Gordon, S. & Martinez, F. O. Alternative activation of macrophages: mechanism and functions. *Immunity* **32**, 593-604, doi:10.1016/j.immuni.2010.05.007 S1074-7613(10)00173-1 [pii] (2010).
69 He, L. & Marneros, A. G. Macrophages are essential for the early wound healing response and the formation of a fibrovascular scar. *Am J Pathol* **182**, 2407-2417, doi:10.1016/j.ajpath.2013.02.032 S0002-9440(13)00211-3 [pii] (2013).
70 Mosmann, T. R. & Coffman, R. L. TH1 and TH2 cells: different patterns of lymphokine secretion lead to different functional properties. *Annu Rev Immunol* **7**, 145-173, doi:10.1146/annurev.iy.07.040189.001045 (1989).
71 Gessner, A., Mohrs, K. & Mohrs, M. Mast cells, basophils, and eosinophils acquire constitutive IL-4 and IL-13 transcripts during lineage differentiation that are sufficient for rapid cytokine production. *J Immunol* **174**, 1063-1072, doi:174/2/1063 [pii] (2005).
72 Stein, M., Keshav, S., Harris, N. & Gordon, S. Interleukin 4 potently enhances murine macrophage mannose receptor activity: a marker of alternative immunologic macrophage activation. *J Exp Med* **176**, 287-292 (1992).
73 Hesse, M. *et al.* Differential regulation of nitric oxide synthase-2 and arginase-1 by type 1/type 2 cytokines in vivo: granulomatous pathology is shaped by the pattern of L-arginine metabolism. *J Immunol* **167**, 6533-6544 (2001).
74 Munder, M. *et al.* Th1/Th2-regulated expression of arginase isoforms in murine macrophages and dendritic cells. *J Immunol* **163**, 3771-3777, doi:ji_v163n7p3771 [pii] (1999).
75 Chang, C. I., Liao, J. C. & Kuo, L. Arginase modulates nitric oxide production in activated macrophages. *Am J Physiol* **274**, H342-348 (1998).
76 Balce, D. R. *et al.* Alternative activation of macrophages by IL-4 enhances the proteolytic capacity of their phagosomes through synergistic mechanisms. *Blood* **118**, 4199-4208, doi:10.1182/blood-2011-01-328906 (2011).
77 Harris, J. *et al.* T helper 2 cytokines inhibit autophagic control of intracellular Mycobacterium tuberculosis. *Immunity* **27**, 505-517, doi:S1074-7613(07)00417-7 [pii] 10.1016/j.immuni.2007.07.022 (2007).
78 Muller, U. *et al.* IL-13 induces disease-promoting type 2 cytokines, alternatively activated macrophages and allergic inflammation during pulmonary infection of mice with Cryptococcus neoformans. *J Immunol* **179**, 5367-5377, doi:179/8/5367 [pii] (2007).

79 Martinez, F. O., Sica, A., Mantovani, A. & Locati, M. Macrophage activation and polarization. *Front Biosci* **13**, 453-461, doi:2692 [pii] (2008).
80 Gerber, J. S. & Mosser, D. M. Reversing lipopolysaccharide toxicity by ligating the macrophage Fc gamma receptors. *J Immunol* **166**, 6861-6868 (2001).
81 Hasko, G., Pacher, P., Deitch, E. A. & Vizi, E. S. Shaping of monocyte and macrophage function by adenosine receptors. *Pharmacol Ther* **113**, 264-275, doi:S0163-7258(06)00150-1 [pii] 10.1016/j.pharmthera.2006.08.003 (2007).
82 Strassmann, G., Patil-Koota, V., Finkelman, F., Fong, M. & Kambayashi, T. Evidence for the involvement of interleukin 10 in the differential deactivation of murine peritoneal macrophages by prostaglandin E2. *J Exp Med* **180**, 2365-2370 (1994).
83 Mahalingam, S. & Lidbury, B. A. Suppression of lipopolysaccharide-induced antiviral transcription factor (STAT-1 and NF-kappa B) complexes by antibody-dependent enhancement of macrophage infection by Ross River virus. *Proc Natl Acad Sci U S A* **99**, 13819-13824, doi:10.1073/pnas.202415999
202415999 [pii] (2002).
84 Autschbach, F. *et al.* In situ expression of interleukin-10 in noninflamed human gut and in inflammatory bowel disease. *Am J Pathol* **153**, 121-130, doi:S0002-9440(10)65552-6 [pii]10.1016/S0002-9440(10)65552-6 (1998).
85 Bonfield, T. L. *et al.* Normal bronchial epithelial cells constitutively produce the anti-inflammatory cytokine interleukin-10, which is downregulated in cystic fibrosis. *Am J Respir Cell Mol Biol* **13**, 257-261, doi:10.1165/ajrcmb.13.3.7544594 (1995).
86 Fernandez, S., Jose, P., Avdiushko, M. G., Kaplan, A. M. & Cohen, D. A. Inhibition of IL-10 receptor function in alveolar macrophages by Toll-like receptor agonists. *J Immunol* **172**, 2613-2620 (2004).
87 Sun, K., Gan, Y. & Metzger, D. W. Analysis of murine genetic predisposition to pneumococcal infection reveals a critical role of alveolar macrophages in maintaining the sterility of the lower respiratory tract. *Infect Immun* **79**, 1842-1847, doi:10.1128/IAI.01143-10IAI.01143-10 [pii] (2011).
88 Lambrecht, B. N. Alveolar macrophage in the driver's seat. *Immunity* **24**, 366-368, doi:S1074-7613(06)00179-8 [pii]10.1016/j.immuni.2006.03.008 (2006).
89 MacLean, J. A. *et al.* Sequestration of inhaled particulate antigens by lung phagocytes. A mechanism for the effective inhibition of pulmonary cell-mediated immunity. *Am J Pathol* **148**, 657-666 (1996).
90 Raoust, E. *et al.* Pseudomonas aeruginosa LPS or flagellin are sufficient to activate TLR-dependent signaling in murine alveolar macrophages and airway epithelial cells. *PLoS One* **4**, e7259, doi:10.1371/journal.pone.0007259 (2009).
91 Barnes, P. J. Alveolar macrophages as orchestrators of COPD. *COPD* **1**, 59-70, doi:MEYLCC37NNM9HJU2 [pii]10.1081/COPD-120028701 (2004).
92 Hashimoto, D. *et al.* Tissue-resident macrophages self-maintain locally throughout adult life with minimal contribution from circulating monocytes. *Immunity* **38**, 792-804, doi:10.1016/j.immuni.2013.04.004S1074-7613(13)00157-X [pii] (2013).

93 Rose, A. S. & Knox, K. S. Bronchoalveolar lavage as a research tool. *Semin Respir Crit Care Med* **28**, 561-573, doi:10.1055/s-2007-991528 (2007).
94 Meyer, K. C. Bronchoalveolar lavage as a diagnostic tool. *Semin Respir Crit Care Med* **28**, 546-560, doi:10.1055/s-2007-991527 (2007).
95 Schroeder, F. & Kinden, D. A. Measurement of phagocytosis using fluorescent latex beads. *J Biochem Biophys Methods* **8**, 15-27 (1983).
96 Desjardins, M. & Griffiths, G. Phagocytosis: latex leads the way. *Curr Opin Cell Biol* **15**, 498-503, doi:S0955067403000838 [pii] (2003).
97 Champion, J. A. & Mitragotri, S. Role of target geometry in phagocytosis. *Proc Natl Acad Sci U S A* **103**, 4930-4934, doi:0600997103 [pii] 10.1073/pnas.0600997103 (2006).
98 Nosanchuk, J. D., Cleare, W., Franzot, S. P. & Casadevall, A. Amphotericin B and fluconazole affect cellular charge, macrophage phagocytosis, and cellular morphology of Cryptococcus neoformans at subinhibitory concentrations. *Antimicrob Agents Chemother* **43**, 233-239 (1999).
99 Nagura, H., Asai, J., Katsumata, Y. & Kojima, K. Role of electric surface charge of cell membrane in phagocytosis. *Acta Pathol Jpn* **23**, 279-290 (1973).
100 Kaksonen, M., Toret, C. P. & Drubin, D. G. Harnessing actin dynamics for clathrin-mediated endocytosis. *Nat Rev Mol Cell Biol* **7**, 404-414, doi:nrm1940 [pii] 10.1038/nrm1940 (2006).
101 Howes, M. T., Mayor, S. & Parton, R. G. Molecules, mechanisms, and cellular roles of clathrin-independent endocytosis. *Curr Opin Cell Biol* **22**, 519-527, doi:10.1016/j.ceb.2010.04.001S0955-0674(10)00045-1 [pii] (2010).
102 Gordon, S. Pattern recognition receptors: doubling up for the innate immune response. *Cell* **111**, 927-930, doi:S0092867402012011 [pii] (2002).
103 Ezekowitz, R. A., Sastry, K., Bailly, P. & Warner, A. Molecular characterization of the human macrophage mannose receptor: demonstration of multiple carbohydrate recognition-like domains and phagocytosis of yeasts in Cos-1 cells. *J Exp Med* **172**, 1785-1794 (1990).
104 Peiser, L., Mukhopadhyay, S. & Gordon, S. Scavenger receptors in innate immunity. *Curr Opin Immunol* **14**, 123-128, doi:S0952791501003077 [pii] (2002).
105 Flannagan, R. S., Jaumouille, V. & Grinstein, S. The cell biology of phagocytosis. *Annu Rev Pathol* **7**, 61-98, doi:10.1146/annurev-pathol-011811-132445 (2012).
106 Brown, E. J. Complement receptors, adhesion, and phagocytosis. *Infect Agents Dis* **1**, 63-70 (1992).
107 Swanson, J. A. & Hoppe, A. D. The coordination of signaling during Fc receptor-mediated phagocytosis. *J Leukoc Biol* **76**, 1093-1103, doi:jlb.0804439 [pii]10.1189/jlb.0804439 (2004).
108 Caron, E., Self, A. J. & Hall, A. The GTPase Rap1 controls functional activation of macrophage integrin alphaMbeta2 by LPS and other inflammatory mediators. *Curr Biol* **10**, 974-978, doi:S0960-9822(00)00641-2 [pii] (2000).

109 Fischetti, V. A. Streptococcal M protein: molecular design and biological behavior. *Clin Microbiol Rev* **2**, 285-314 (1989).
110 China, B., Sory, M. P., N'Guyen, B. T., De Bruyere, M. & Cornelis, G. R. Role of the YadA protein in prevention of opsonization of Yersinia enterocolitica by C3b molecules. *Infect Immun* **61**, 3129-3136 (1993).
111 Foster, T. J. Immune evasion by staphylococci. *Nat Rev Microbiol* **3**, 948-958, doi:nrmicro1289 [pii]10.1038/nrmicro1289 (2005).
112 Chekeni, F. B. & Ravichandran, K. S. The role of nucleotides in apoptotic cell clearance: implications for disease pathogenesis. *J Mol Med (Berl)* **89**, 13-22, doi:10.1007/s00109-010-0673-7 (2011).
113 Paidassi, H., Tacnet-Delorme, P., Arlaud, G. J. & Frachet, P. How phagocytes track down and respond to apoptotic cells. *Crit Rev Immunol* **29**, 111-130, doi:0772bd76689c273e,756c284a5bc74384 [pii] (2009).
114 Freeman, G. J., Casasnovas, J. M., Umetsu, D. T. & DeKruyff, R. H. TIM genes: a family of cell surface phosphatidylserine receptors that regulate innate and adaptive immunity. *Immunol Rev* **235**, 172-189, doi:10.1111/j.0105-2896.2010.00903.xIMR903 [pii] (2010).
115 Park, S. Y. *et al.* Rapid cell corpse clearance by stabilin-2, a membrane phosphatidylserine receptor. *Cell Death Differ* **15**, 192-201, doi:4402242 [pii]10.1038/sj.cdd.4402242 (2008).
116 Park, D. *et al.* BAI1 is an engulfment receptor for apoptotic cells upstream of the ELMO/Dock180/Rac module. *Nature* **450**, 430-434, doi:nature06329 [pii]10.1038/nature06329 (2007).
117 Brown, S. *et al.* Apoptosis disables CD31-mediated cell detachment from phagocytes promoting binding and engulfment. *Nature* **418**, 200-203, doi:10.1038/nature00811 nature00811 [pii] (2002).
118 Griffin, F. M., Jr., Griffin, J. A., Leider, J. E. & Silverstein, S. C. Studies on the mechanism of phagocytosis. I. Requirements for circumferential attachment of particle-bound ligands to specific receptors on the macrophage plasma membrane. *J Exp Med* **142**, 1263-1282 (1975).
119 Swanson, J. A. & Baer, S. C. Phagocytosis by zippers and triggers. *Trends Cell Biol* **5**, 89-93 (1995).
120 May, R. C. & Machesky, L. M. Phagocytosis and the actin cytoskeleton. *J Cell Sci* **114**, 1061-1077 (2001).
121 Anderson, C. L., Shen, L., Eicher, D. M., Wewers, M. D. & Gill, J. K. Phagocytosis mediated by three distinct Fc gamma receptor classes on human leukocytes. *J Exp Med* **171**, 1333-1345 (1990).
122 van de Winkel, J. G. & Capel, P. J. Human IgG Fc receptor heterogeneity: molecular aspects and clinical implications. *Immunol Today* **14**, 215-221, doi:0167-5699(93)90166-I [pii]10.1016/0167-5699(93)90166-I (1993).
123 Tridandapani, S. *et al.* Regulated expression and inhibitory function of Fcgamma RIIb in human monocytic cells. *J Biol Chem* **277**, 5082-5089, doi:10.1074/jbc.M110277200M110277200 [pii] (2002).

124 Greenberg, S. Signal transduction of phagocytosis. *Trends Cell Biol* **5**, 93-99, doi:S0962892400889576 [pii] (1995).
125 Isakov, N. Immunoreceptor tyrosine-based activation motif (ITAM), a unique module linking antigen and Fc receptors to their signaling cascades. *J Leukoc Biol* **61**, 6-16 (1997).
126 Ravetch, J. V. & Bolland, S. IgG Fc receptors. *Annu Rev Immunol* **19**, 275-290, doi:19/1/275 [pii]
10.1146/annurev.immunol.19.1.275 (2001).
127 Korade-Mirnics, Z. & Corey, S. J. Src kinase-mediated signaling in leukocytes. *J Leukoc Biol* **68**, 603-613 (2000).
128 Wang, A. V., Scholl, P. R. & Geha, R. S. Physical and functional association of the high affinity immunoglobulin G receptor (Fc gamma RI) with the kinases Hck and Lyn. *J Exp Med* **180**, 1165-1170 (1994).
129 Johnson, S. A. *et al.* Phosphorylated immunoreceptor signaling motifs (ITAMs) exhibit unique abilities to bind and activate Lyn and Syk tyrosine kinases. *J Immunol* **155**, 4596-4603 (1995).
130 Tridandapani, S. *et al.* The adapter protein LAT enhances fcgamma receptor-mediated signal transduction in myeloid cells. *J Biol Chem* **275**, 20480-20487, doi:10.1074/jbc.M909462199
M909462199 [pii] (2000).
131 Gu, H., Botelho, R. J., Yu, M., Grinstein, S. & Neel, B. G. Critical role for scaffolding adapter Gab2 in Fc gamma R-mediated phagocytosis. *J Cell Biol* **161**, 1151-1161, doi:10.1083/jcb.200212158
jcb.200212158 [pii] (2003).
132 Yu, M., Lowell, C. A., Neel, B. G. & Gu, H. Scaffolding adapter Grb2-associated binder 2 requires Syk to transmit signals from FcepsilonRI. *J Immunol* **176**, 2421-2429, doi:176/4/2421 [pii] (2006).
133 Kiefer, F. *et al.* The Syk protein tyrosine kinase is essential for Fcgamma receptor signaling in macrophages and neutrophils. *Mol Cell Biol* **18**, 4209-4220 (1998).
134 Botelho, R. J. *et al.* Localized biphasic changes in phosphatidylinositol-4,5-bisphosphate at sites of phagocytosis. *J Cell Biol* **151**, 1353-1368 (2000).
135 Liao, F., Shin, H. S. & Rhee, S. G. Tyrosine phosphorylation of phospholipase C-gamma 1 induced by cross-linking of the high-affinity or low-affinity Fc receptor for IgG in U937 cells. *Proc Natl Acad Sci U S A* **89**, 3659-3663 (1992).
136 Ninomiya, N. *et al.* Involvement of phosphatidylinositol 3-kinase in Fc gamma receptor signaling. *J Biol Chem* **269**, 22732-22737 (1994).
137 Garcia-Garcia, E. & Rosales, C. Signal transduction during Fc receptor-mediated phagocytosis. *J Leukoc Biol* **72**, 1092-1108 (2002).
138 Thrasher, A. J. & Burns, S. O. WASP: a key immunological multitasker. *Nat Rev Immunol* **10**, 182-192, doi:10.1038/nri2724nri2724 [pii] (2010).
139 Schonder, A. A. Craniopharyngioma in the elderly patient: case report. *J Am Geriatr Soc* **23**, 545-547 (1975).

140 Suzaki, E., Kobayashi, H., Kodama, Y., Masujima, T. & Terakawa, S. Video-rate dynamics of exocytotic events associated with phagocytosis in neutrophils. *Cell Motil Cytoskeleton* **38**, 215-228, doi:10.1002/(SICI)1097-0169(1997)38:3<215::AID-CM1>3.0.CO;2-4 [pii] 10.1002/(SICI)1097-0169(1997)38:3<215::AID-CM1>3.0.CO;2-4 (1997).
141 Desjardins, M. Biogenesis of phagolysosomes: the 'kiss and run' hypothesis. *Trends Cell Biol* **5**, 183-186 (1995).
142 Desjardins, M., Huber, L. A., Parton, R. G. & Griffiths, G. Biogenesis of phagolysosomes proceeds through a sequential series of interactions with the endocytic apparatus. *J Cell Biol* **124**, 677-688 (1994).
143 Pitt, A., Mayorga, L. S., Stahl, P. D. & Schwartz, A. L. Alterations in the protein composition of maturing phagosomes. *J Clin Invest* **90**, 1978-1983, doi:10.1172/JCI116077 (1992).
144 Lee, W. L., Kim, M. K., Schreiber, A. D. & Grinstein, S. Role of ubiquitin and proteasomes in phagosome maturation. *Mol Biol Cell* **16**, 2077-2090, doi:E04-06-0464 [pii] 10.1091/mbc.E04-06-0464 (2005).
145 de Chastellier, C. & Thilo, L. Phagosome maturation and fusion with lysosomes in relation to surface property and size of the phagocytic particle. *Eur J Cell Biol* **74**, 49-62 (1997).
146 Vieira, O. V. *et al.* Distinct roles of class I and class III phosphatidylinositol 3-kinases in phagosome formation and maturation. *J Cell Biol* **155**, 19-25, doi:10.1083/jcb.200107069155/1/19 [pii] (2001).
147 Stenmark, H. Rab GTPases as coordinators of vesicle traffic. *Nat Rev Mol Cell Biol* **10**, 513-525, doi:10.1038/nrm2728nrm2728 [pii] (2009).
148 Huotari, J. & Helenius, A. Endosome maturation. *EMBO J* **30**, 3481-3500, doi:10.1038/emboj.2011.286emboj2011286 [pii] (2011).
149 Desjardins, M., Nzala, N. N., Corsini, R. & Rondeau, C. Maturation of phagosomes is accompanied by changes in their fusion properties and size-selective acquisition of solute materials from endosomes. *J Cell Sci* **110 (Pt 18)**, 2303-2314 (1997).
150 Duclos, S. *et al.* Rab5 regulates the kiss and run fusion between phagosomes and endosomes and the acquisition of phagosome leishmanicidal properties in RAW 264.7 macrophages. *J Cell Sci* **113 Pt 19**, 3531-3541 (2000).
151 Vieira, O. V. *et al.* Modulation of Rab5 and Rab7 recruitment to phagosomes by phosphatidylinositol 3-kinase. *Mol Cell Biol* **23**, 2501-2514 (2003).
152 Mills, I. G., Urbe, S. & Clague, M. J. Relationships between EEA1 binding partners and their role in endosome fusion. *J Cell Sci* **114**, 1959-1965 (2001).
153 Callaghan, J., Nixon, S., Bucci, C., Toh, B. H. & Stenmark, H. Direct interaction of EEA1 with Rab5b. *Eur J Biochem* **265**, 361-366, doi:ejb743 [pii] (1999).
154 Fairn, G. D. & Grinstein, S. How nascent phagosomes mature to become phagolysosomes. *Trends Immunol* **33**, 397-405, doi:10.1016/j.it.2012.03.003 S1471-4906(12)00053-1 [pii] (2012).

155 Peplowska, K., Markgraf, D. F., Ostrowicz, C. W., Bange, G. & Ungermann, C. The CORVET tethering complex interacts with the yeast Rab5 homolog Vps21 and is involved in endo-lysosomal biogenesis. *Dev Cell* **12**, 739-750, doi:S1534-5807(07)00106-2 [pii] 10.1016/j.devcel.2007.03.006 (2007).
156 Plemel, R. L. *et al.* Subunit organization and Rab interactions of Vps-C protein complexes that control endolysosomal membrane traffic. *Mol Biol Cell* **22**, 1353-1363, doi:10.1091/mbc.E10-03-0260mbc.E10-03-0260 [pii] (2011).
157 Harrison, R. E., Bucci, C., Vieira, O. V., Schroer, T. A. & Grinstein, S. Phagosomes fuse with late endosomes and/or lysosomes by extension of membrane protrusions along microtubules: role of Rab7 and RILP. *Mol Cell Biol* **23**, 6494-6506 (2003).
158 Hackam, D. J. *et al.* Regulation of phagosomal acidification. Differential targeting of Na+/H+ exchangers, Na+/K+-ATPases, and vacuolar-type H+-atpases. *J Biol Chem* **272**, 29810-29820 (1997).
159 Lukacs, G. L., Rotstein, O. D. & Grinstein, S. Phagosomal acidification is mediated by a vacuolar-type H(+)-ATPase in murine macrophages. *J Biol Chem* **265**, 21099-21107 (1990).
160 Drose, S. & Altendorf, K. Bafilomycins and concanamycins as inhibitors of V-ATPases and P-ATPases. *J Exp Biol* **200**, 1-8 (1997).
161 Kinchen, J. M. & Ravichandran, K. S. Phagosome maturation: going through the acid test. *Nat Rev Mol Cell Biol* **9**, 781-795, doi:10.1038/nrm2515nrm2515 [pii] (2008).
162 Nunes, P., Demaurex, N. & Dinauer, M. C. Regulation Of The NADPH Oxidase And Associated Ion Fluxes During Phagocytosis. *Traffic*, doi:10.1111/tra.12115 (2013).
163 Winterbourn, C. C. Reconciling the chemistry and biology of reactive oxygen species. *Nat Chem Biol* **4**, 278-286, doi:nchembio.85 [pii]10.1038/nchembio.85 (2008).
164 Aktan, F. iNOS-mediated nitric oxide production and its regulation. *Life Sci* **75**, 639-653, doi:10.1016/j.lfs.2003.10.042S0024320504002887 [pii] (2004).
165 Jyoti, A. *et al.* Interaction of inducible nitric oxide synthase with Rac2 regulates reactive oxygen and nitrogen species generation in the human neutrophil phagosomes: Implication in microbial killing. *Antioxid Redox Signal*, doi:10.1089/ars.2012.4970 (2013).
166 Pillay, C. S., Elliott, E. & Dennison, C. Endolysosomal proteolysis and its regulation. *Biochem J* **363**, 417-429 (2002).
167 Unanue, E. R. Antigen-presenting function of the macrophage. *Annu Rev Immunol* **2**, 395-428, doi:10.1146/annurev.iy.02.040184.002143 (1984).
168 Neefjes, J., Jongsma, M. L., Paul, P. & Bakke, O. Towards a systems understanding of MHC class I and MHC class II antigen presentation. *Nat Rev Immunol* **11**, 823-836, doi:10.1038/nri3084nri3084 [pii] (2011).
169 Rudensky, A. & Beers, C. Lysosomal cysteine proteases and antigen presentation. *Ernst Schering Res Found Workshop*, 81-95 (2006).
170 Lehrer, R. I., Lichtenstein, A. K. & Ganz, T. Defensins: antimicrobial and cytotoxic peptides of mammalian cells. *Annu Rev Immunol* **11**, 105-128, doi:10.1146/annurev.iy.11.040193.000541 (1993).

171 Neumann, E. J. *et al.* Assessment of the economic impact of porcine reproductive and respiratory syndrome on swine production in the United States. *J Am Vet Med Assoc* **227**, 385-392 (2005).
172 Wensvoort, G. *et al.* Mystery swine disease in The Netherlands: the isolation of Lelystad virus. *Vet Q* **13**, 121-130, doi:10.1080/01652176.1991.9694296 (1991).
173 Collins, J. E. *et al.* Isolation of swine infertility and respiratory syndrome virus (isolate ATCC VR-2332) in North America and experimental reproduction of the disease in gnotobiotic pigs. *J Vet Diagn Invest* **4**, 117-126 (1992).
174 Li, Y. *et al.* Emergence of a highly pathogenic porcine reproductive and respiratory syndrome virus in the Mid-Eastern region of China. *Vet J* **174**, 577-584, doi:S1090-0233(07)00267-5 [pii]10.1016/j.tvjl.2007.07.032 (2007).
175 Tian, K. *et al.* Emergence of fatal PRRSV variants: unparalleled outbreaks of atypical PRRS in China and molecular dissection of the unique hallmark. *PLoS One* **2**, e526, doi:10.1371/journal.pone.0000526 (2007).
176 Murtaugh, M. P., Stadejek, T., Abrahante, J. E., Lam, T. T. & Leung, F. C. The ever-expanding diversity of porcine reproductive and respiratory syndrome virus. *Virus Res* **154**, 18-30, doi:S0168-1702(10)00292-3 [pii]10.1016/j.virusres.2010.08.015 (2010).
177 Nelsen, C. J., Murtaugh, M. P. & Faaberg, K. S. Porcine reproductive and respiratory syndrome virus comparison: divergent evolution on two continents. *J Virol* **73**, 270-280 (1999).
178 Shi, M. *et al.* Molecular epidemiology of PRRSV: a phylogenetic perspective. *Virus Res* **154**, 7-17, doi:10.1016/j.virusres.2010.08.014 S0168-1702(10)00291-1 [pii] (2010).
179 Cavanagh, D. Nidovirales: a new order comprising Coronaviridae and Arteriviridae. *Arch Virol* **142**, 629-633 (1997).
180 Snijder, E. J. & Meulenberg, J. J. The molecular biology of arteriviruses. *J Gen Virol* **79 (Pt 5)**, 961-979 (1998).
181 Zimmerman, J. J. *et al.* Studies of porcine reproductive and respiratory syndrome (PRRS) virus infection in avian species. *Vet Microbiol* **55**, 329-336 (1997).
182 Drake, J. W. Rates of spontaneous mutation among RNA viruses. *Proc Natl Acad Sci U S A* **90**, 4171-4175 (1993).
183 Ward, C. D., Stokes, M. A. & Flanegan, J. B. Direct measurement of the poliovirus RNA polymerase error frequency in vitro. *J Virol* **62**, 558-562 (1988).
184 Fijalkowska, I. J., Schaaper, R. M. & Jonczyk, P. DNA replication fidelity in Escherichia coli: a multi-DNA polymerase affair. *FEMS Microbiol Rev* **36**, 1105-1121, doi:10.1111/j.1574-6976.2012.00338.x (2012).
185 Barr, J. N. & Fearns, R. How RNA viruses maintain their genome integrity. *J Gen Virol* **91**, 1373-1387, doi:10.1099/vir.0.020818-0 vir.0.020818-0 [pii] (2010).
186 Steinhauer, D. A. & Holland, J. J. Rapid evolution of RNA viruses. *Annu Rev Microbiol* **41**, 409-433, doi:10.1146/annurev.mi.41.100187.002205 (1987).

187 Park, B. K. & Joo, H. S. Induction of dual infections in newborn and three-week-old pigs by use of two plaque size variants of porcine reproductive and respiratory syndrome virus. *Am J Vet Res* **58**, 257-259 (1997).
188 Wensvoort, G. *et al.* Antigenic comparison of Lelystad virus and swine infertility and respiratory syndrome (SIRS) virus. *J Vet Diagn Invest* **4**, 134-138 (1992).
189 Christianson, W. T. *et al.* Pathogenesis of porcine reproductive and respiratory syndrome virus infection in mid-gestation sows and fetuses. *Can J Vet Res* **57**, 262-268 (1993).
190 Albina, E., Madec, F., Cariolet, R. & Torrison, J. Immune response and persistence of the porcine reproductive and respiratory syndrome virus in infected pigs and farm units. *Vet Rec* **134**, 567-573 (1994).
191 Wills, R. W., Doster, A. R., Galeota, J. A., Sur, J. H. & Osorio, F. A. Duration of infection and proportion of pigs persistently infected with porcine reproductive and respiratory syndrome virus. *J Clin Microbiol* **41**, 58-62 (2003).
192 Pitkin, A., Deen, J. & Dee, S. Further assessment of fomites and personnel as vehicles for the mechanical transport and transmission of porcine reproductive and respiratory syndrome virus. *Can J Vet Res* **73**, 298-302 (2009).
193 Christopher-Hennings, J. *et al.* Detection of porcine reproductive and respiratory syndrome virus in boar semen by PCR. *J Clin Microbiol* **33**, 1730-1734 (1995).
194 Wills, R. W. *et al.* Porcine reproductive and respiratory syndrome virus: a persistent infection. *Vet Microbiol* **55**, 231-240 (1997).
195 Batista, L., Dee, S. A., Rossow, K. D., Deen, J. & Pijoan, C. Assessing the duration of persistence and shedding of porcine reproductive and respiratory syndrome virus in a large population of breeding-age gilts. *Can J Vet Res* **66**, 196-200 (2002).
196 Meulenberg, J. J. *et al.* Lelystad virus, the causative agent of porcine epidemic abortion and respiratory syndrome (PEARS), is related to LDV and EAV. *Virology* **192**, 62-72, doi:S0042-6822(83)71008-1 [pii]
10.1006/viro.1993.1008 (1993).
197 den Boon, J. A. *et al.* Processing and evolution of the N-terminal region of the arterivirus replicase ORF1a protein: identification of two papainlike cysteine proteases. *J Virol* **69**, 4500-4505 (1995).
198 Mardassi, H., Massie, B. & Dea, S. Intracellular synthesis, processing, and transport of proteins encoded by ORFs 5 to 7 of porcine reproductive and respiratory syndrome virus. *Virology* **221**, 98-112, doi:S0042-6822(96)90356-6 [pii]
10.1006/viro.1996.0356 (1996).
199 Meulenberg, J. J. *et al.* Characterization of proteins encoded by ORFs 2 to 7 of Lelystad virus. *Virology* **206**, 155-163, doi:S0042-6822(95)80030-1 [pii] (1995).
200 Dea, S., Gagnon, C. A., Mardassi, H., Pirzadeh, B. & Rogan, D. Current knowledge on the structural proteins of porcine reproductive and respiratory syndrome (PRRS) virus: comparison of the North American and European isolates. *Arch Virol* **145**, 659-688 (2000).

201 Egli, C., Thur, B., Liu, L. & Hofmann, M. A. Quantitative TaqMan RT-PCR for the detection and differentiation of European and North American strains of porcine reproductive and respiratory syndrome virus. *J Virol Methods* **98**, 63-75, doi:S0166093401003585 [pii] (2001).

202 Duan, X., Nauwynck, H. J. & Pensaert, M. B. Virus quantification and identification of cellular targets in the lungs and lymphoid tissues of pigs at different time intervals after inoculation with porcine reproductive and respiratory syndrome virus (PRRSV). *Vet Microbiol* **56**, 9-19, doi:S0378-1135(96)01347-8 [pii] 10.1016/S0378-1135(96)01347-8 (1997).

203 Lawson, S. R., Rossow, K. D., Collins, J. E., Benfield, D. A. & Rowland, R. R. Porcine reproductive and respiratory syndrome virus infection of gnotobiotic pigs: sites of virus replication and co-localization with MAC-387 staining at 21 days post-infection. *Virus Res* **51**, 105-113, doi:S0168170297000865 [pii] (1997).

204 Duan, X., Nauwynck, H. J. & Pensaert, M. B. Effects of origin and state of differentiation and activation of monocytes/macrophages on their susceptibility to porcine reproductive and respiratory syndrome virus (PRRSV). *Arch Virol* **142**, 2483-2497 (1997).

205 Thanawongnuwech, R., Halbur, P. G. & Thacker, E. L. The role of pulmonary intravascular macrophages in porcine reproductive and respiratory syndrome virus infection. *Anim Health Res Rev* **1**, 95-102, doi:S1466252300000086 [pii] (2000).

206 Beyer, J. *et al.* Porcine reproductive and respiratory syndrome virus (PRRSV): kinetics of infection in lymphatic organs and lung. *J Vet Med B Infect Dis Vet Public Health* **47**, 9-25 (2000).

207 Halbur, P. G. *et al.* Immunohistochemical identification of porcine reproductive and respiratory syndrome virus (PRRSV) antigen in the heart and lymphoid system of three-week-old colostrum-deprived pigs. *Vet Pathol* **32**, 200-204 (1995).

208 Sur, J. H. *et al.* Porcine reproductive and respiratory syndrome virus replicates in testicular germ cells, alters spermatogenesis, and induces germ cell death by apoptosis. *J Virol* **71**, 9170-9179 (1997).

209 Loving, C. L., Brockmeier, S. L. & Sacco, R. E. Differential type I interferon activation and susceptibility of dendritic cell populations to porcine arterivirus. *Immunology* **120**, 217-229, doi:IMM2493 [pii] 10.1111/j.1365-2567.2006.02493.x (2007).

210 Chang, H. C., Peng, Y. T., Chang, H. L., Chaung, H. C. & Chung, W. B. Phenotypic and functional modulation of bone marrow-derived dendritic cells by porcine reproductive and respiratory syndrome virus. *Vet Microbiol* **129**, 281-293, doi:S0378-1135(07)00617-7 [pii] 10.1016/j.vetmic.2007.12.002 (2008).

211 Kim, H. S., Kwang, J., Yoon, I. J., Joo, H. S. & Frey, M. L. Enhanced replication of porcine reproductive and respiratory syndrome (PRRS) virus in a homogeneous subpopulation of MA-104 cell line. *Arch Virol* **133**, 477-483 (1993).

212 Wang, W. W. *et al.* [The role of vimentin during PRRSV infection of Marc-145 cells]. *Bing Du Xue Bao* **27**, 456-461 (2011).

213 Provost, C. *et al.* Identification of a new cell line permissive to porcine reproductive and respiratory syndrome virus infection and replication which is phenotypically distinct from MARC-145 cell line. *Virol J* **9**, 267, doi:10.1186/1743-422X-9-267 1743-422X-9-267 [pii] (2012).
214 Silversides, D. W., Music, N., Jacques, M., Gagnon, C. A. & Webby, R. Investigation of the species origin of the St. Jude Porcine Lung epithelial cell line (SJPL) made available to researchers. *J Virol* **84**, 5454-5455, doi:10.1128/JVI.00042-10 JVI.00042-10 [pii] (2010).
215 Kreutz, L. C. Cellular membrane factors are the major determinants of porcine reproductive and respiratory syndrome virus tropism. *Virus Res* **53**, 121-128, doi:S0168170297001342 [pii] (1998).
216 Lee, Y. J. *et al.* Generation of a porcine alveolar macrophage cell line for the growth of porcine reproductive and respiratory syndrome virus. *J Virol Methods* **163**, 410-415, doi:10.1016/j.jviromet.2009.11.003 S0166-0934(09)00473-X [pii] (2010).
217 Calvert, J. G. *et al.* CD163 expression confers susceptibility to porcine reproductive and respiratory syndrome viruses. *J Virol* **81**, 7371-7379, doi:JVI.00513-07 [pii] 10.1128/JVI.00513-07 (2007).
218 Shanmukhappa, K., Kim, J. K. & Kapil, S. Role of CD151, A tetraspanin, in porcine reproductive and respiratory syndrome virus infection. *Virol J* **4**, 62, doi:1743-422X-4-62 [pii]10.1186/1743-422X-4-62 (2007).
219 Van Gorp, H., Van Breedam, W., Delputte, P. L. & Nauwynck, H. J. Sialoadhesin and CD163 join forces during entry of the porcine reproductive and respiratory syndrome virus. *J Gen Virol* **89**, 2943-2953, doi:10.1099/vir.0.2008/005009-089/12/2943 [pii] (2008).
220 Kreutz, L. C. & Ackermann, M. R. Porcine reproductive and respiratory syndrome virus enters cells through a low pH-dependent endocytic pathway. *Virus Res* **42**, 137-147, doi:0168-1702(96)01313-5 [pii] (1996).
221 Nauwynck, H. J., Duan, X., Favoreel, H. W., Van Oostveldt, P. & Pensaert, M. B. Entry of porcine reproductive and respiratory syndrome virus into porcine alveolar macrophages via receptor-mediated endocytosis. *J Gen Virol* **80 (Pt 2)**, 297-305 (1999).
222 Van Gorp, H., Van Breedam, W., Delputte, P. L. & Nauwynck, H. J. The porcine reproductive and respiratory syndrome virus requires trafficking through CD163-positive early endosomes, but not late endosomes, for productive infection. *Arch Virol* **154**, 1939-1943, doi:10.1007/s00705-009-0527-1 (2009).
223 Marsh, M. & Bron, R. SFV infection in CHO cells: cell-type specific restrictions to productive virus entry at the cell surface. *J Cell Sci* **110 (Pt 1)**, 95-103 (1997).
224 Mercer, J., Schelhaas, M. & Helenius, A. Virus entry by endocytosis. *Annu Rev Biochem* **79**, 803-833, doi:10.1146/annurev-biochem-060208-104626 (2010).
225 Jusa, E. R., Inaba, Y., Kouno, M. & Hirose, O. Effect of heparin on infection of cells by porcine reproductive and respiratory syndrome virus. *Am J Vet Res* **58**, 488-491 (1997).

226 Delputte, P. L., Vanderheijden, N., Nauwynck, H. J. & Pensaert, M. B. Involvement of the matrix protein in attachment of porcine reproductive and respiratory syndrome virus to a heparinlike receptor on porcine alveolar macrophages. *J Virol* **76**, 4312-4320 (2002).
227 O'Neill, A. S., van den Berg, T. K. & Mullen, G. E. Sialoadhesin - a macrophage-restricted marker of immunoregulation and inflammation. *Immunology* **138**, 198-207, doi:10.1111/imm.12042 (2013).
228 Klaas, M. & Crocker, P. R. Sialoadhesin in recognition of self and non-self. *Semin Immunopathol* **34**, 353-364, doi:10.1007/s00281-012-0310-3 (2012).
229 Van Breedam, W. *et al.* The M/GP(5) glycoprotein complex of porcine reproductive and respiratory syndrome virus binds the sialoadhesin receptor in a sialic acid-dependent manner. *PLoS Pathog* **6**, e1000730, doi:10.1371/journal.ppat.1000730 (2010).
230 Vanderheijden, N. *et al.* Involvement of sialoadhesin in entry of porcine reproductive and respiratory syndrome virus into porcine alveolar macrophages. *J Virol* **77**, 8207-8215 (2003).
231 Das, P. B. *et al.* The minor envelope glycoproteins GP2a and GP4 of porcine reproductive and respiratory syndrome virus interact with the receptor CD163. *J Virol* **84**, 1731-1740, doi:10.1128/JVI.01774-09
JVI.01774-09 [pii] (2010).
232 Akila, P., Prashant, V., Suma, M. N., Prashant, S. N. & Chaitra, T. R. CD163 and its expanding functional repertoire. *Clin Chim Acta* **413**, 669-674, doi:10.1016/j.cca.2012.01.028
S0009-8981(12)00049-6 [pii] (2012).
233 Kristiansen, M. *et al.* Identification of the haemoglobin scavenger receptor. *Nature* **409**, 198-201, doi:10.1038/35051594 (2001).
234 Sanchez-Torres, C. *et al.* Expression of porcine CD163 on monocytes/macrophages correlates with permissiveness to African swine fever infection. *Arch Virol* **148**, 2307-2323, doi:10.1007/s00705-003-0188-4 (2003).
235 Sanchez, C. *et al.* The porcine 2A10 antigen is homologous to human CD163 and related to macrophage differentiation. *J Immunol* **162**, 5230-5237 (1999).
236 Blackwell, J. L. & Brinton, M. A. Translation elongation factor-1 alpha interacts with the 3' stem-loop region of West Nile virus genomic RNA. *J Virol* **71**, 6433-6444 (1997).
237 Nanda, S. K., Johnson, R. F., Liu, Q. & Leibowitz, J. L. Mitochondrial HSP70, HSP40, and HSP60 bind to the 3' untranslated region of the Murine hepatitis virus genome. *Arch Virol* **149**, 93-111, doi:10.1007/s00705-003-0196-4 (2004).
238 Zeman, D. *et al.* Laboratory investigation of PRRS virus infection in three swine herds. *J Vet Diagn Invest* **5**, 522-528 (1993).
239 Done, S. H. & Paton, D. J. Porcine reproductive and respiratory syndrome: clinical disease, pathology and immunosuppression. *Vet Rec* **136**, 32-35 (1995).
240 Rossow, K. D. *et al.* Pathogenesis of porcine reproductive and respiratory syndrome virus infection in gnotobiotic pigs. *Vet Pathol* **32**, 361-373 (1995).

241 Gray, J. T., Stabel, T. J. & Fedorka-Cray, P. J. Effect of dose on the immune response and persistence of Salmonella choleraesuis infection in swine. *Am J Vet Res* **57**, 313-319 (1996).
242 Wills, R. W. *et al.* Synergism between porcine reproductive and respiratory syndrome virus (PRRSV) and Salmonella choleraesuis in swine. *Vet Microbiol* **71**, 177-192 (2000).
243 Stevenson, G. W., Van Alstine, W. G., Kanitz, C. L. & Keffaber, K. K. Endemic porcine reproductive and respiratory syndrome virus infection of nursery pigs in two swine herds without current reproductive failure. *J Vet Diagn Invest* **5**, 432-434 (1993).
244 Feng, W. *et al.* In utero infection by porcine reproductive and respiratory syndrome virus is sufficient to increase susceptibility of piglets to challenge by Streptococcus suis type II. *J Virol* **75**, 4889-4895, doi:10.1128/JVI.75.10.4889-4895.2001 (2001).
245 Solano, G. I., Bautista, E., Molitor, T. W., Segales, J. & Pijoan, C. Effect of porcine reproductive and respiratory syndrome virus infection on the clearance of Haemophilus parasuis by porcine alveolar macrophages. *Can J Vet Res* **62**, 251-256 (1998).
246 Thanawongnuwech, R., Thacker, E. L. & Halbur, P. G. Effect of porcine reproductive and respiratory syndrome virus (PRRSV) (isolate ATCC VR-2385) infection on bactericidal activity of porcine pulmonary intravascular macrophages (PIMs): in vitro comparisons with pulmonary alveolar macrophages (PAMs). *Vet Immunol Immunopathol* **59**, 323-335, doi:S0165-2427(97)00078-0 [pii] (1997).
247 Chiou, M. T., Jeng, C. R., Chueh, L. L., Cheng, C. H. & Pang, V. F. Effects of porcine reproductive and respiratory syndrome virus (isolate tw91) on porcine alveolar macrophages in vitro. *Vet Microbiol* **71**, 9-25, doi:S0378-1135(99)00159-5 [pii] (2000).
248 Riber, U., Nielsen, J. & Lind, P. In utero infection with PRRS virus modulates cellular functions of blood monocytes and alveolar lung macrophages in piglets. *Vet Immunol Immunopathol* **99**, 169-177, doi:10.1016/j.vetimm.2004.02.008 S0165242704000698 [pii] (2004).
249 Gonzalez-Navajas, J. M., Lee, J., David, M. & Raz, E. Immunomodulatory functions of type I interferons. *Nat Rev Immunol* **12**, 125-135, doi:10.1038/nri3133 nri3133 [pii] (2012).
250 Patel, D. *et al.* Porcine reproductive and respiratory syndrome virus inhibits type I interferon signaling by blocking STAT1/STAT2 nuclear translocation. *J Virol* **84**, 11045-11055, doi:10.1128/JVI.00655-10 JVI.00655-10 [pii] (2010).
251 Van Reeth, K., Labarque, G., Nauwynck, H. & Pensaert, M. Differential production of proinflammatory cytokines in the pig lung during different respiratory virus infections: correlations with pathogenicity. *Res Vet Sci* **67**, 47-52, doi:10.1053/rvsc.1998.0277 S0034-5288(98)90277-6 [pii] (1999).
252 Buddaert, W., Van Reeth, K. & Pensaert, M. In vivo and in vitro interferon (IFN) studies with the porcine reproductive and respiratory syndrome virus (PRRSV). *Adv Exp Med Biol* **440**, 461-467 (1998).

253 Suradhat, S., Thanawongnuwech, R. & Poovorawan, Y. Upregulation of IL-10 gene expression in porcine peripheral blood mononuclear cells by porcine reproductive and respiratory syndrome virus. *J Gen Virol* **84**, 453-459 (2003).
254 Suradhat, S. & Thanawongnuwech, R. Upregulation of interleukin-10 gene expression in the leukocytes of pigs infected with porcine reproductive and respiratory syndrome virus. *J Gen Virol* **84**, 2755-2760 (2003).
255 Asai, T. *et al.* Elevated serum haptoglobin in pigs infected with porcine reproductive and respiratory syndrome virus. *Vet Immunol Immunopathol* **70**, 143-148, doi:S0165-2427(99)00069-0 [pii] (1999).
256 Lopez Fuertes, L. *et al.* Analysis of cellular immune response in pigs recovered from porcine respiratory and reproductive syndrome infection. *Virus Res* **64**, 33-42, doi:S0168-1702(99)00073-8 [pii] (1999).
257 Yoon, I. J., Joo, H. S., Goyal, S. M. & Molitor, T. W. A modified serum neutralization test for the detection of antibody to porcine reproductive and respiratory syndrome virus in swine sera. *J Vet Diagn Invest* **6**, 289-292 (1994).
258 Yoon, K. J., Wu, L. L., Zimmerman, J. J., Hill, H. T. & Platt, K. B. Antibody-dependent enhancement (ADE) of porcine reproductive and respiratory syndrome virus (PRRSV) infection in pigs. *Viral Immunol* **9**, 51-63 (1996).
259 Lopez, O. J. & Osorio, F. A. Role of neutralizing antibodies in PRRSV protective immunity. *Vet Immunol Immunopathol* **102**, 155-163, doi:S0165-2427(04)00236-3 [pii] 10.1016/j.vetimm.2004.09.005 (2004).
260 Costers, S. *et al.* GP4 of porcine reproductive and respiratory syndrome virus contains a neutralizing epitope that is susceptible to immunoselection in vitro. *Arch Virol* **155**, 371-378, doi:10.1007/s00705-009-0582-7 (2010).
261 Mateu, E. & Diaz, I. The challenge of PRRS immunology. *Vet J* **177**, 345-351, doi:S1090-0233(07)00203-1 [pii]10.1016/j.tvjl.2007.05.022 (2008).
262 Sanford, K. K., Earle, W. R. & Likely, G. D. The growth in vitro of single isolated tissue cells. *J Natl Cancer Inst* **9**, 229-246 (1948).
263 Truong, H. M. *et al.* A highly pathogenic porcine reproductive and respiratory syndrome virus generated from an infectious cDNA clone retains the in vivo virulence and transmissibility properties of the parental virus. *Virology* **325**, 308-319, doi:10.1016/j.virol.2004.04.046S0042682204003514 [pii] (2004).
264 Dulbecco, R. & Vogt, M. Some problems of animal virology as studied by the plaque technique. *Cold Spring Harb Symp Quant Biol* **18**, 273-279 (1953).
265 Ross, J. D. & Syverton, J. T. Use of tissue cultures in virus research. *Annu Rev Microbiol* **11**, 459-508, doi:10.1146/annurev.mi.11.100157.002331 (1957).
266 Weischenfeldt, J. & Porse, B. Bone Marrow-Derived Macrophages (BMM): Isolation and Applications. *CSH Protoc* **2008**, pdb prot5080, doi:10.1101/pdb.prot50802008/12/pdb.prot5080 [pii] (2008).
267 Bradley, T. R. & Metcalf, D. The growth of mouse bone marrow cells in vitro. *Aust J Exp Biol Med Sci* **44**, 287-299 (1966).

268 Striz, I. *et al.* The phenotype of alveolar macrophages and its correlation with immune cells in bronchoalveolar lavage. *Eur Respir J* **6**, 1287-1294 (1993).
269 Boyum, A. Isolation of mononuclear cells and granulocytes from human blood. Isolation of monuclear cells by one centrifugation, and of granulocytes by combining centrifugation and sedimentation at 1 g. *Scand J Clin Lab Invest Suppl* **97**, 77-89 (1968).
270 Yates, R. M., Hermetter, A. & Russell, D. G. The kinetics of phagosome maturation as a function of phagosome/lysosome fusion and acquisition of hydrolytic activity. *Traffic* **6**, 413-420, doi:TRA284 [pii]10.1111/j.1600-0854.2005.00284.x (2005).
271 Yates, R. M. & Russell, D. G. Real-time spectrofluorometric assays for the lumenal environment of the maturing phagosome. *Methods Mol Biol* **445**, 311-325, doi:10.1007/978-1-59745-157-4_20 (2008).
272 Yates, R. M., Hermetter, A. & Russell, D. G. Recording phagosome maturation through the real-time, spectrofluorometric measurement of hydrolytic activities. *Methods Mol Biol* **531**, 157-171, doi:10.1007/978-1-59745-396-7_11 (2009).
273 Stanley, E. R., Cifone, M., Heard, P. M. & Defendi, V. Factors regulating macrophage production and growth: identity of colony-stimulating factor and macrophage growth factor. *J Exp Med* **143**, 631-647 (1976).
274 Boltz-Nitulescu, G. *et al.* Differentiation of rat bone marrow cells into macrophages under the influence of mouse L929 cell supernatant. *J Leukoc Biol* **41**, 83-91 (1987).
275 Thacker, E. L., Halbur, P. G., Paul, P. S. & Thacker, B. J. Detection of intracellular porcine reproductive and respiratory syndrome virus nucleocapsid protein in porcine macrophages by flow cytometry. *J Vet Diagn Invest* **10**, 308-311 (1998).
276 Kapetanovic, R. *et al.* Pig bone marrow-derived macrophages resemble human macrophages in their response to bacterial lipopolysaccharide. *J Immunol* **188**, 3382-3394, doi:10.4049/jimmunol.1102649jimmunol.1102649 [pii] (2012).
277 Daeron, M. Fc receptor biology. *Annu Rev Immunol* **15**, 203-234, doi:10.1146/annurev.immunol.15.1.203 (1997).
278 Linehan, S. A., Martinez-Pomares, L. & Gordon, S. Mannose receptor and scavenger receptor: two macrophage pattern recognition receptors with diverse functions in tissue homeostasis and host defense. *Adv Exp Med Biol* **479**, 1-14, doi:10.1007/0-306-46831-X_1 (2000).
279 Vieira, O. V., Botelho, R. J. & Grinstein, S. Phagosome maturation: aging gracefully. *Biochem J* **366**, 689-704, doi:10.1042/BJ20020691BJ20020691 [pii] (2002).
280 Rybicka, J. M., Balce, D. R., Chaudhuri, S., Allan, E. R. & Yates, R. M. Phagosomal proteolysis in dendritic cells is modulated by NADPH oxidase in a pH-independent manner. *EMBO J* **31**, 932-944, doi:10.1038/emboj.2011.440emboj2011440 [pii] (2012).
281 Rybicka, J. M., Balce, D. R., Khan, M. F., Krohn, R. M. & Yates, R. M. NADPH oxidase activity controls phagosomal proteolysis in macrophages through modulation of the lumenal redox environment of phagosomes. *Proc Natl Acad Sci U S A* **107**, 10496-10501, doi:10.1073/pnas.0914867107 0914867107 [pii] (2010).
282 Honey, K. & Rudensky, A. Y. Lysosomal cysteine proteases regulate antigen presentation. *Nat Rev Immunol* **3**, 472-482, doi:10.1038/nri1110nri1110 [pii] (2003).

283 Opriessnig, T. *et al.* Comparison of molecular and biological characteristics of a modified live porcine reproductive and respiratory syndrome virus (PRRSV) vaccine (ingelvac PRRS MLV), the parent strain of the vaccine (ATCC VR2332), ATCC VR2385, and two recent field isolates of PRRSV. *J Virol* **76**, 11837-11844 (2002).
284 Li, X., Qiu, L., Yang, Z., Dang, R. & Wang, X. Emergency vaccination alleviates highly pathogenic porcine reproductive and respiratory syndrome virus infection after contact exposure. *BMC Vet Res* **9**, 26, doi:10.1186/1746-6148-9-261746-6148-9-26 [pii] (2013).
285 Ding, Z. *et al.* Proteomic alteration of Marc-145 cells and PAMs after infection by porcine reproductive and respiratory syndrome virus. *Vet Immunol Immunopathol* **145**, 206-213, doi:10.1016/j.vetimm.2011.11.005S0165-2427(11)00450-8 [pii] (2012).
286 Irvine, K. M. *et al.* A CSF-1 receptor kinase inhibitor targets effector functions and inhibits pro-inflammatory cytokine production from murine macrophage populations. *FASEB J* **20**, 1921-1923, doi:fj.06-5848fje [pii]10.1096/fj.06-5848fje (2006).
287 Sagong, M. *et al.* Human telomerase reverse transcriptase-immortalized porcine monomyeloid cell lines for the production of porcine reproductive and respiratory syndrome virus. *J Virol Methods* **179**, 26-32, doi:10.1016/j.jviromet.2011.08.016 S0166-0934(11)00350-8 [pii] (2012).
288 Raschke, W. C., Baird, S., Ralph, P. & Nakoinz, I. Functional macrophage cell lines transformed by Abelson leukemia virus. *Cell* **15**, 261-267, doi:0092-8674(78)90101-0 [pii] (1978).
289 Stanley, E. R. *et al.* Biology and action of colony--stimulating factor-1. *Mol Reprod Dev* **46**, 4-10, doi:10.1002/(SICI)1098-2795(199701)46:1<4::AID-MRD2>3.0.CO;2-V [pii] 10.1002/(SICI)1098-2795(199701)46:1<4::AID-MRD2>3.0.CO;2-V (1997).
290 Chen, X., Liu, H., Focia, P. J., Shim, A. H. & He, X. Structure of macrophage colony stimulating factor bound to FMS: diverse signaling assemblies of class III receptor tyrosine kinases. *Proc Natl Acad Sci U S A* **105**, 18267-18272, doi:10.1073/pnas.0807762105 [pii] (2008).
291 Elegheert, J. *et al.* Allosteric competitive inactivation of hematopoietic CSF-1 signaling by the viral decoy receptor BARF1. *Nat Struct Mol Biol* **19**, 938-947, doi:10.1038/nsmb.2367nsmb.2367 [pii] (2012).
292 Pandit, J. *et al.* Three-dimensional structure of dimeric human recombinant macrophage colony-stimulating factor. *Science* **258**, 1358-1362 (1992).
293 Domenech, N. *et al.* Identification of porcine macrophages with monoclonal antibodies in formalin-fixed, paraffin-embedded tissues. *Vet Immunol Immunopathol* **94**, 77-81, doi:S0165242703000849 [pii] (2003).
294 Ezquerra, A. *et al.* Porcine myelomonocytic markers and cell populations. *Dev Comp Immunol* **33**, 284-298, doi:10.1016/j.dci.2008.06.002 S0145-305X(08)00130-4 [pii] (2009).
295 Wang, R., Nan, Y., Yu, Y., Yang, Z. & Zhang, Y. J. Variable interference with interferon signal transduction by different strains of porcine reproductive and respiratory syndrome virus. *Vet Microbiol*, doi:S0378-1135(13)00384-2 [pii] 10.1016/j.vetmic.2013.07.022 (2013).

296 Yoon, K. J., Wu, L. L., Zimmerman, J. J. & Platt, K. B. Field isolates of porcine reproductive and respiratory syndrome virus (PRRSV) vary in their susceptibility to antibody dependent enhancement (ADE) of infection. *Vet Microbiol* **55**, 277-287 (1997).
297 Feng, L. *et al.* Generation and characterization of a porcine endometrial endothelial cell line susceptible to porcine reproductive and respiratory syndrome virus. *Virus Res* **171**, 209-215, doi:10.1016/j.virusres.2012.11.015 S0168-1702(12)00460-1 [pii] (2013).
298 Cafruny, W. A. *et al.* Porcine reproductive and respiratory syndrome virus (PRRSV) infection spreads by cell-to-cell transfer in cultured MARC-145 cells, is dependent on an intact cytoskeleton, and is suppressed by drug-targeting of cell permissiveness to virus infection. *Virol J* **3**, 90, doi:1743-422X-3-90 [pii] 10.1186/1743-422X-3-90 (2006).
299 LaBarre, D. D. & Lowy, R. J. Improvements in methods for calculating virus titer estimates from TCID50 and plaque assays. *J Virol Methods* **96**, 107-126, doi:S0166-0934(01)00316-0 [pii] (2001).
300 Fairbairn, L., Kapetanovic, R., Sester, D. P. & Hume, D. A. The mononuclear phagocyte system of the pig as a model for understanding human innate immunity and disease. *J Leukoc Biol* **89**, 855-871, doi:10.1189/jlb.1110607 jlb.1110607 [pii] (2011).
301 Sumikoshi, M. *et al.* Human influenza virus infection and apoptosis induction in human vascular endothelial cells. *J Med Virol* **80**, 1072-1078, doi:10.1002/jmv.21185 (2008).
302 Takizawa, T. *et al.* Induction of programmed cell death (apoptosis) by influenza virus infection in tissue culture cells. *J Gen Virol* **74 (Pt 11)**, 2347-2355 (1993).
303 Avirutnan, P., Malasit, P., Seliger, B., Bhakdi, S. & Husmann, M. Dengue virus infection of human endothelial cells leads to chemokine production, complement activation, and apoptosis. *J Immunol* **161**, 6338-6346 (1998).
304 Thome, M. *et al.* Viral FLICE-inhibitory proteins (FLIPs) prevent apoptosis induced by death receptors. *Nature* **386**, 517-521, doi:10.1038/386517a0 (1997).
305 Ma, Z. *et al.* Porcine Reproductive and Respiratory Syndrome Virus Nonstructural Protein 4 Induces Apoptosis Dependent on Its 3C-Like Serine Protease Activity. *PLoS One* **8**, e69387, doi:10.1371/journal.pone.0069387PONE-D-13-13130 [pii] (2013).
306 Sur, J. H., Doster, A. R. & Osorio, F. A. Apoptosis induced in vivo during acute infection by porcine reproductive and respiratory syndrome virus. *Vet Pathol* **35**, 506-514 (1998).
307 Sun, Y., Han, M., Kim, C., Calvert, J. G. & Yoo, D. Interplay between interferon-mediated innate immunity and porcine reproductive and respiratory syndrome virus. *Viruses* **4**, 424-446, doi:10.3390/v4040424viruses-04-00424 [pii] (2012).
308 Costers, S., Lefebvre, D. J., Delputte, P. L. & Nauwynck, H. J. Porcine reproductive and respiratory syndrome virus modulates apoptosis during replication in alveolar macrophages. *Arch Virol* **153**, 1453-1465, doi:10.1007/s00705-008-0135-5 (2008).
309 Boschert, K. R., Schoeb, T. R., Chandler, D. B. & Dillehay, D. L. Inhibition of phagocytosis and interleukin-1 production in pulmonary macrophages from rats with sialodacryoadenitis virus infection. *J Leukoc Biol* **44**, 87-92 (1988).

310 Hang do, T. T. *et al.* Differential effect of prior influenza infection on alveolar macrophage phagocytosis of Staphylococcus aureus and Escherichia coli: involvement of interferon-gamma production. *Microbiol Immunol* **55**, 751-759, doi:10.1111/j.1348-0421.2011.00383.x (2011).
311 Couper, K. N., Blount, D. G. & Riley, E. M. IL-10: the master regulator of immunity to infection. *J Immunol* **180**, 5771-5777, doi:180/9/5771 [pii] (2008).
312 Franke-Ullmann, G. *et al.* Characterization of murine lung interstitial macrophages in comparison with alveolar macrophages in vitro. *J Immunol* **157**, 3097-3104 (1996).
313 Wood, P. R., Simes, R. J. & Nelson, D. S. Activity of mouse macrophages purified by adherence to, and removal from, a plastic surface. *J Immunol Methods* **28**, 117-124 (1979).
314 Davies, J. Q. & Gordon, S. Isolation and culture of murine macrophages. *Methods Mol Biol* **290**, 91-103, doi:1-59259-838-2:091 [pii] (2005).
315 Kumar, S. *et al.* Mouse macrophage innate immune response to Chikungunya virus infection. *Virol J* **9**, 313, doi:10.1186/1743-422X-9-3131743-422X-9-313 [pii] (2012).
316 Glass, W. G., Rosenberg, H. F. & Murphy, P. M. Chemokine regulation of inflammation during acute viral infection. *Curr Opin Allergy Clin Immunol* **3**, 467-473, doi:10.1097/01.all.0000104448.09202.9100130832-200312000-00008 [pii] (2003).